DP-904

AEC RESEARCH AND DEVELOPMENT REPORT

PAPERS PRESENTED AT THE X-RAY PREFERRED ORIENTATION MEETING AT SAVANNAH RIVER LABORATORY JUNE 7, 8, 1962

Edited by
E. F. STURCKEN

DUPONT
REG. U.S. PAT. OFF.

ISSUED BY

Savannah River Laboratory

Aiken, South Carolina

LEGAL NOTICE

Printed in USA. Price $2.50
Available from the Clearinghouse for Federal Scientific and Technical Information, National Bureau of Standards, U. S. Department of Commerce, Springfield, Virginia

664508

DP-904

Metals, Ceramics, and Materials
(TID-4500, 31st Ed.)

PAPERS PRESENTED AT THE X-RAY PREFERRED ORIENTATION MEETING AT SAVANNAH RIVER LABORATORY JUNE 7, 8, 1962

Edited by

Edward F. Sturcken

Approved by

P. H. Permar, Research Manager
Pile Materials Division

July 1964

E. I. DU PONT DE NEMOURS & COMPANY
SAVANNAH RIVER LABORATORY
AIKEN, SOUTH CAROLINA

CONTRACT AT(07-2)-1 WITH THE
UNITED STATES ATOMIC ENERGY COMMISSION

ABSTRACT

A meeting was held by representatives of the USAEC feed materials, national laboratories, and production reactor sites to discuss techniques for measurement of grain orientation in uranium and the development of methods for predicting the irradiation growth that occurs in uranium fuel elements because of preferred grain orientation.

The papers on X-ray diffraction techniques described intersite exchange of standards, X-ray diffraction from highly radioactive materials, techniques for measuring texture gradients, and the measurement of grain size from statistical fluctuation in X-ray diffraction intensity. Papers on preferred orientation measurements included the effects of various heat treatments and fabrication procedures on the texture, texture gradients, and grain size of uranium fuel elements of various geometrical shapes. Papers concerning the development of theories for predicting irradiation growth included the strain tensor theory for irradiation growth (growth index method), the form of a theory that would include the interaction between grains during growth, deformation modes of uranium single crystals, and crystal structure variations in uranium at low temperature.

CONTENTS

Page

Session III. Physical Metallurgy and Structure Studies of Uranium

INTRODUCTION

A meeting to discuss the application of X-ray diffraction techniques to the measurement of preferred orientation in uranium was held at Savannah River Laboratory, Aiken, South Carolina, on June 7, 8, 1962 with the following persons attending:

W. I. Clark
Hanford Atomic Products Operation

H. E. Kissinger
Hanford Atomic Products Operation

H. C. Kloepper, Jr.
Mallinckrodt Chemical Works

B. G. LeFevre
Savannah River Laboratory

P. R. Morris
National Lead Company of Ohio

V. Morton
National Lead Company of Ohio

M. H. Mueller
Argonne National Laboratory

Leonard Robins
Bridgeport Brass Co.

R. B. Russell
Nuclear Metals, Inc.

J. W. Starbuck
Mallinckrodt Chemical Works

E. A. Starke
Savannah River Laboratory

E. F. Sturcken
Savannah River Laboratory

R. N. Thudium
National Lead Company of Ohio

R. S. Wood, Jr.
Savannah River Plant

The meeting was composed of persons interested in the measurement of grain orientation in uranium and the use of these measurements to predict the irradiation growth that occurs in uranium fuel elements because of preferred grain orientation. The papers and proceedings of previous meetings of this group are reported in the following AEC reports: NLCO-804, November 1959, edited by P. R. Morris of the National Lead Company of Ohio; ANL-6359, December 1960, edited by M. H. Mueller of Argonne National Laboratory; HW-74429, August 1962, edited by W. Gary Jolley of Hanford Atomic Products Operation; and NMI-4992, May 1963, edited by R. B. Russell of Nuclear Metals, Inc.

COMPUTATION PROCEDURE FOR DETERMINING AREA WEIGHTS FOR X-RAY DIFFRACTION STUDIES

R. N. Thudium

National Lead Company of Ohio

ABSTRACT

A method has been devised to determine area weights for any combination of planes of an orthogonal crystal structure. A program has been written for a General Precision LGP-30 digital computer and is operable to compute area weights for any combination of planes of uranium. Areas of spherical polygons for 18 and 20 plane sets of uranium have been tabulated.

INTRODUCTION

The Growth Index[1] has been modified by Morris[2] and Sturcken.[3] Morris's area weight treatment[2] makes the following two assumptions.

- A pole represents all points within a spherical polygon obtained by making arcs of great circles equidistant between a pole and each of its nearest neighbors.
- A finite set of poles may be employed to adequately sample an unknown continuous function.

The second assumption was made in other methods.[1,3] As the texture increases, it becomes necessary to increase the number of poles or sampling points. The G_3 and the modified texture coefficient $[A_W\ TC/A_W]$ developed by Morris[2] depend upon these assumptions.

Until recently, two laborious techniques[4,5] have been employed for determining area weights. Accuracy of these techniques was ±5%. A technique was needed to obtain area weights quickly with greater accuracy.

SUMMARY

A method was devised to determine area weights of any combination of planes of uranium. A computer program was written for calculating these area weights. The program was tested using 18- and 20-plane sets of uranium. Accuracy of results is ±0.005%. Time required to make a computation is approximately three minutes for each plane.

DISCUSSION

In a previous technique,[5] poles of 18 crystallographic planes of uranium were projected on the surface of a sphere. Arcs of great circles were drawn equidistant between a pole and each of its nearest neighbors, thus forming a spherical polygon about each pole (see Figure 1).

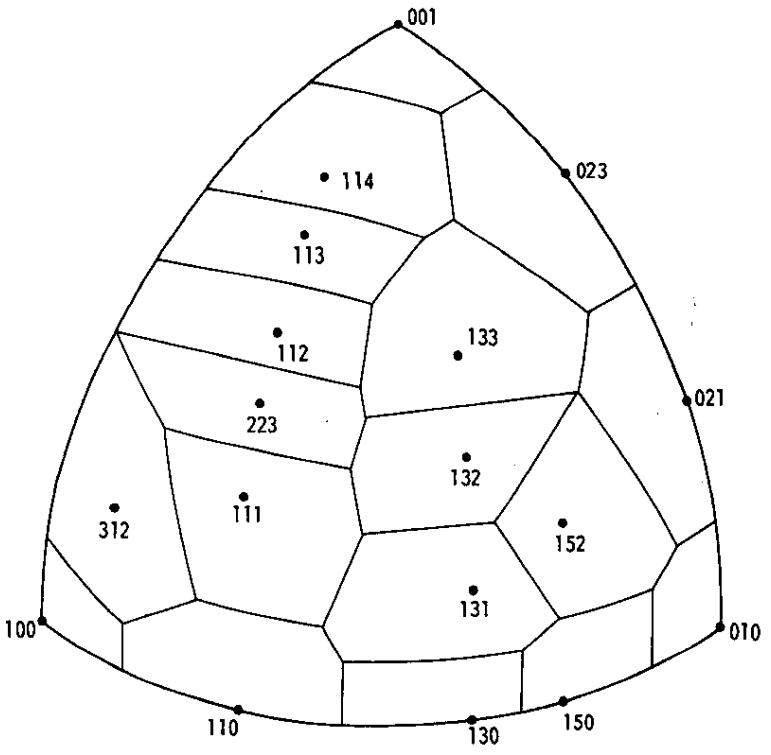

FIG. 1 EIGHTEEN-PLANE SET OF SPHERICAL POLYGONS FOR URANIUM

The pole of a crystallographic plane of an orthorhombic crystal structure may be represented by a unit vector[6] with Miller indices (hkl) and lattice parameters a, b, and c. If $\vec{i}$, $\vec{j}$, and $\vec{k}$ are unit base vectors along the a, b, and c axes, respectively, intercepts of the (hkl) plane with the three principal axes may be represented by the vectors

$$\frac{(a)}{(h)}\vec{i},\ \frac{(b)}{(k)}\vec{j},\ \text{and}\ \frac{(c)}{(l)}\vec{k}$$

as shown in Figure 2.

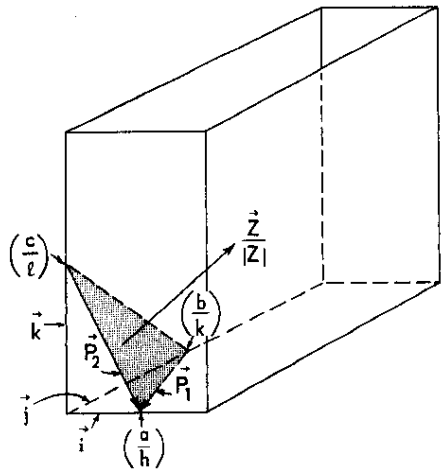

FIG. 2 UNIT NORMAL VECTOR $\frac{\vec{Z}}{|Z|}$ OF (hkl) PLANE

Vectors $\vec{P}_1$ and $\vec{P}_2$ will be

$$\vec{P}_1 = \frac{(a)}{(h)}\vec{i} - \frac{(b)}{(k)}\vec{j} \qquad (1)$$

$$\vec{P}_2 = \frac{(a)}{(h)}\vec{i} - \frac{(c)}{(l)}\vec{k} \qquad (2)$$

A vector normal to the (hkl) plane of $\vec{P}_1$ and $\vec{P}_2$ is found by taking the vector product of $\vec{P}_1$ and $\vec{P}_2$.

$$\vec{Z} = \vec{P}_1 \times \vec{P}_2 \qquad (3)$$

The normal vector $\vec{Z}$ is divided by its absolute magnitude, $|Z|$, giving the unit normal vector of the (hkl) plane $\frac{\vec{Z}}{|Z|}$.

Substituting $\vec{P}_1$ and $\vec{P}_2$ from Equations 1 and 2 in Equation 3

$$\vec{Z} = \vec{P}_1 \times \vec{P}_2 = \begin{vmatrix} \vec{i} & \vec{j} & \vec{k} \\ \frac{a}{h} & -\frac{b}{k} & 0 \\ \frac{a}{h} & 0 & -\frac{c}{l} \end{vmatrix} = \frac{bc}{kl}\vec{i} + \frac{ac}{hl}\vec{j} + \frac{ab}{hk}\vec{k}$$

where

$$|Z| = \left[\left(\frac{bc}{kl}\right)^2 + \left(\frac{ac}{hl}\right)^2 + \left(\frac{ab}{hk}\right)^2\right]^{\frac{1}{2}}$$

and

$$\frac{\vec{Z}}{|Z|} = \frac{\frac{bc}{kl}\vec{i} + \frac{ac}{hl}\vec{j} + \frac{ab}{hk}\vec{k}}{\left[\left(\frac{bc}{kl}\right)^2 + \left(\frac{ac}{hl}\right)^2 + \left(\frac{ab}{hk}\right)^2\right]^{\frac{1}{2}}}$$

$$= \frac{hbc\,\vec{i} + kac\,\vec{j} + lab\,\vec{k}}{[(hbc)^2 + (kac)^2 + (lab)^2]^{\frac{1}{2}}} \qquad (4)$$

Consider the unit vector poles of four (hkl) planes of uranium, $\vec{A}$, $\vec{B}$, $\vec{C}$, and $\vec{D}$.

$$\frac{\vec{Z}_A}{|Z_A|} = A_1\vec{i} + A_2\vec{j} + A_3\vec{k} = \vec{A}$$

$$\frac{\vec{Z}_B}{|Z_B|} = B_1\vec{i} + B_2\vec{j} + B_3\vec{k} = \vec{B}$$

$$\frac{\vec{Z}_C}{|Z_C|} = C_1\vec{i} + C_2\vec{j} + C_3\vec{k} = \vec{C}$$

$$\frac{\vec{Z}_D}{|Z_D|} = D_1\vec{i} + D_2\vec{j} + D_3\vec{k} = \vec{D}$$

where A_i, B_i, C_i, and D_i are determined as in Equation 4.

Consider Figure 3, where $\vec{A}$ is the vector pole of the plane of interest, $\vec{B}$ and $\vec{C}$ are nearest neighbors, and $\vec{D}$ is 90 degrees from $\vec{A}$. Then by adding $\vec{A}$ and $\vec{B}$, and $\vec{A}$ and $\vec{C}$,

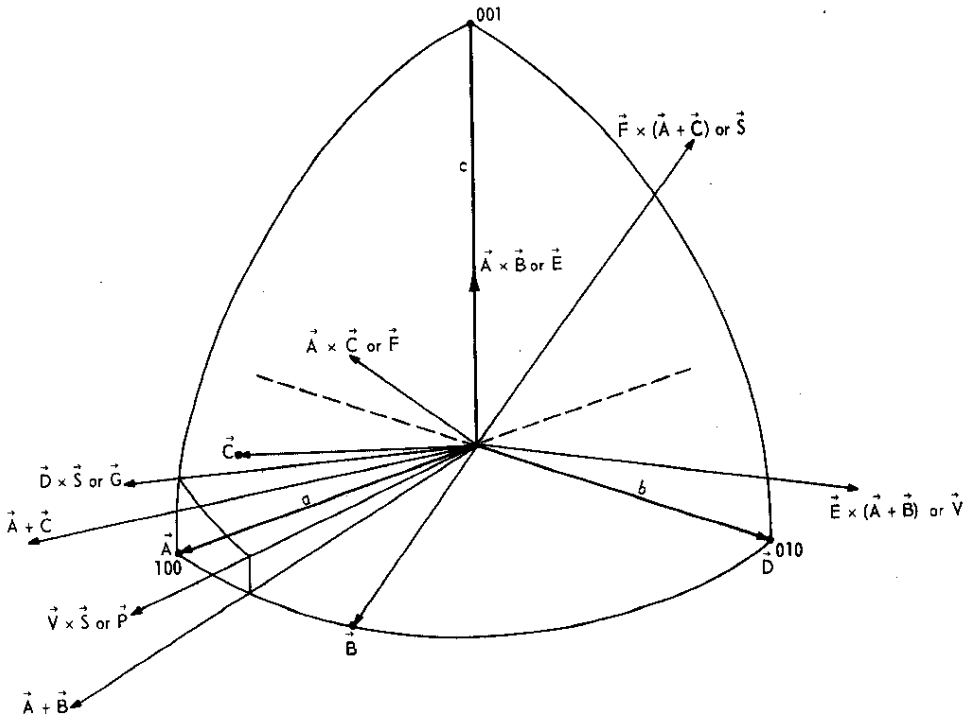

FIG. 3 VECTORS, SUMS OF VECTORS, AND VECTOR PRODUCTS

vectors midway between $\vec{A}$ and $\vec{B}$ and midway between $\vec{A}$ and $\vec{C}$ are obtained.

The sums are:

$$\vec{A} + \vec{B} = (A_1 + B_1)\,\vec{i} + (A_2 + B_2)\,\vec{j} + (A_3 + B_3)\,\vec{k} \qquad (5)$$

and

$$\vec{A} + \vec{C} = (A_1 + C_1)\,\vec{i} + (A_2 + C_2)\,\vec{j} + (A_3 + C_3)\,\vec{k} \qquad (6)$$

Then by taking the vector products of $\vec{A}$ and $\vec{B}$, and $\vec{A}$ and $\vec{C}$, vectors normal to $\vec{A}$ and $\vec{B}$, and $\vec{A}$ and $\vec{C}$, respectively, are obtained as shown in Figure 3.

The products are:

$$\vec{A} \times \vec{B} = \begin{vmatrix} \vec{i} & \vec{j} & \vec{k} \\ A_1 & A_2 & A_3 \\ B_1 & B_2 & B_3 \end{vmatrix}$$

$$= (A_2B_3 - A_3B_2)\,\vec{i} + (A_3B_1 - A_1B_3)\,\vec{j} + (A_1B_2 - A_2B_1)\,\vec{k}$$

$$= E_1\,\vec{i} + E_2\,\vec{j} + E_3\,\vec{k}$$

$$= \vec{E} \qquad (7)$$

and

$$\vec{A} \times \vec{C} = (A_2C_3 - A_3C_2)\,\vec{i} + (A_3C_1 - A_1C_3)\,\vec{j} + (A_1C_2 - A_2C_1)\,\vec{k}$$
$$= F_1\,\vec{i} + F_2\,\vec{j} + F_3\,\vec{k}$$
$$= \vec{F} \qquad (8)$$

The vector products of $\vec{E}$ and $(\vec{A} + \vec{B})$ and $\vec{F}$ and $(\vec{A} + \vec{C})$ give vectors normal to $\vec{E}$ and $(\vec{A} + \vec{B})$, and to $\vec{F}$ and $(\vec{A} + \vec{C})$, respectively. These vectors are normal to the great circles making up two sides of the spherical polygon. The products are:

$$\vec{E} \times (\vec{A} + \vec{B}) = \begin{vmatrix} \vec{i} & \vec{j} & \vec{k} \\ E_1 & E_2 & E_3 \\ (A_1+B_1) & (A_2+B_2) & (A_3+B_3) \end{vmatrix}$$
$$= [E_2(A_3 + B_3) - E_3(A_2 + B_2)]\,\vec{i}$$
$$+ [E_3(A_1 + B_1) - E_1(A_3 + B_3)]\,\vec{j}$$
$$+ [E_1(A_2 + B_2) - E_2(A_1 + B_1)]\,\vec{k}$$
$$= V_1\,\vec{i} + V_2\,\vec{j} + V_3\,\vec{k}$$
$$= \vec{V} \qquad (9)$$

and

$$\vec{F} \times (\vec{A} + \vec{C}) = [F_2(A_3 + C_3) - F_3(A_2 + C_2)]\,\vec{i}$$
$$+ [F_3(A_1 + C_1) - F_1(A_3 + C_3)]\,\vec{j}$$
$$+ [F_1(A_2 + C_2) - F_2(A_1 + C_1)]\,\vec{k}$$
$$= S_1\,\vec{i} + S_2\,\vec{j} + S_3\,\vec{k}$$
$$= \vec{S} \qquad (10)$$

Then the vector product of $\vec{V}$ and $\vec{S}$, taken in a counter-clockwise direction, gives a vector normal to $\vec{V}$ and $\vec{S}$, which is in the direction of the point of intersection of the sides of the spherical polygon as shown in Figure 3. The vector

product is:

$$V \times S = \begin{vmatrix} \vec{i} & \vec{j} & \vec{k} \\ V_1 & V_2 & V_3 \\ S_1 & S_2 & S_3 \end{vmatrix}$$

$$= (V_2S_3 - V_3S_2)\,\vec{i} + (V_3S_1 - V_1S_3)\,\vec{j} + (V_1S_2 - V_2S_1)\,\vec{k}$$

$$= P_1\,\vec{i} + P_2\,\vec{j} + P_3\,\vec{k}$$

$$= \vec{P} \qquad (11)$$

The vector product of $\vec{D}$ and $\vec{S}$, taken in a counter-clockwise direction, gives a vector normal to $\vec{D}$ and $\vec{S}$, which is in the direction of the point of intersection of the great circles as shown in Figure 3. The vector product is:

$$\vec{D} \times \vec{S} = \begin{vmatrix} \vec{i} & \vec{j} & \vec{k} \\ D_1 & D_2 & D_3 \\ S_1 & S_2 & S_3 \end{vmatrix}$$

$$= (D_2S_3 - D_3S_2)\,\vec{i} + (D_3S_1 - D_1S_3)\,\vec{j} + (D_1S_2 - D_2S_1)\,\vec{k}$$

$$= G_1\,\vec{i} + G_2\,\vec{j} + G_3\,\vec{k}$$

$$= \vec{G}$$

The vectors $\vec{A}$, $(\vec{A} + \vec{B})$, $\vec{P}$, and $\vec{G}$ (which shall be said to form an $\vec{A}$, $(\vec{A} + \vec{B})$, $\vec{P}$, $\vec{G}$ type) are divided by their absolute magnitudes, giving the unit vectors

$$\frac{\vec{A}}{|A|},\ \frac{\vec{A} + \vec{B}}{|A + B|},\ \frac{\vec{P}}{|P|},\ \text{and}\ \frac{\vec{G}}{|G|}$$

The termini of these vectors on a unit sphere are the vertices of a spherical polygon as shown in Figure 4 where

$$\frac{\vec{A}}{|A|} = \frac{A_1\,\vec{i} + A_2\,\vec{j} + A_3\,\vec{k}}{[(A_1)^2 + (A_2)^2 + (A_3)^2]^{\frac{1}{2}}}$$

$$= J_{11}\,\vec{i} + J_{12}\,\vec{j} + J_{13}\,\vec{k}$$

$$= \vec{J}_1$$

$$\frac{\vec{A}+\vec{B}}{|A+B|} = \frac{(A_1+B_1)\,\vec{i} + (A_2+B_2)\,\vec{j} + (A_3+B_3)\,\vec{k}}{[(A_1+B_1)^2 + (A_2+B_2)^2 + (A_3+B_3)^2]^{\frac{1}{2}}}$$

$$= J_{21}\,\vec{i} + J_{22}\,\vec{j} + J_{23}\,\vec{k}$$

$$= \vec{J}_2$$

$$\frac{\vec{P}}{|P|} = \frac{P_1\,\vec{i} + P_2\,\vec{j} + P_3\,\vec{k}}{[(P_1)^2 + (P_2)^2 + (P_3)^2]^{\frac{1}{2}}}$$

$$= J_{31}\,\vec{i} + J_{32}\,\vec{j} + J_{33}\,\vec{k}$$

$$= \vec{J}_3$$

and

$$\frac{\vec{G}}{|G|} = \frac{G_1\,\vec{i} + G_2\,\vec{j} + G_3\,\vec{k}}{[(G_1)^2 + (G_2)^2 + (G_3)^2]^{\frac{1}{2}}}$$

$$= J_{41}\,\vec{i} + J_{42}\,\vec{j} + J_{43}\,\vec{k}$$

$$= \vec{J}_4$$

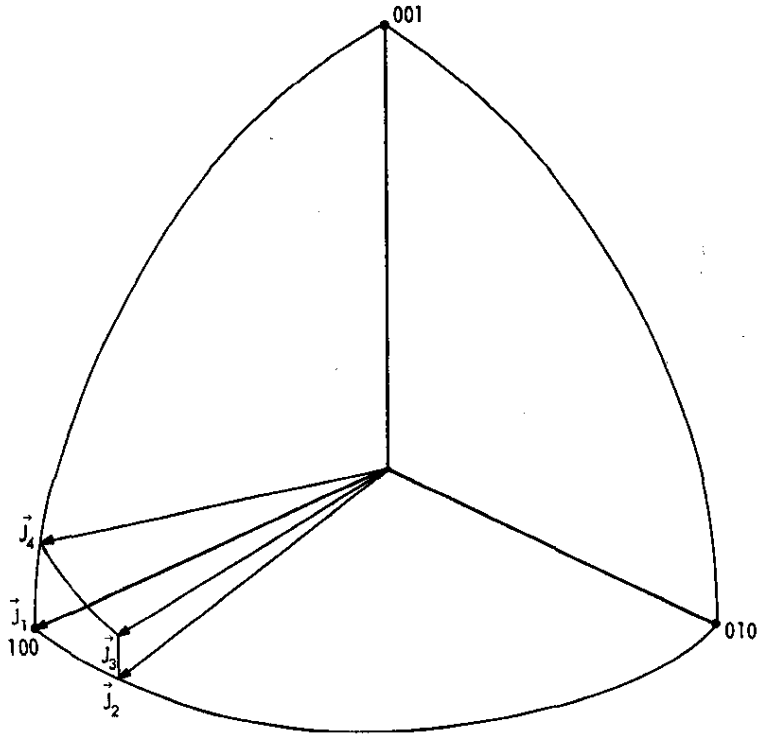

FIG. 4 NORMALIZED VECTORS OF THE SPHERICAL POLYGON

The spherical polygon is divided into spherical triangles, and chords, $\vec{l}_i$, of each triangle are determined by subtracting vectors. The chord length, l_i, is given by

$$l_i = [(\vec{l}_i)(\vec{l}_i)]^{\frac{1}{2}}$$

Thus

$$\begin{aligned} l_1 &= [(\vec{J}_1 - \vec{J}_2)(\vec{J}_1 - \vec{J}_2)]^{\frac{1}{2}} \\ &= \Big\{[(J_{11} - J_{21})\,\vec{i} + (J_{12} - J_{22})\,\vec{j} \\ &\quad + (J_{13} - J_{23})\,\vec{k}][(J_{11} - J_{21})\,\vec{i} \\ &\quad + (J_{12} + J_{22})\,\vec{j} + (J_{13} - J_{23})\,\vec{k}]\Big\}^{\frac{1}{2}} \\ &= [(J_{11} - J_{21})^2 + (J_{12} - J_{22})^2 + (J_{13} - J_{23})^2]^{\frac{1}{2}} \end{aligned}$$

Likewise

$$l_2 = [(J_{21} - J_{31})^2 + (J_{22} - J_{32})^2 + (J_{23} - J_{33})^2]^{\frac{1}{2}}$$

$$l_3 = [(J_{11} - J_{31})^2 + (J_{12} - J_{32})^2 + (J_{13} - J_{33})^2]^{\frac{1}{2}}$$

$$l_4 = [(J_{31} - J_{41})^2 + (J_{32} - J_{42})^2 + (J_{33} - J_{43})^2]^{\frac{1}{2}}$$

$$l_5 = [(J_{11} - J_{41})^2 + (J_{12} - J_{42})^2 + (J_{13} - J_{43})^2]^{\frac{1}{2}}$$

The angles, θ_i, subtended at the origin by the chords are determined by

$$\frac{\theta_i}{2} = \text{arc sin } \frac{l_i}{2r}$$

where r = 1, and i = 1, 2, 3, 4, 5.

$$\frac{\theta_i}{2} = \text{arc sin } \frac{l_i}{2}$$

The sums

$$\tfrac{1}{2}S_1 = \tfrac{1}{4}(\theta_1 + \theta_2 + \theta_3) \qquad (12)$$

and

$$\tfrac{1}{2}S_5 = \tfrac{1}{4}(\theta_3 + \theta_4 + \theta_5) \qquad (12)$$

are formed.

The spherical excess in degrees, E_1, of the spherical triangle is given by

$$E_1 = 4 \arctan \left\{ [\tan \tfrac{1}{2}S_1][\tan \tfrac{1}{2}(S_1 - \theta_1)] \right.$$
$$\left. [\tan \tfrac{1}{2}(S_1 - \theta_2)][\tan \tfrac{1}{2}(S_1 - \theta_3)] \right\}^{\frac{1}{2}}$$

and

$$E_2 = 4 \arctan \left\{ [\tan \tfrac{1}{2}S_5][\tan \tfrac{1}{2}(S_5 - \theta_3)] \right.$$
$$\left. [\tan \tfrac{1}{2}(S_5 - \theta_4)][\tan \tfrac{1}{2}(S_5 - \theta_5)] \right\}^{\frac{1}{2}}$$

The area of the spherical polygon about $\vec{A}$ is equal to

$$\text{Area } \vec{A} = \frac{\pi r^2 (E_1 + E_2)}{180} \qquad (13)$$

If the area of the octant of the sphere is set equal to unity, then $r^2 = \frac{2}{\pi}$. Equation 13 becomes

$$\text{Area } \vec{A} = \frac{(E_1 + E_2)}{90}$$

This describes one type of spherical polygon: $\vec{A}$, $(\vec{A} + \vec{B})$, $\vec{P}$, and $\vec{G}$. Other types that make up spherical polygons are:

$\vec{A}$, $\vec{G}$, $\vec{P}$, $(\vec{A} + \vec{B})$

$\vec{A}$, $(\vec{A} + \vec{B})$, $\vec{P}$, $(\vec{A} + \vec{C})$

$\vec{A}$, $\vec{G}$, $\vec{P}$, $\vec{G}$

$(\vec{A} + \vec{B})$, $\vec{P}$, $\vec{G}$

$\vec{G}$, $\vec{P}$, $(\vec{A} + \vec{B})$

$(\vec{A} + \vec{B})$, $\vec{P}$, $(\vec{A} + \vec{C})$

$\vec{G}$, $\vec{P}$, $\vec{G}$

All $\vec{P}$

In the above groupings, there may be multiple $\vec{P}$ in any group. Figure 5 shows the computer flow chart.

Each $\vec{P}/|P|$ may be determined at least three times by taking different vector products of vectors normal to planes

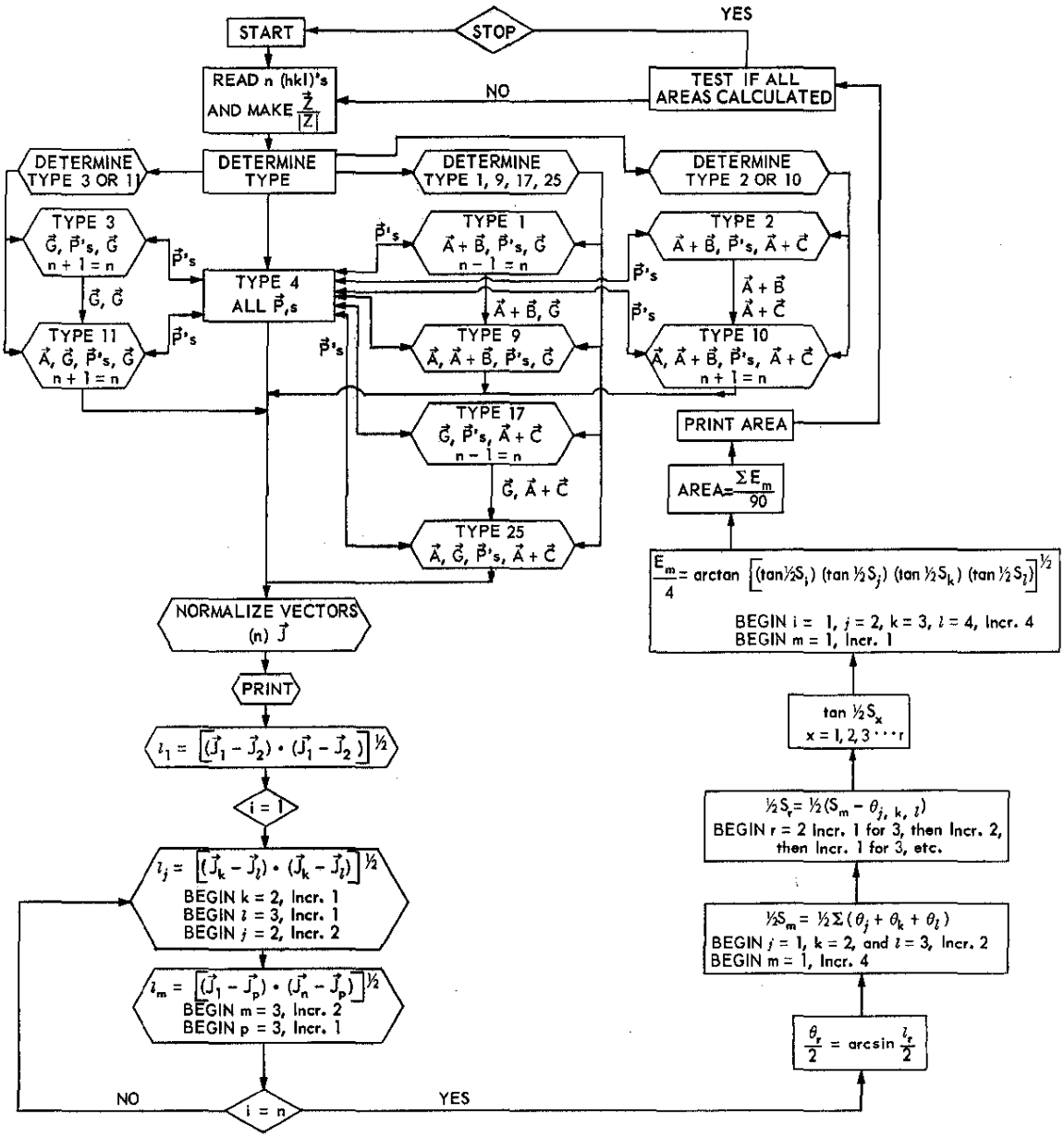

FIG. 5 COMPUTER FLOW CHART

of the great circles. Thus, a check is made of nearest neighbors of a pole. Nearest neighbors are first roughly determined by sketching spherical polygons on an inverse pole figure. Then the $\vec{P}/|P|$'s are compared to the seventh decimal. If disagreement is greater than five in the seventh decimal, a new set of nearest neighbors are tried. Finally, the sum of areas for all spherical polygons must be within 0.01% of the area of the octant (the area of the octant is taken as unity).

In Table I are given the diffraction planes of the 18-plane set, calculated random intensities, area weight factors, squares of direction cosines, and products of area weight factors and squares of direction cosines. Table II gives similar information for the 20-plane set.

Using the data from Table I

$$\frac{1}{18} \sum_{i=1}^{18} (\cos^2 \beta_i - \cos^2 \alpha_i) = +0.028$$

$$\sum_{i=1}^{18} A_{wi} (\cos^2 \beta_i - \cos^2 \alpha_i) = +0.002$$

Using the data from Table II

$$\frac{1}{20} \sum_{i=1}^{20} (\cos^2 \beta_i - \cos^2 \alpha_i) = +0.092$$

$$\sum_{i=1}^{20} A_{wi} (\cos^2 \beta_i - \cos^2 \alpha_i) = +0.007$$

TABLE I

Area Weight Data for the 18-Plane Set of Uranium

Plane	I_o	A_w	$\cos^2 \alpha$	$\cos^2 \beta$	$\cos^2 \gamma$	$A_w \cos^2 \alpha$	$A_w \cos^2 \beta$	$A_w \cos^2 \gamma$
020	6.34	0.03129	0.00000	1.00000	0.00000	0.00000	0.03129	0.00000
110	72.7	0.06532	0.80877	0.19123	0.00000	0.05283	0.01249	0.00000
021	100.0	0.05820	0.00000	0.74035	0.25965	0.00000	0.04309	0.01511
002	51.4	0.03033	0.00000	0.00000	1.00000	0.00000	0.00000	0.03033
111	58.3	0.07413	0.63769	0.16078	0.21153	0.04727	0.01118	0.01568
112	48.3	0.05339	0.39013	0.09224	0.51763	0.02083	0.00492	0.02764
130	3.37	0.03602	0.31969	0.68031	0.00000	0.01152	0.02450	0.00000
131	40.0	0.07074	0.28904	0.61508	0.09588	0.02045	0.04351	0.00678
023	16.8	0.06535	0.00000	0.24059	0.75941	0.00000	0.01572	0.04963
200	8.82	0.02380	1.00000	0.00000	0.00000	0.02380	0.00000	0.00000
113	11.6	0.04691	0.23686	0.05601	0.70713	0.01111	0.00263	0.03317
132	3.65	0.05243	0.22447	0.47769	0.29784	0.01177	0.02505	0.01562
133	15.3	0.08009	0.16358	0.34809	0.48833	0.01310	0.02788	0.03911
114	10.2	0.07267	0.15282	0.03613	0.81105	0.01111	0.00263	0.05894
150	7.43	0.03784	0.14469	0.85531	0.00000	0.00548	0.03236	0.00000
223	12.2	0.04836	0.50434	0.11925	0.37641	0.02439	0.00577	0.01820
152	12.8	0.06963	0.12139	0.71755	0.16106	0.00845	0.04996	0.01121
312	8.85	0.08346	0.85201	0.02238	0.12561	0.07111	0.00187	0.01048
Σ		0.99996	5.84548	6.34299	5.81153	0.33322	0.33485	0.33190
$\frac{1}{18}\Sigma$			0.3247	0.3524	0.3229			

TABLE II

Area Weight Data for the 20-Plane Set of Uranium

Plane	I_o	A_W	$\cos^2 \alpha$	$\cos^2 \beta$	$\cos^2 \gamma$	$A_W \cos^2 \alpha$	$A_W \cos^2 \beta$	$A_W \cos^2 \gamma$
020	6.34	0.01770	0.00000	1.00000	0.00000	0.00000	0.01770	0.00000
110	72.7	0.06532	0.80877	0.19123	0.00000	0.05283	0.01249	0.00000
021	100.0	0.03545	0.00000	0.74035	0.25965	0.00000	0.02625	0.00920
002	51.4	0.03033	0.00000	0.00000	1.00000	0.00000	0.00000	0.03033
111	58.3	0.07413	0.63769	0.15078	0.21153	0.04727	0.01118	0.01568
022	3.58	0.03432	0.00000	0.41619	0.58382	0.00000	0.01428	0.02004
112	48.3	0.05339	0.39013	0.09224	0.51763	0.02083	0.00492	0.02764
130	3.37	0.03602	0.31969	0.68031	0.00000	0.01152	0.02450	0.00000
131	40.0	0.07074	0.28904	0.61508	0.09588	0.02045	0.04351	0.00678
023	16.8	0.04728	0.00000	0.24059	0.75941	0.00000	0.01138	0.03590
200	8.82	0.02380	1.00000	0.00000	0.00000	0.02380	0.00000	0.00000
041	4.83	0.03437	0.00000	0.91940	0.08061	0.00000	0.03160	0.00277
113	11.6	0.04691	0.23686	0.05601	0.70713	0.01111	0.00263	0.03317
132	3.65	0.05243	0.22447	0.47769	0.29784	0.01177	0.02505	0.01562
133	15.3	0.07394	0.16358	0.34809	0.48833	0.01210	0.02574	0.03611
114	10.2	0.07267	0.15282	0.03613	0.81105	0.01111	0.00263	0.05894
150	7.43	0.03690	0.14469	0.85531	0.00000	0.00534	0.03156	0.00000
223	12.2	0.04836	0.50434	0.11925	0.37641	0.02439	0.00577	0.01820
152	12.8	0.06243	0.12139	0.71755	0.16106	0.00758	0.04480	0.01005
312	8.85	0.08346	0.85201	0.02238	0.12561	0.07111	0.00187	0.01048
	Σ	0.99995	5.84548	7.67858	6.47596	0.33121	0.33786	0.33091
$\frac{1}{20}$	Σ		0.2923	0.3839	0.3238			

REFERENCES

1. Sturcken, E. F. An X-ray Method for Predicting the Stability of Natural Uranium at Low Burnup. E. I. du Pont de Nemours & Co., Savannah River Laboratory, Aiken, S. C. USAEC Report DP-251 (1957) (declassified with deletions 10-4-61).

2. Morris, P. R. Comparative Measurements of the Velocity of Propagation of an Ultrasonic Pulse in Uranium Fuel Elements. National Lead Company of Ohio, Cincinnati, Ohio. USAEC Report NLCO-764 (1958).

3. Sturcken, E. F. "A Generalized Growth Index Formalism." Papers Presented at the X-ray Preferred Orientation Meeting Held at National Lead Company of Ohio, November 9 and 10, 1959. P. R. Morris, Ed. National Lead Company of Ohio, Cincinnati, Ohio. USAEC Report NLCO-804 (1960).

4. Morris, P. R. "Reducing the Effects of Nonuniform Pole Distribution in Inverse Pole Studies." J. Appl. Phys. 30, 595-96 (1959).

5. Thudium, R. N. and P. R. Morris. "Brief Description of the Area Weight Treatment for the 18-Plane Set." Papers and Discussion from the X-ray Preferred Orientation Meeting Held at Argonne National Laboratory, December 15 and 16, 1960. M. H. Mueller, Ed. Argonne National Laboratory, Argonne, Ill. USAEC Report ANL-6359 (1961).

6. LeGeros, J. P. "A Growth Mechanism Based Upon Lattice Distortion." Papers Presented at the X-ray Preferred Orientation Meeting Held at National Lead Company of Ohio, November 9 and 10, 1959. National Lead Company of Ohio, Cincinnati, Ohio. USAEC Report NLCO-804 (1960).

X-RAY DIFFRACTION OF HIGHLY IRRADIATED URANIUM FUEL ELEMENTS

Wesley I. Clark

General Electric Company
Hanford Atomic Products Operation

ABSTRACT

A description is given of the double diffracting X-ray unit in the Radiometallurgy Facility at the Hanford Laboratories. This equipment is a modified General Electric XRD-3 diffraction unit, using a copper X-ray tube mounted on the rotating goniometer. The diffracted beam from the sample passes through a shielded slit and is diffracted again by a single aluminum crystal orientated for the characteristic Cu $K\alpha_1$ X-rays. The aluminum crystal separates the diffraction pattern from the background produced by the irradiated sample. The intensity of the diffracted X-rays is measured with a shielded proportional counter.

This equipment is being used to study the diffraction patterns of irradiated nuclear fuel elements. One such study was to determine the grain orientation of uranium fuel elements that failed during irradiation. Diffraction patterns of samples reading 400 r at 10 inches have been obtained with this equipment.

The radioactivity of the fission products produced during irradiation presents two main problems in obtaining X-ray diffraction data from irradiated fuel elements. First, the operator must be protected from excessive exposure, and second, the diffracted X-ray beam must be detected in the presence of the high radioactivity of the sample. For both of these problems, the level of activity of the proposed diffraction samples will dictate the amount of shielding necessary for both the operator and the detector tube.

In the Radiometallurgy Facility at the Hanford Laboratories Operation the problem of personnel exposure was solved by enclosing the X-ray diffraction unit within a 6-inch lead brick cave. The cave measures 5 x 4 feet by 3 feet high with a 1/2-inch steel top. The high voltage cable and cooling water hoses to the X-ray tube enter through the top of the cave. The controls and drive to the goniometer along with the electrical leads for lighting, to the proportional counter, etc., pass through the walls of the cave. Viewing is provided through an 8 x 10 inch lead glass window mounted in the wall directly in front of the sample holder. The sample is positioned in the sample holder by a simple, over-the-wall manipulator. The sample holder can be moved to scan across the sample to the right or left of the centerline of the X-ray beam, but does not rotate. An air piston holds the sample in position during the diffraction run.

Detecting and differentiating the X-ray beam from the high background produced by the sample can be accomplished with either electronic discrimination or with an X-ray optical system. A proportional counter and pulse height analyzer are used in some units to discriminate between the diffracted X-ray beam and the background. In these units, the counter is heavily shielded from the sample except for a small channel through which the X-ray beam passes.

The X-ray optical system consists of a diffraction unit joined to a fixed-angle X-ray spectrometer. In this system, a single crystal is used as a monochromator to separate the diffracted X-ray beam from the high background. A counter tube is positioned to detect the X-ray beam diffracted by the crystal. The X-ray optical system is advantageous in that it eliminates a straight line between the sample and the counter tube. The geometry of this equipment (Figure 1) is covered in greater detail by Cummings and Gruber.[1]

By using the X-ray optical system, we are able to obtain X-ray diffraction patterns of irradiated samples reading in excess of 400 r at 10 inches. This reading would be approximately 2 x 10^7 counts/second. Although electronic discrimination is used to cleanup the diffraction pattern, the primary separation of the X-ray beam from the background is achieved with the single crystal monochromator.

A General Electric XRD-3 diffraction unit was modified to accomodate the additional equipment needed to obtain

---

[1] Cummings, W. V. and W. J. Gruber. Techniques for X-ray Diffraction Studies of Radioactive Materials. General Electric Co., Hanford Atomic Products Operation, Richland, Wash. USAEC Report HW-56170 (1960).

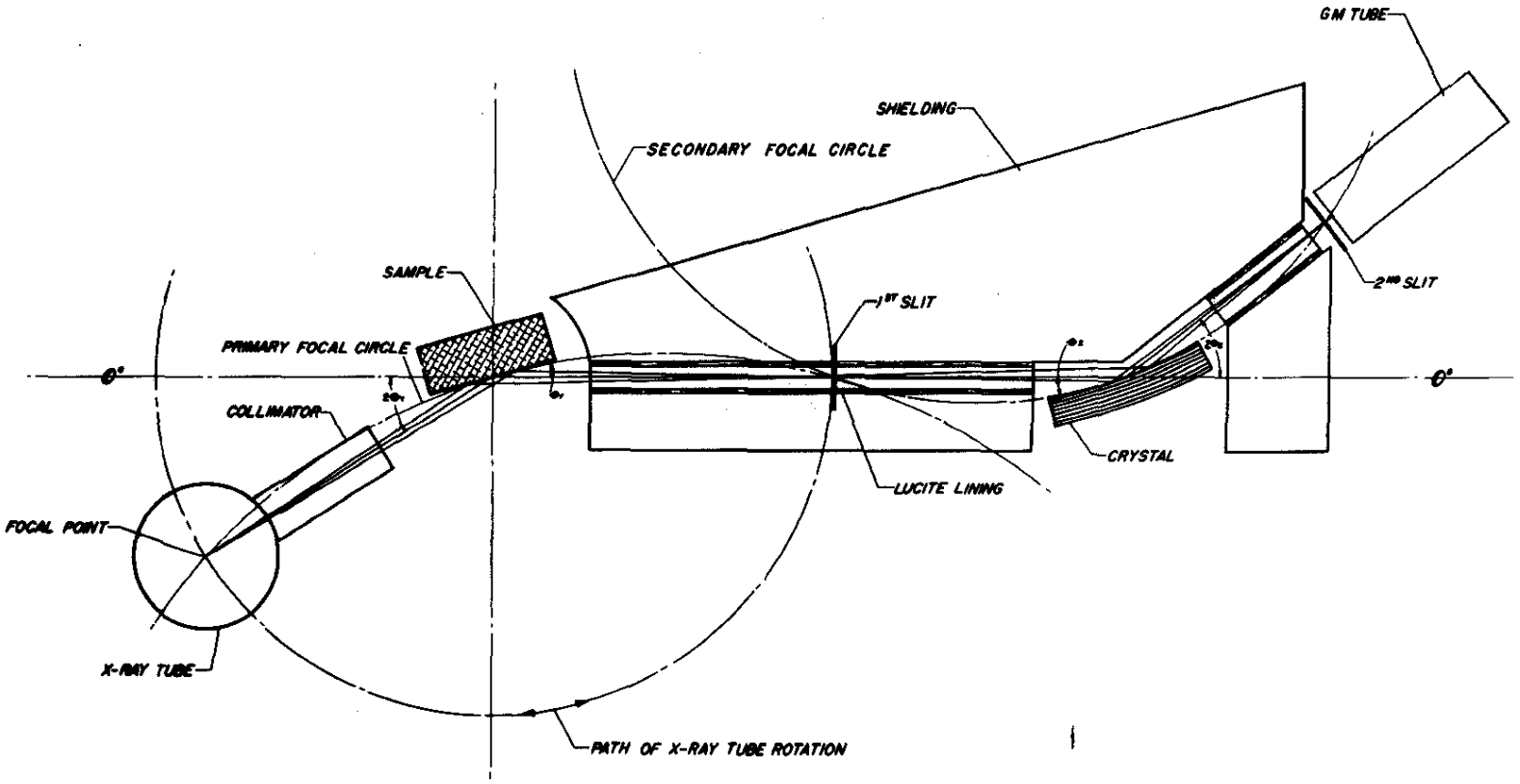

FIG. 1 DOUBLE DIFFRACTION ARRANGEMENT

diffraction patterns of the highly radioactive samples. The goniometer unit was removed from the top of the power console, mounted on a metal plate, and placed on a separate table. A copper target X-ray tube was mounted vertically on the movable ring of the goniometer in place of the detector tube assembly. Due to the large weight of the spectrometer and shielding for the detector tube, the spectrometer unit was mounted stationary. Mounting the X-ray tube vertically was necessary due to the length of the tube housing. A stationary slit, located at the former position of the focal point of the X-ray tube, is the common point on the focal circles of both the diffraction unit and the spectrometer.

The spectrometer consists of the above mentioned slit, a single crystal of aluminum, a second slit, and the proportional counter tube. The two slits and the surface of the aluminum crystal are on the focal circle of the fixed angle spectrometer. A single crystal of aluminum was cut along the (111) plane, ground, and polished on a 12-inch radius and then bent to a 12-inch circle. This combination of grinding and bending produced a focusing crystal with a 6-inch radius. The crystal was aligned at a fixed angle to diffract the characteristic Cu $K\alpha_1$ wavelength from the target of the X-ray tube. The second slit with the proportional counter directly behind it, was placed on the focal circle of the crystal, in position to detect the doubly diffracted X-rays.

Bending the path of the X-rays with the single crystal enabled 10 inches of lead shielding to be placed between the sample and the detector tube. The X-ray beam passes through a channel in the lead shielding. By using a single-channel pulse height analyzer in conjunction with the optic system, a 400 r, irradiated uranium sample produced a background of 40 counts/second. The maximum peaks of uranium metal usually fall in the range of 80 to 200 counts/second with a background count of 2 to 40 counts/second, depending on the level of radioactivity from the irradiated sample.

[Since the above discription was written, the equipment has been modified. The main change was to install a horizontal X-ray tube in place of the vertical tube (Figure 2). The new tube holder houses a Phillips high-intensity X-ray tube. The Phillips tube is smaller than the General Electric tube and will run at 50 kv and 40 ma (the standard G. E. X-ray tube is rated at 50 kv and 16 ma). The new tube has increased the intensity of the diffraction peaks at least 2 fold.]

The double diffracting X-ray equipment has been used for various studies on a number of different materials. These

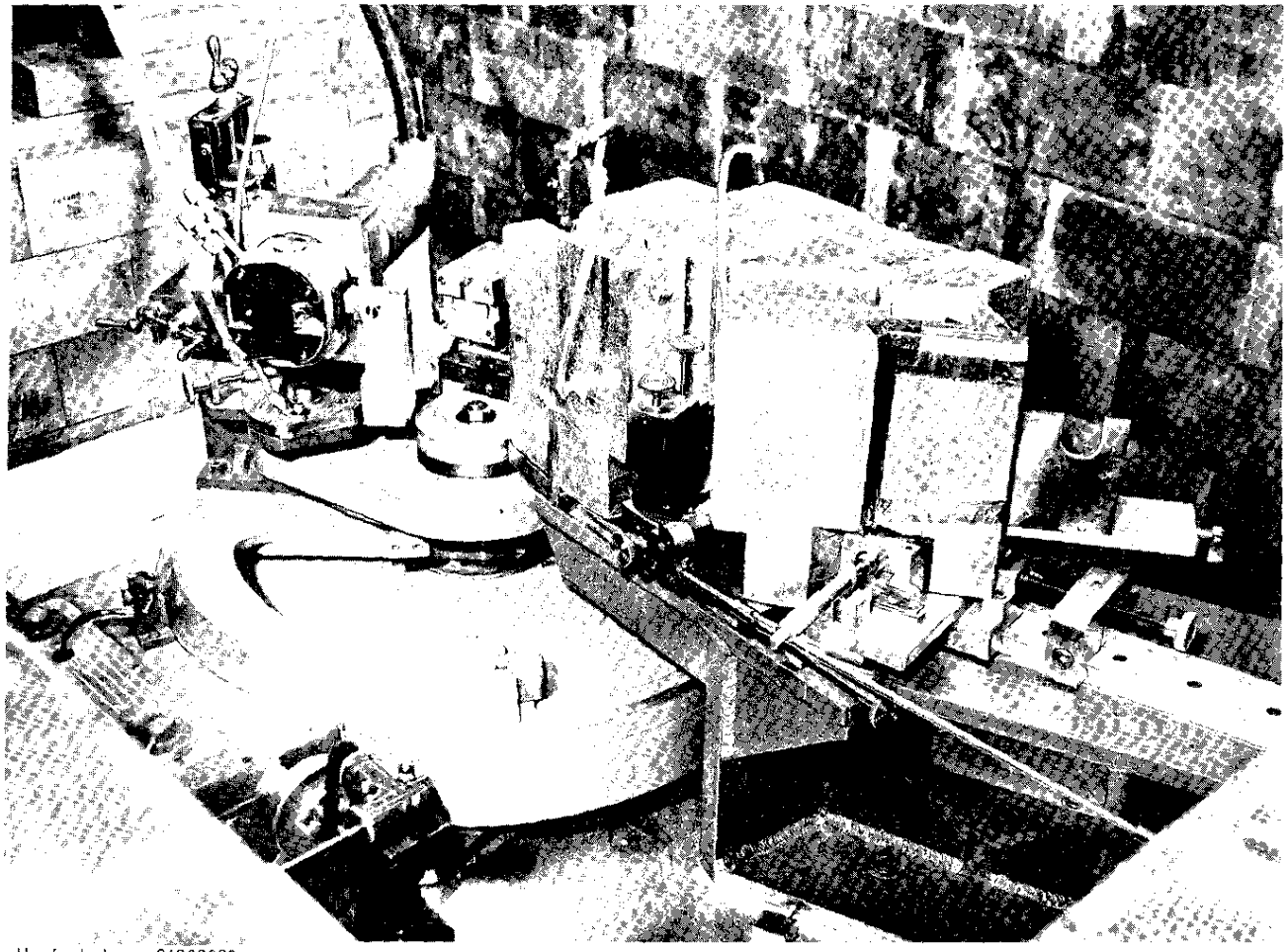

Hanford photo 06308083

FIG. 2 X-RAY DIFFRACTION EQUIPMENT SHOWING HORIZONTAL X-RAY TUBE IN PLACE

studies have included secondary phase identification in uranium dioxide, line broadening, lattice parameter determinations, and preferred orientation studies.

The samples that were studied for preferred orientation were fuel elements that failed during irradiation. Five fuel element failures and a normal fuel element adjacent to a failure were run to determine the grain orientation of the uranium. The sample was cut transversely from the fuel element, and the resulting disk was ground and polished as a normal metallurgical sample. After polishing, the sample was given a deep electrochemical etch to remove the worked metal. The rate of surface oxidation was reduced by giving the sample a light cathodic etch and holding the sample under a vacuum until it was to be run on the diffraction equipment. The sample was positioned in the sample holder and the diffraction data were recorded. In order to obtain an average texture coefficient of the total surface, the sample was rotated 90° in the stationary sample holder between diffraction runs. Four diffraction patterns were averaged to obtain the average texture coefficient for each of the 18 planes studied.

Analysis of the pole figure charts from these samples indicated a slight difference in the degree of orientation between the failed and the nonfailed samples. The orientation of the samples was similar to that for the unirradiated samples.

The results of these determinations are not conclusive at this time. A sufficient number of control samples have not been run to determine what the normal fuel element looks like after irradiation. The future program calls for determining the orientation on more normal, nonfailed fuel elements, to determine the limits of grain orientation in normal irradiated fuel elements. Part of this program will be to compare preirradiation data from small pieces cut from the fuel element with the grain orientation after irradiation. From these studies, we hope to learn what changes in orientation take place during irradiation.

Work performed under Contract No. AT (45-1)-1350 between the U. S. Atomic Energy Commission and the General Electric Co.

INTERSITE EXCHANGE OF TUNGSTEN STANDARD SAMPLES

R. S. Wood, Jr.

E. I. du Pont de Nemours & Co.
Savannah River Plant

SUMMARY

Tungsten diffraction standards were prepared by J. P. LeGeros of the Savannah River Plant for X-ray diffraction and were presented to members of the Preferred Orientation Committee at the December 1961 meeting. Each member was asked to diffract six planes and calculate a standardized value for each plane.

There were wide and statistically significant differences between data from the various sites. Data was tested by the t test, however, and the hypothesis that the data came from the same population is at least 85% correct.

More work in intersite standardization of methods is needed if meaningful intersite exchange of data is to be accomplished.

Editorial Note: An investigation by the editor revealed that the difference among the measurements of the standards at the various laboratories was due to differences in the standards. Even though the standards were chosen from a single section of tungsten it is believed that variations were introduced during the preparation of the standards. The standards were mechanically polished in an identical fashion, but a final electropolish was not used. The point is illustrated in Tables I and II as follows: note in Table I that a great difference exists between values by SRL and SRP for two different standard samples. However, when the SRP standard was measured by SRL (see Table II), the SRP and SRL results were nearly identical.

DISCUSSION

The samples were prepared from 1/4-inch-diameter tungsten welding rods cut into 3/8-inch lengths. Ten sections were mounted per sample and bonded with Koldweld.* The chemical analysis made at the Savannah River Plant indicated approximately pure tungsten with trace amounts of nickel, iron, and silicon. Samples were ground using successively 120, 180, 240, 320, and 600 grit paper, and then polished with 14, 6, and 1/4 micron abrasive on cloth. All samples were polished simultaneously, and approximately 1/16-inch was ground [grinding generally introduces cold work] from the surface to remove effects of cold work. All mounted samples were arranged identically.

Each committee member was requested to diffract the 011, 020, 112, 022, 013, and 123 planes of tungsten. The X-ray diffraction data from each member was submitted to the Savannah River Plant and was standardized for each diffraction run using the following formula:

$$C_{hkl} = \frac{I_{hkl}}{\frac{\Sigma I_{hkl}}{N}}$$

where hkl = Miller Index

I_{hkl} = the intensity

C_{hkl} = standardized value

N = number of planes (6)

This calculation is similar to the texture coefficient calculation used in preferred orientation work. The precision for each plane at the 95% confidence level was calculated from each laboratory using the relation:

$$\text{Precision} = \frac{t_{95}\ \sigma_{hkl}}{\sqrt{NR}}$$

where t_{95} = t value at 95% confidence level

---

* Product of Precision Dental Mfg. Co., Chicago, Ill.

σ_{hkl} = standard deviation

NR = number of diffraction runs

Although 6 planes were diffracted, the data was subsequently modified to exclude the 011 plane because of a coincidence loss encountered by one member during the diffraction of this intense peak. Table I shows the modified data. In the analysis of the data, it was hypothesized that each plane, as diffracted by the various members, was part of the same statistical population. t tests were made using standardized intensity values to determine if this assumption was true. The t tests indicated that the hypothesis was correct 85% of the time. However, when the extremes for any one plane were compared, the differences were so great that intersite exchange of data would be of limited use.

TABLE I

5 Plane Set of X-ray Diffraction Results From Tungsten Standard Samples

hkl	SRP No. 1 10 Runs		Nuclear Metals No. 2 3 Runs		Hanford No. 3 8 Runs		SRL No. 4 8 Runs		MCW No. 5 10 Runs		Bridgeport Brass No. 7 8 Runs		Total Samples 47 Runs		t Test Smallest with $\bar{C}_{hkl}$	t Test Largest with $\bar{C}_{hkl}$
	$\bar{C}_{hkl}$	Prec	$\bar{C}_{hkl}$	Prec	$\bar{C}_{hkl}$	Prec	$\bar{C}_{hkl}$	Prec	$\bar{C}_{hkl}$	Prec	$\bar{C}_{hkl}$	Prec	$\bar{C}_{hkl}$	Prec		
020	0.8368	.0101	0.7891	.0352	0.8825	.0208	1.1153	.0127	1.1056	.0113	0.6730	.0293	0.9182	.0492	1.496	.77
112	1.0897	.0075	1.2265	.1737	0.9850	.0364	0.6738	.0088	0.7472	.0072	1.2329	.0494	0.9613	.0634	1.333	1.259
022	0.6724	.0064	0.6928	.0369	0.9408	.0406	0.9275	.0075	0.8794	.0093	0.7681	.0401	0.8232	.0326	1.357	1.059
013	0.8962	.0064	0.8909	.0943	0.8987	.0254	1.2288	.0075	1.1544	.0623	0.8576	.0338	1.0013	.0448	0.943	1.492
123	1.5047	.0136	1.4026	.0509	1.2928	.0426	1.0545	.0175	1.1134	.0082	1.4683	.0842	1.2960	.0551	1.287	1.112

TABLE II

SRL Diffraction Intensity Measurements
Performed on the SRP Tungsten Standard

hkl	Run 1	Run 2	Run 3	Run 4	Run 5	Run 6	Run 7	Run 8	Run 9	Run 10
200	0.84351	0.84065	0.84324	0.83643	0.84383	0.85120	0.83588	0.83773	0.84187	0.84626
211	1.14186	1.13561	1.14504	1.13869	1.12096	1.13797	1.12844	1.13795	1.12332	1.11926
220	0.61613	0.61802	0.60689	0.62623	0.61680	0.61568	0.61611	0.62068	0.61401	0.61706
310	0.90670	0.90024	0.90295	0.91039	0.91239	0.89581	0.90556	0.90737	0.90987	0.91785
321	1.49177	1.50546	1.50081	1.48821	1.50597	1.49928	1.51395	1.49621	1.51088	1.49950

	SRL Measurements		SRP Measurements for Comparison	
hkl	Average of 10 Runs	Prec	Average of 10 Runs From Table I	Prec
200	0.84206	.00346	0.8368	.0101
211	1.13291	.00657	1.0897	.0075
220	0.61676	.00346	0.6724	.0064
310	0.90691	.00452	0.8962	.0064
321	1.50120	.00579	1.5047	.0136

TECHNIQUES FOR MEASURING TEXTURE GRADIENTS IN TUBULAR URANIUM FUEL ELEMENTS

B. G. LeFevre and E. F. Sturcken

E. I. du Pont de Nemours & Co.
Savannah River Laboratory

INTRODUCTION

It is known that beta treatment of uranium can induce preferred orientation (texture).[1-3] The preferred orientation is believed to be caused by rapid cooling (causing steep thermal gradients and, perhaps, associated stress gradients) through the β - α transformation range. The type of preferred orientation produced has been measured. The grains generally have their "a" crystallographic axis in the direction of the thermal gradient, and the preferred orientation is most severe near the surface[1,3] of the metal, where the cooling rate and temperature gradient are most severe, and diminishes toward the center of the metal. The preferred orientation is of importance because it causes irradiation growth[4] in the fuel elements.

The fact that the preferred orientation changes with depth in the wall of the fuel element poses a special problem for making X-ray diffraction measurements of preferred orientation (PO) and for interpreting the PO in terms of the amount of irradiation growth it will cause. Measurements must be made at a number of depths in the fuel element wall, and a sufficient number of measurements must be made at each depth to overcome the statistical fluctuations in diffraction intensity due to the large grain size of beta-treated uranium. Because of texture gradients and temperature gradients, the strain arising from irradiation growth will be different at different depths in the wall of the tube. The growth will be so complex, that to predict it, it will be necessary to use an empirical approach in which the measured texture gradient will be calibrated against observed irradiation growth.

This report describes the development of techniques for measuring texture gradients and the application of these techniques to the measurement of texture gradients in thick-walled, tubular uranium fuel elements. The sample preparation

techniques are modifications of methods first developed at National Lead Company of Ohio by Morton and Thudium.[5,6]

The tubes studied were 8 inches long x 2.754-inch OD x 0.420-inch wall and 8-inch long x 1.374-inch OD x 0.420-inch wall. The tubes were heat treated by submerging (vertically) in molten 50/50 wt % NaCl/KCl at 730 ±10°C for 8-10 minutes, then transferring within 10 ±2 seconds to "Houghton-K" oil at 55 ±10°C.

SUMMARY

Sampling techniques were developed for measuring preferred orientation gradients in thick-walled tubular elements by X-ray diffraction. The techniques enable texture coefficients and growth indices to be determined for the radial, tangential, and longitudinal directions at various points across the wall of the tube.

The techniques were used to determine texture gradients in beta-heat-treated, oil-quenched uranium fuel elements. The results of the study were as follows:

1. PO measurements across the walls of two large diameter (2.754-inch OD x 0.420-inch wall thickness) and two small diameter (1.374-inch OD x 0.420-inch wall thickness) fuel elements showed that all fuel elements had texture gradients that were most severe on the surfaces of the elements and least severe in the centers of the elements.

2. Contrary to previous conceptions, the texture was not a "skin" effect but varied from the surface to the center of the element.

3. The magnitude of the textures for the elements measured were as follows:

	Growth Index* (G_3)		
	Inner Surface	Center	Outer Surface
Longitudinal	+0.04	0.0	+0.09
Tangential	+0.07	-0.02	+0.13
Radial	-0.07	+0.06	-0.10

* A value of $G_3 = 0.087$ caused a length change of 48.5% for 0.17 atom % burnup in uranium rods irradiated[7] (unrestrained) in NaK capsules. Cladding restraint would reduce this value by a factor of 10 or greater.

4. Textures were generally similar for the tangential and longitudinal directions, probably because these directions have similar thermal gradients during heat treatment.

5. The magnitude of the growth index is generally larger on the outer surface than on the inner surface, probably because of the steeper thermal gradient during transformation.

6. Calculation of thermal expansion coefficient (TEC) gradients from the X-ray data[8] shows that for the tangential and longitudinal directions the TEC is approximately 5 to 10% higher in the center than on the outside of the element, but for the radial direction the TEC is approximately 10% higher on the outside than in the center of the element.

7. Inverse pole figures were constructed to show the types of PO at the center and on the outside surface of the fuel element. The figures show that the outer surfaces of the element have relatively large numbers of (100) plane poles oriented radially and (011), (041), and (010) plane poles oriented tangentially. The center of the element has fairly large numbers of (023) and (041) plane poles oriented radially and large numbers of (100) poles oriented tangentially.

DISCUSSION OF EXPERIMENTAL PROCEDURE

PREPARATION OF X-RAY SPECIMENS

The texture gradients in the fuel elements were measured by using the sampling scheme shown in Figure 1. The machining and mounting techniques are discussed in detail in the Appendix.

For the radial direction, a single composite sample was prepared from thin slices cut from the tube parallel to and "straddling" the radius. To determine the grain orientation as a function of wall thickness of the tube, this sample was examined at different depths from outer surface to inner surface. The radial slices were made thin enough that the maximum deviation of the polished surface from a true radial direction was $\pm 4.5^{\circ}$.

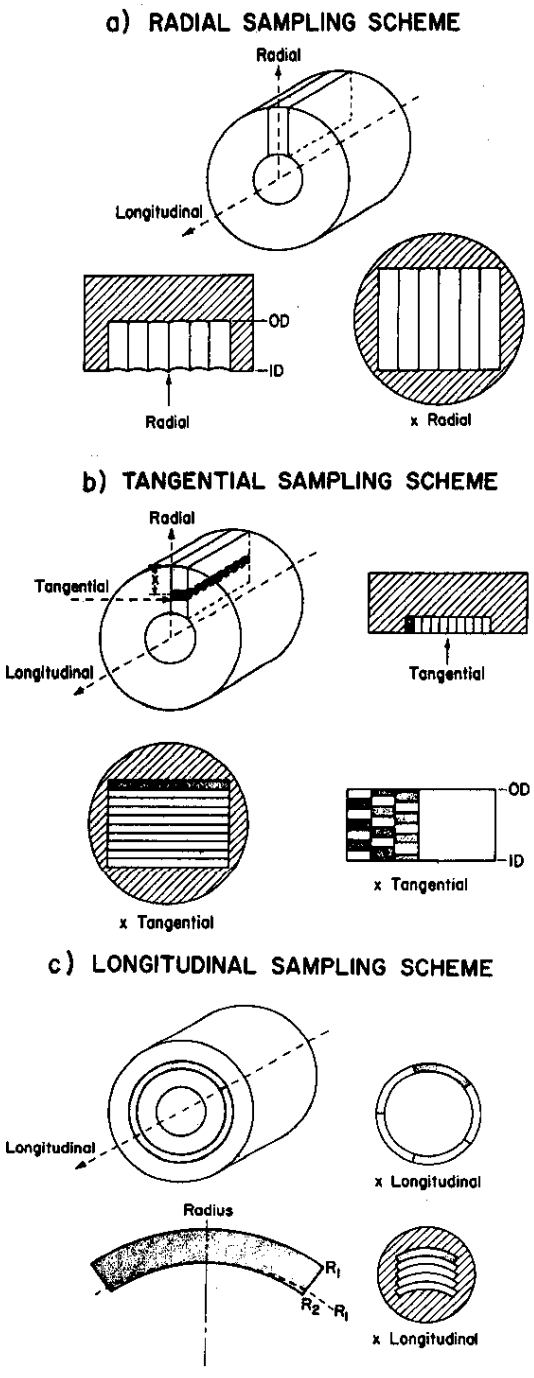

FIG. 1 SAMPLING METHOD FOR MEASURING TEXTURE GRADIENTS

For the tangential direction, a set of ten composite samples was prepared, each sample composed of thin strips taken from a particular depth in the wall of the tube. The strips composing the mounted samples were made 0.060 inch thick, so that each sample represented the average grain orientation of the tube in a tangential direction over a range of ±0.030 inch along the radius.

For the longitudinal direction, a sampling scheme similar to that of the tangential direction was used. Ten samples were prepared, each one composed of ring segments taken from a particular depth in the tube wall and mounted in a longitudinal direction. The rings were 0.060 inch thick, so that each sample represented an average orientation in a longitudinal direction over a range of 0.060 inch along the radius.

X-RAY MEASUREMENTS

The X-ray measurements were made by the techniques described previously[4,9] with a Norelco diffractometer and recording unit. Diffraction peaks of 21 crystallographic planes were studied with Cu Kα radiation.

The samples were placed in a one-inch diameter rotating specimen holder, and the incident X-ray beam was limited to a size of approximately 1/2-inch by 1/2-inch square (at 30° 2θ) at the center of the sample surface. With the sample rotating, an area of approximately 0.3 square inch on the sample surface was illuminated by the beam. The incident beam was collimated by an adjustable slit mounted near the sample, as shown in Figure 2. This method of collimating produced a sharply defined beam of uniform intensity upon the sample.

Several scans, each at a new grain depth, were averaged to obtain a reliable G_3 value for each point. This was necessary, since too few grains are "seen" in a single scan to get statistically significant intensity measurements. For the radial direction the G_3 value at each point was determined by averaging four or six scans, and for the tangential and longitudinal directions three runs were averaged for each point. Between successive runs approximately 0.002 inch of metal was removed by grinding and polishing through #1 diamond dust, and an additional 0.0005 to 0.001 inch was removed by electropolishing in a chromic-acetic acid solution.

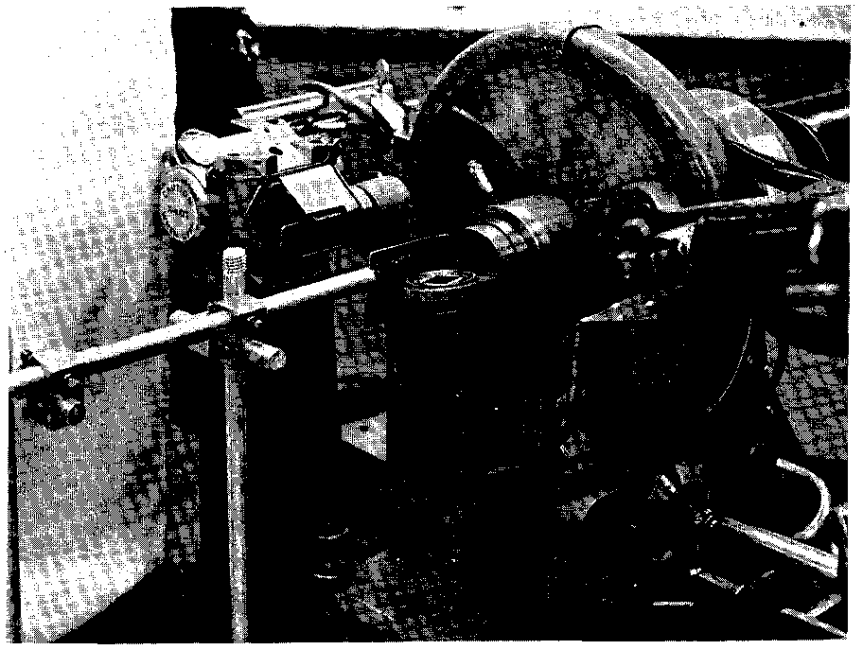

FIG. 2 VIEW OF X-RAY DIFFRACTOMETER SHOWING ADJUSTABLE SLIT MOUNTED NEAR SAMPLE

PRELIMINARY PO MEASUREMENTS

Preliminary measurements were made in the radial direction only on four tubes (two 2.754-inch OD x 0.420-inch wall and two 1.374-inch OD x 0.420-inch wall) by a different specimen preparation technique to get an approximation of the shape of the texture gradient and the number of scans necessary to accurately determine it. This was done by mounting a section of the tube as shown in Figure 3 and making X-ray scans at various depth intervals with the X-ray beam confined to a small area of approximately 0.05 square inch in the center of the sample. This technique has serious limitations for determining texture gradients accurately, since the beam must be limited to a small area in order to hold the direction of interest within a reasonable tolerance. The small beam area results in a large scatter in the data. The advantage of the method is that the specimens are easy to prepare. The technique was used only as a method of obtaining preliminary data quickly. Three to five runs were averaged for a single G_3 value, with approximately 0.003 inch of metal being removed by polishing between successive runs.

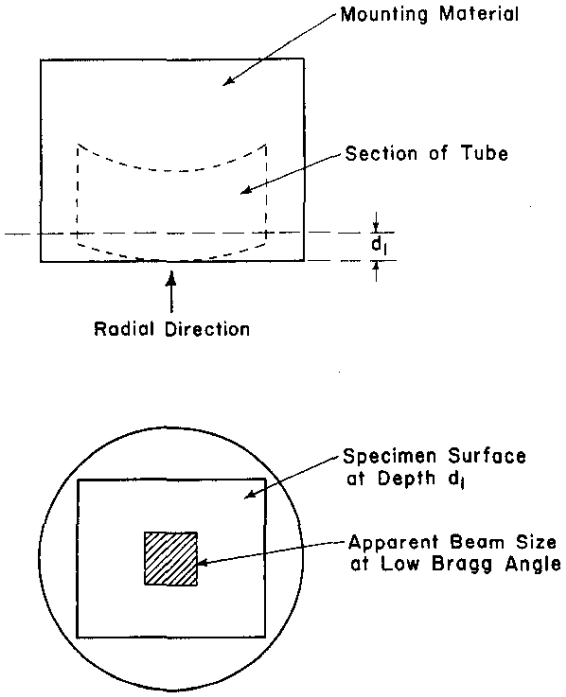

FIG. 3 TECHNIQUE FOR MAKING PRELIMINARY TEXTURE GRADIENT MEASUREMENTS IN RADIAL DIRECTION OF FUEL ELEMENT

LIMITATIONS

Certain errors are inherent in the problem of measuring texture gradients in tubular elements because of the finite thicknesses of the pieces that go into the composite samples (Figure 1). These deviations from the ideal case can be minimized, but not completely eliminated, since the pieces must be machined to some practical size.

For a radial sample the direction being studied at any point deviates from a true radial direction by as much as ± arctan T/2R, where T is the thickness of the strips composing the sample, and R is the perpendicular distance from the center of the tube to the specimen surface. If the strips are made 1/8 inch thick, the maximum deviation for a 2.754-inch OD x 0.420-inch wall element is ±4.5 degrees at the inner radius of the tube.

For tangential and longitudinal samples, each X-ray measurement represents the average grain orientation over an interval of T inches along the radius, where T is the thickness of the strips (or ring segments) composing the sample. For this reason the pieces would have to be made very small in order to detect sharp changes in orientation.

RESULTS

GROWTH INDEX MEASUREMENTS

Figure 4 shows how G_3 varies as a function of wall thickness for the radial, tangential, and longitudinal directions of the 2.754-inch-OD x 0.420-inch-wall-thickness tube that was studied in detail. The vertical spread on each point represents the extreme values in the group that were averaged, and the vertical dotted lines represent the inner and outer walls of a fuel element machined to cladding dimensions.

The curves in Figure 4 show that the grain orientation varies smoothly and continuously across the wall of the tube. The curves are approximately symmetrical about the center of the wall, as would be expected if the texture gradient is dependent upon the thermal gradient during quenching from the beta phase, as it is reported to be.[1] For each direction, the G_3 value near the OD is greater in magnitude than that near the ID. This is consistent with the fact that during quenching the thermal gradient is greater near the outer surface than the inner surface. It is also consistent with the observation that during irradiation the OD changes more than the ID.

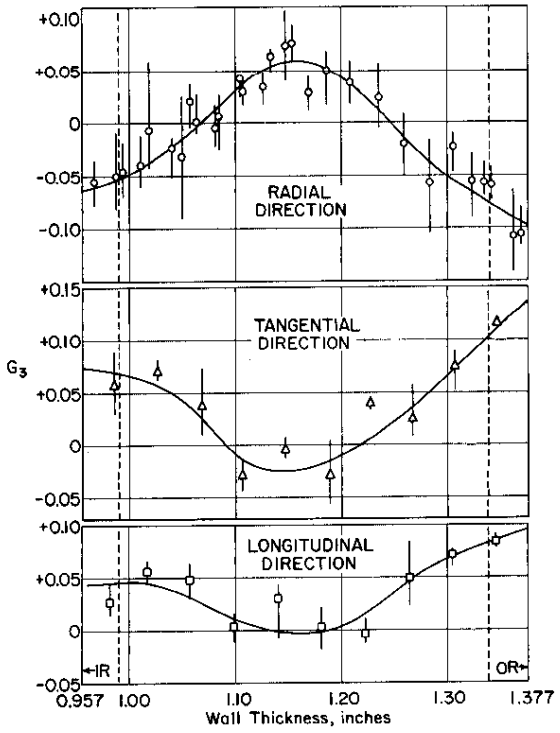

FIG. 4 GROWTH INDEX, G_3, VS WALL THICKNESS IN BETA-TREATED OIL-QUENCHED TUBE. Alloy composition: 534 ppm C, 28 ppm Si, 15 ppm Al, 117 ppm Fe. (Identification No. 92770B-17)

The preliminary measurements made on the four oil-quenched fuel elements in the radial direction indicate that similar texture gradients exist in all of the elements (Figures 5 and 6); however, detailed examination in three directions was not made for each one. Because of the large scatter in the preliminary data no attempt was made to draw curves through the points.

RELATION OF TEXTURE GRADIENTS TO IRRADIATION GROWTH OF FUEL ELEMENTS

It is very difficult to predict the type of growth which will result from the observed texture gradients. Each incremental annulus of the tube has a different growth index and operates at a different irradiation temperature and with different restraining stresses. Since growth is temperature dependent,[10] for a given growth index, the growth will be highest for the lowest temperature and lowest for the highest temperature. Each annulus will be restrained and will interact with its neighboring annuli. The varying temperature of the metal will cause it to be strongest on its coolest annuli and weakest on its hottest annuli. The varying TEC will introduce additional complexity. Considering only the texture gradient, the general "tendencies" for growth are shown schematically in Figure 7. The wall of the tube may be divided into three regions each having roughly the same thickness: annuli near the outer and inner surfaces which tend to shrink radially and grow tangentially, and a center annulus which tends to grow radially and shrink tangentially. Quantitative prediction of growth will require some irradiation tests of tubes with measured texture gradients.

INVERSE POLE FIGURES FOR URANIUM TUBES

The type of texture present in each of these regions is shown by inverse pole figures in Figure 8. The outer annuli have a high concentration of (100) plane poles oriented in the radial direction and high concentrations of (010), (041), and (011) plane poles oriented in the tangential direction. This leads to a negative radial G_3 and a positive tangential G_3. In the center annulus there is a fairly high concentration of (023) and (041) poles, together with an absence of (100) and (10ℓ) type poles in the radial direction, which leads to a positive radial G_3. This high concentration of (100) poles oriented tangentially in this region gives a negative tangential G_3.

THERMAL EXPANSION COEFFICIENT GRADIENT

The same grain orientation data that are used to calculate G_3 may also be used to calculate the thermal expansion coefficient[8,11] (α_N) of the sample.

Curves showing how α_N varies as a function of wall thickness for the radial, tangential, and longitudinal directions are shown in Figure 9. For each direction the α_N curve looks like an inverted G_3 curve, with the vertical axis different, however; again the slight asymmetry between the inner and outer surfaces is present. The maximum variation of α_N across the wall is approximately 10% for the radial direction, 10% for the tangential direction, and 5% for the longitudinal direction. Thermal expansion coefficients were also calculated from the preliminary radial data that were gathered, and curves are shown in Figures 10 and 11.

The thermal expansion coefficients are averaged over the temperature range of 27 to 300°C. Strictly speaking the expansion coefficients should be evaluated at each temperature interval across the fuel element. However, the present results are intended to be only qualitative in nature.

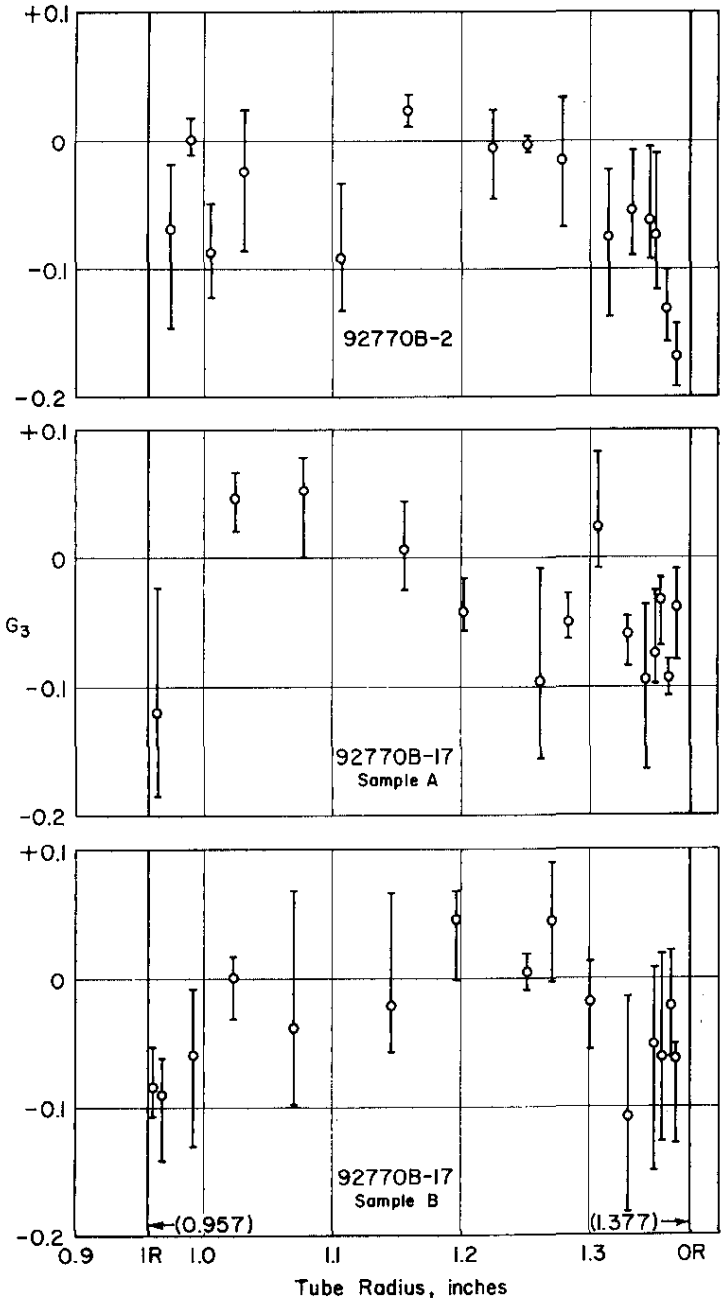

FIG. 5 G_3 VS WALL THICKNESS FOR RADIAL DIRECTION OF URANIUM TUBES (2.754" OD X 0.420" WALL THICKNESS)

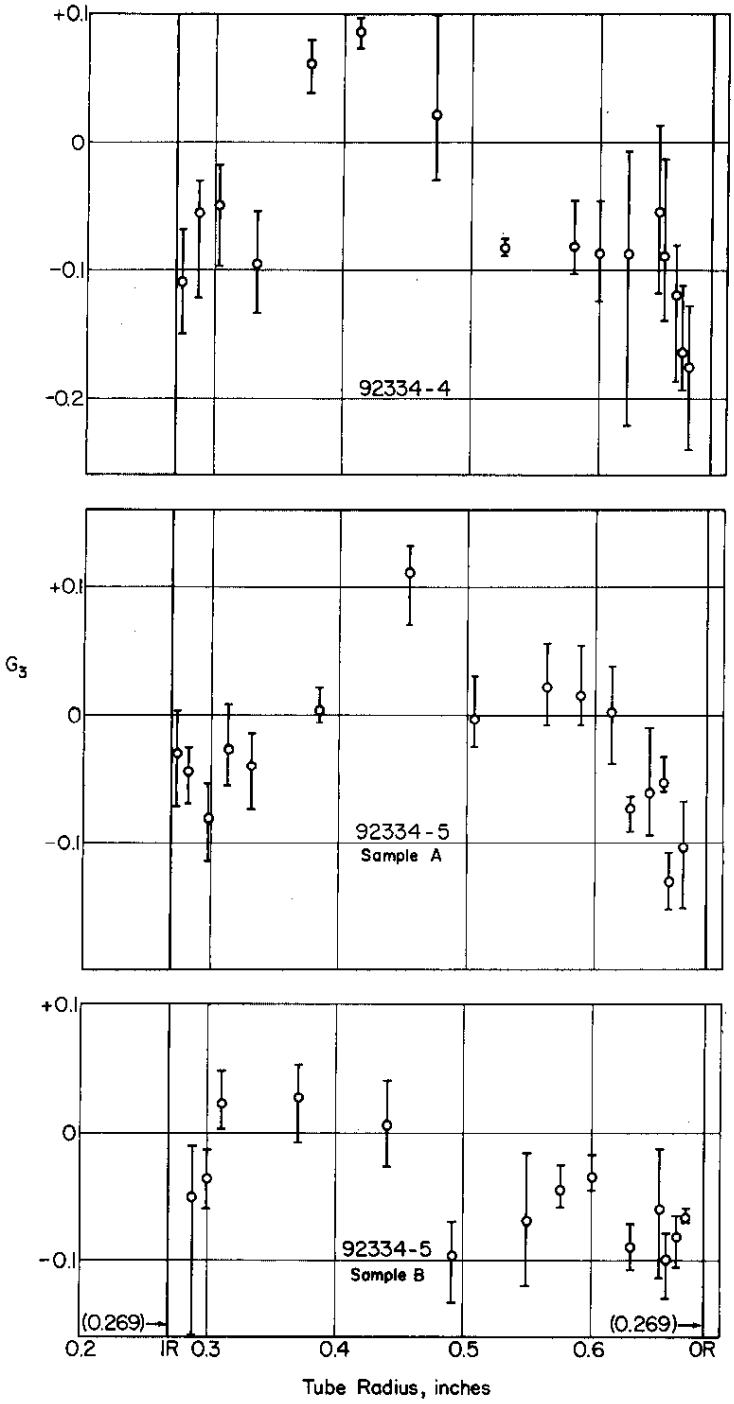

FIG. 6 G_3 VS WALL THICKNESS FOR RADIAL DIRECTION OF URANIUM TUBES (1.374" OD X 0.420" WALL THICKNESS)

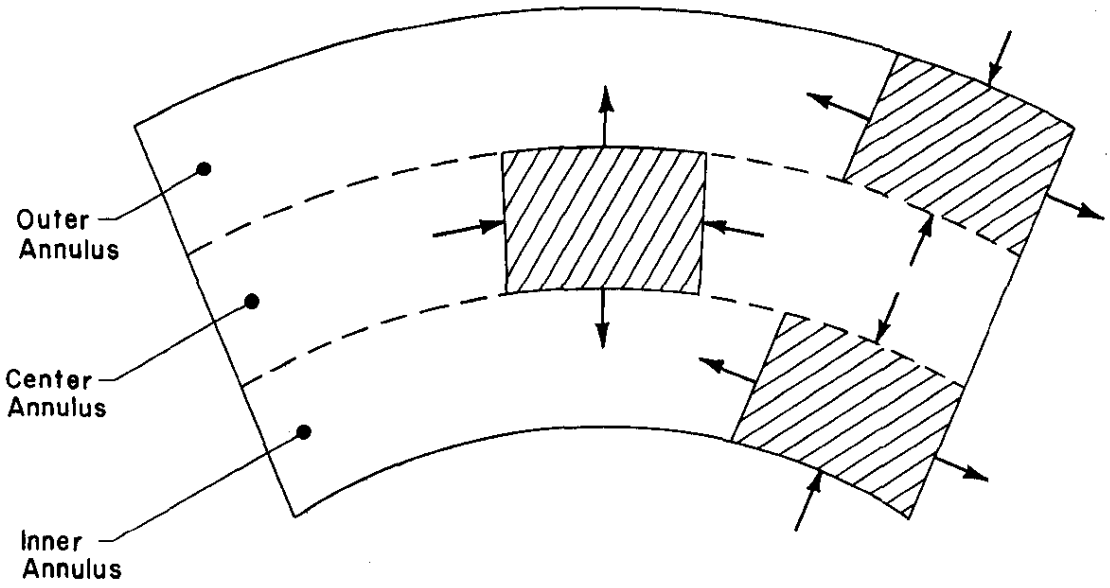

FIG. 7 GENERAL GROWTH TENDENCIES FOR BETA-TREATED OIL-QUENCHED TUBES. The arrows indicate only the directions of the growth tendencies and not the magnitudes.

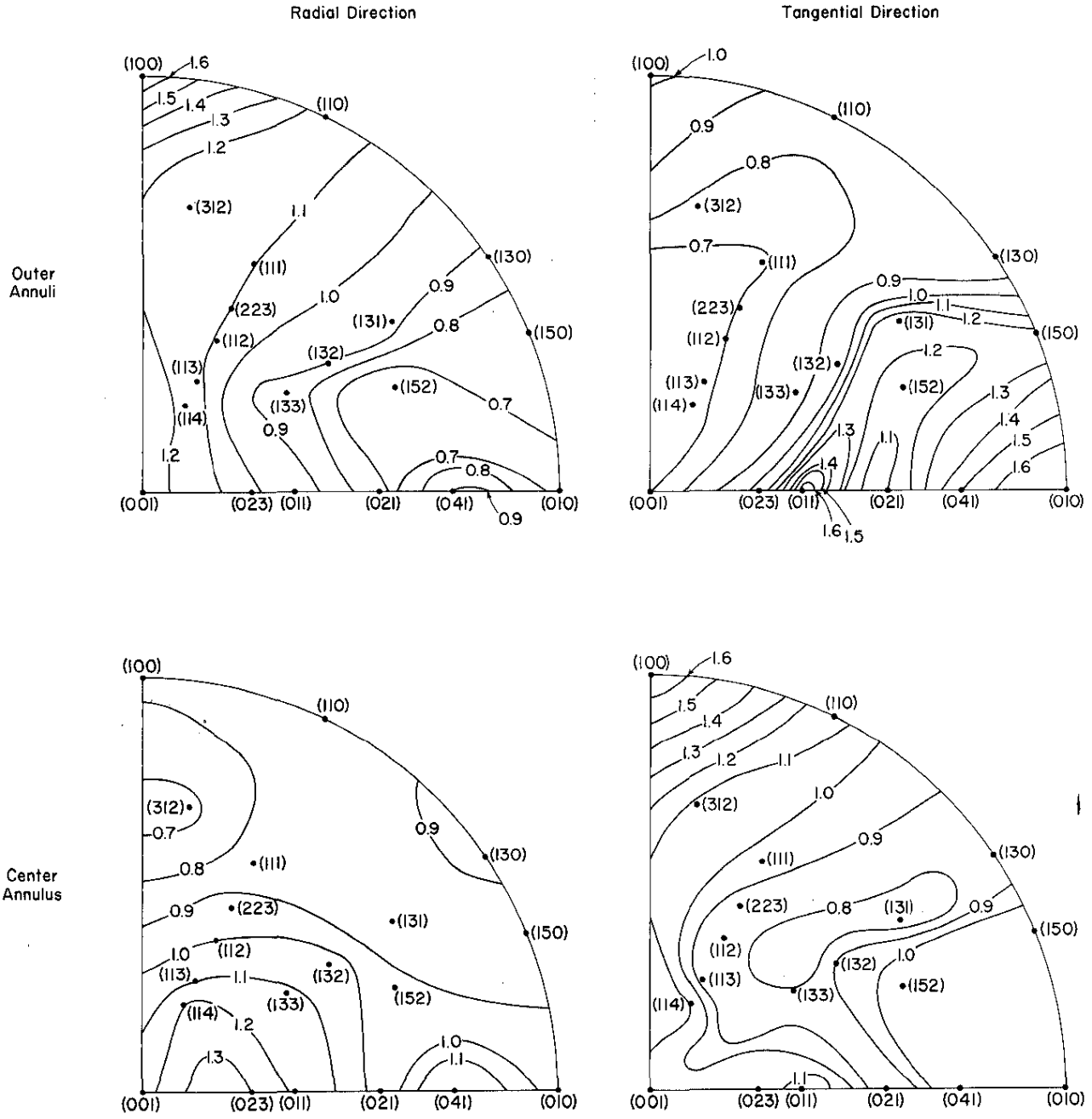

FIG. 8 INVERSE POLE FIGURES SHOWING TYPE OF PREFERRED ORENTATION IN BETA-TREATED, OIL-QUENCHED URANIUM TUBES

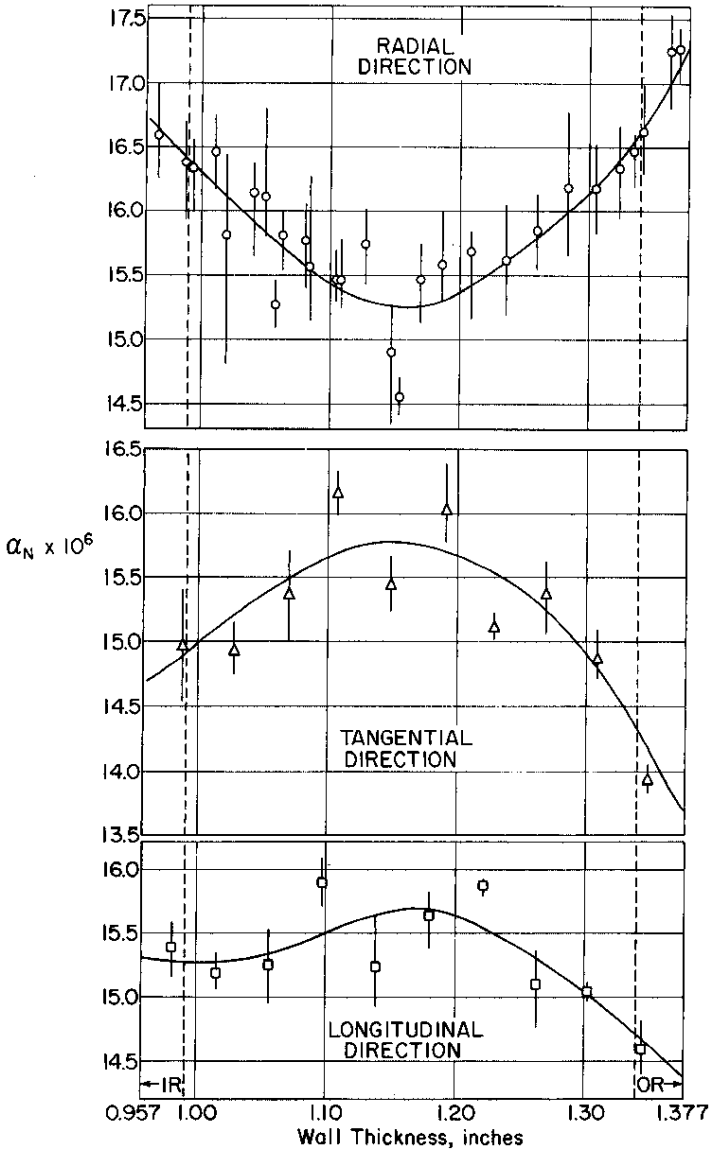

FIG. 9 THERMAL EXPANSION COEFFICIENTS VS WALL THICKNESS IN BETA-TREATED OIL-QUENCHED TUBE. Coefficients were calculated using the equation in Reference 11 and the single crystal thermal expansion coefficients for uranium that were measured by Lloyd[12]. Alloy composition: 534 ppm C, 28 ppm Si, 15 ppm Al, 117 ppm Fe (Identification No. 92770B-17)

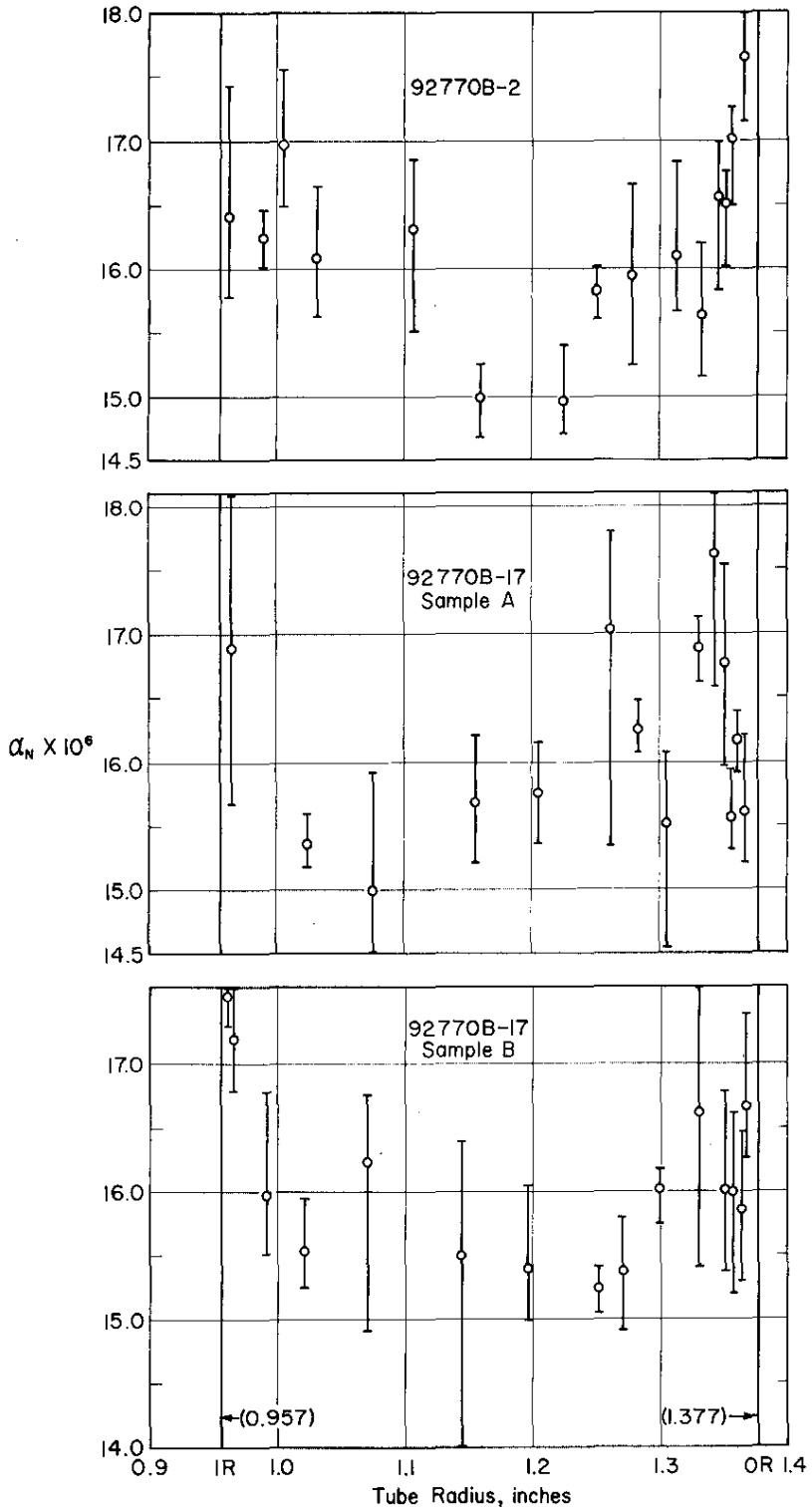

FIG. 10 α_N VS WALL THICKNESS FOR RADIAL DIRECTION OF URANIUM TUBES (2.754" OD X 0.420" WALL THICKNESS)

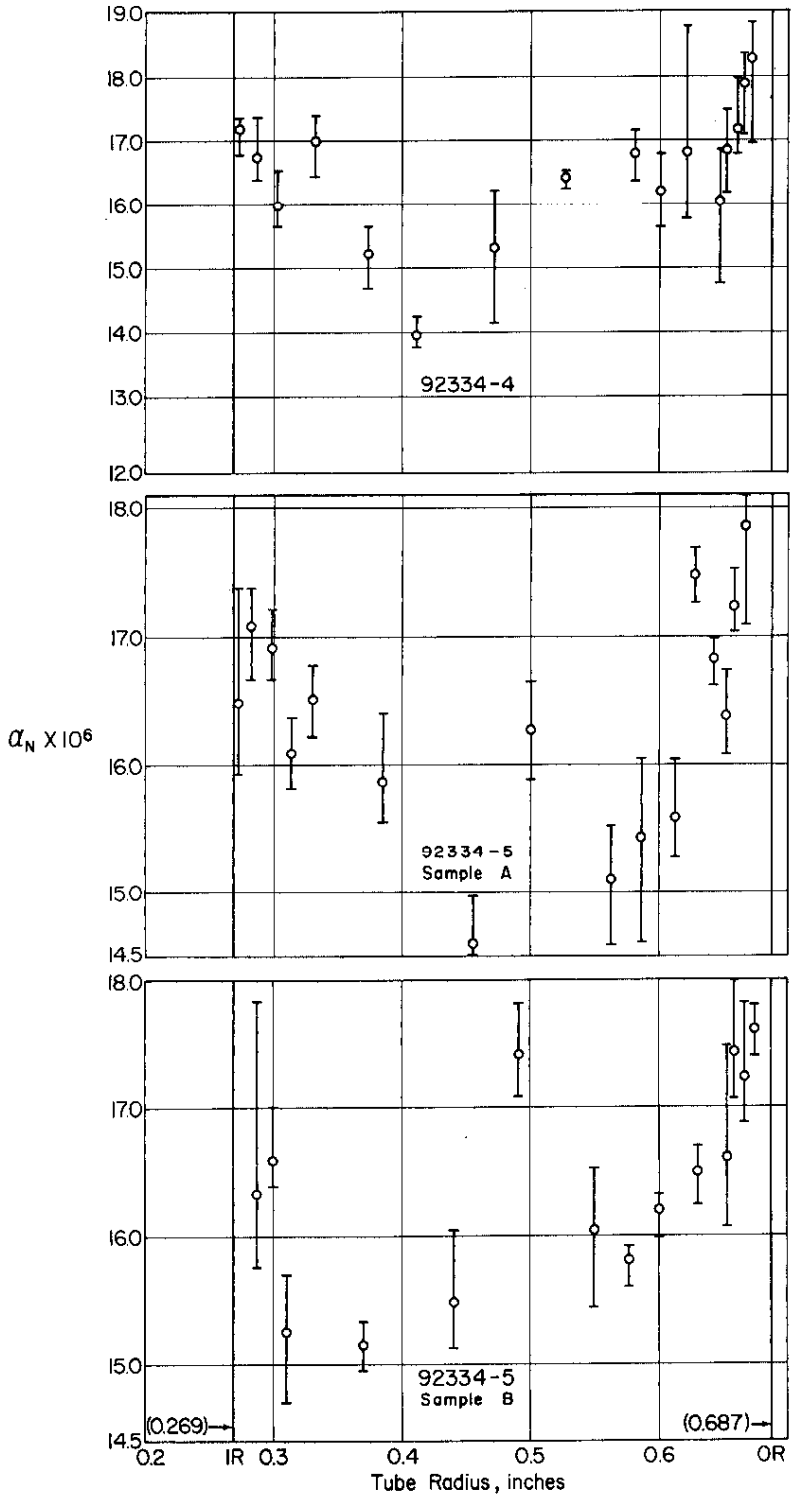

FIG. 11 α_N VS WALL THICKNESS FOR RADIAL DIRECTION OF URANIUM TUBES (1.374" OD X 0.420" WALL THICKNESS)

APPENDIX

PREPARATION OF SPECIMENS FOR TEXTURE GRADIENT MEASUREMENTS

Machining of Samples

RADIAL SAMPLES

Sampling Scheme

Figure 1a shows the sampling scheme used for the radial direction. Longitudinal strips are cut from a section of the tube straddling the radius. Several of these strips are then mounted together to give a composite sample. To measure the radial texture gradient as a function of radial position, the sample is then ground perpendicular to the radius, and X-ray scans are made in whatever increments are necessary to give the desired number of points.

Machining Technique

General Description. The radial strips described above are cut on a milling machine in the manner shown in Figure 12. A section of the tube is cut off and placed on a steel mandrel, and the strips are cut by "straddle milling"; the cutters are held apart the correct distance by steel spacers. The cuts are made completely through the wall of the tube in one pass. On specimens prepared from large diameter tubes, 1/16-inch carbide slitting saws were used at a speed of 43 rpm and 1/4-inch/minute feed. These machining variables, i.e., cutters and speeds, are important since reasonable tolerances are difficult to hold if different cutters and/or speeds are used. If the strips are made 1/8 inch thick, sixteen of them can be machined from a section of a 2.754-inch OD x 0.420-inch-wall tube.

Mandrel. A steel mandrel is used to hold the material during machining. It is shown in detail in Figure 12. The central shaft of the mandrel fits snug against the inner wall of the tube, and the lock nut on the end holds the ring firmly, so that the cuts can be made completely through the wall of the tube without any slippage or misalignment of the piece being cut. The grooves in the mandrel are precut by the machinist to help guide the cutters.

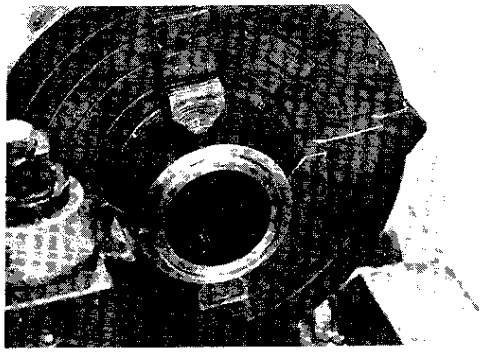

Lathe Cutting the Ring

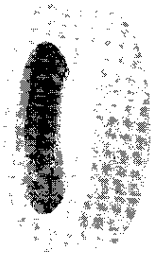

Ring

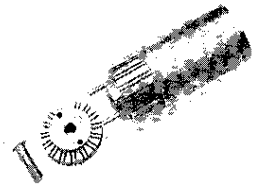

Mandrel for Mounting Ring

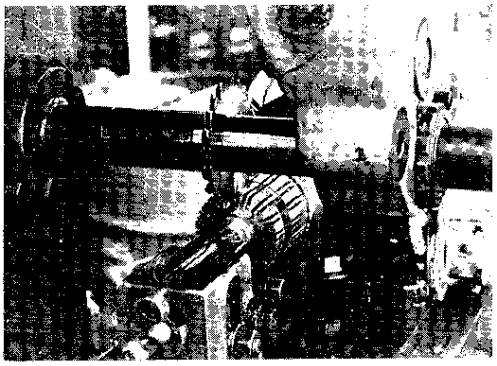

Straddle Milling Radial Strips

FIG. 12 METHOD USED TO MACHINE RADIAL SECTIONS
(see also Figure 1a)

TANGENTIAL SAMPLES

Sampling Scheme

Figure 1b shows the method used to make tangential samples. Note that a series of composite samples are made, each representing a certain point along the radius of the tube. A section of the tube is first cut into strips similar to those of the radial samples, except that one surface is along a true radius, rather than simply parallel to a radius. These pieces are then cut into strips 60 mils wide and mounted together with the true tangential surface exposed as shown. Each of the pieces in a single sample is taken from the same point, x, along the radius. In order to measure the preferred orientation at ten points along the wall of the fuel element, it would be necessary to stagger the smaller strips in the manner shown in Figure 1b.

Machining Technique

General Description. To machine the larger strips a straddle-milling method identical to that of the radial scheme is used, except that the cuts are made along a true radius rather than astraddle of it. To cut the smaller strips a milling machine is used in the manner shown in Figure 13. One-sixteenth-inch carbide cutters, with 43 rpm and 1/4-inch table feed, are used in both operations.

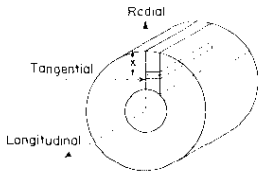

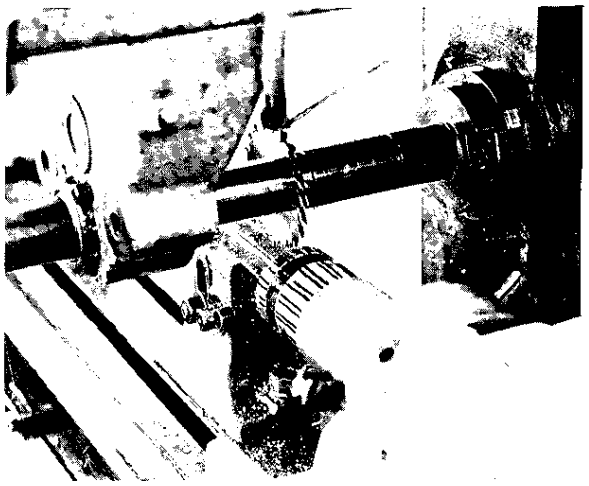

Straddle Milling Radial Strips

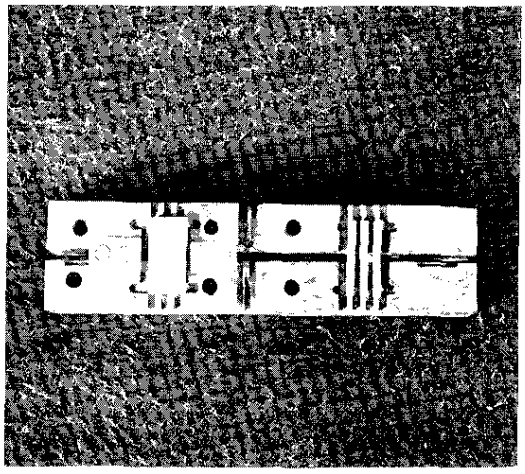

Mount for Cutting Strips into Smaller Segments from OD to ID

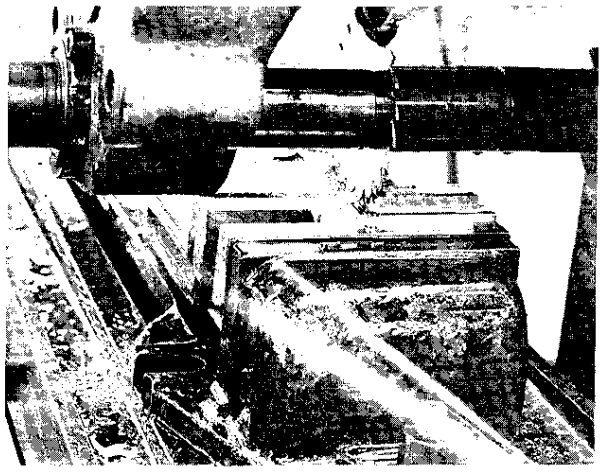

Milling Small Segments from OD to ID

FIG. 13 METHOD USED TO MACHINE TANGENTIAL SPECIMENS

Mandrel and Holder. The mandrel used in cutting the larger tangential pieces is identical in nature to the one used for machining radial strips. A brass holder is used for cutting the smaller strips and is shown in detail in Figure 13.

LONGITUDINAL SAMPLES

Sampling Scheme

The sampling scheme used for the longitudinal direction is shown in Figure 1c. The method is similar to that of the tangential in that a series of composite samples are made, each representing a certain point along the radius of the tube; however, instead of cutting strips from flat sections, a series of concentric rings 60 mils thick are cut from the tube, and the rings are cut into segments. The segments from a given ring are then mounted together into one sample representing a single point along the radius of the tube. The inner radii of the segments are changed as shown in Figure 1c to make them fit more snugly in the composite sample.

Machining Techniques

The machining of the concentric rings is done on a lathe, Figure 14. The rings are cut into segments using an aluminum mandrel on a milling machine (Figure 14). Thin slitting saws, 20-mils thick, may be used here to save material, since the rings are thin and the direction of the cuts not too critical. The segments are "radiused" on a lathe by the method shown in Figure 14. Emery paper is glued to a shaft with the same radius as that desired, allowing for the thickness of the paper. A shaft is necessary for each size ring; however, "Micarta,"* which is cheap and easily machined, may be used, and turned down to smaller diameters as the work progresses to smaller rings.

Mounting of Samples

REMOVAL OF COLD WORK

Before the machined pieces are grouped and mounted into composite samples, whether for the radial, tangential, or longitudinal direction, it is necessary to remove the cold-worked layers on the lateral surfaces, i.e., the surfaces perpendicular to the surface being scanned. These cold-worked layers are produced by the machining process, and it was determined by observing the triplet on several machined samples that a cold-worked layer as deep as 3 mils is produced by the carbide slitting saws (a lesser amount is produced by the lathe and by grinding). If the pieces composing the sample are only 60 mils in width, the cold-worked material then composes as much as 10% of the total area being scanned.

* Trademark of Westinghouse Electric Corp.

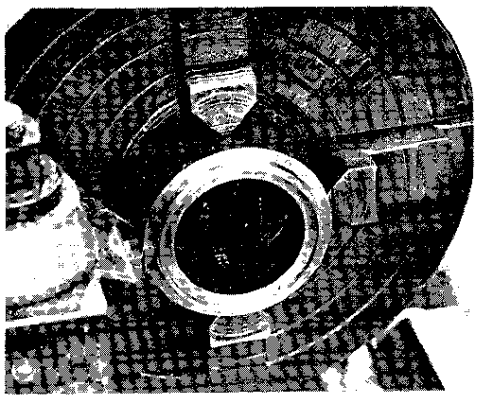

Turning Rings in the Lathe

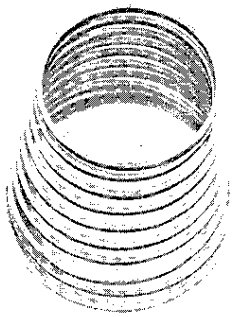

Rings of Various Diameters

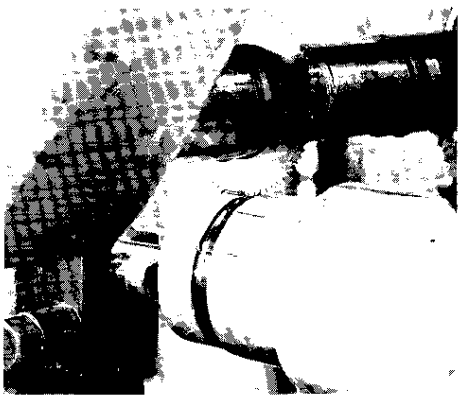

Milling the Segments from the Rings

Radiusing the Inner Surface of the Rings to Make Them Fit Snugly in the Composite Sample

FIG. 14 METHOD USED TO MACHINE LONGITUDINAL SECTIONS

It is therefore necessary to remove about 4 mils from each of these surfaces. On the radial pieces it can be removed by grinding and electropolishing, but on the longitudinal and tangential pieces it is best done by electropolishing alone, since these pieces are very small.

MOUNTING TECHNIQUES

The X-ray samples are mounted in a clear epoxy resin, or some similar material that is not attacked by the electropolish solution and does not give diffraction spectra. The pieces are placed together on a flat, machined block inside a one-inch-diameter ring, with the viewing surface down (Figure 15a). Care must be taken to see that the pieces fit together tightly to eliminate voids and that they are not tilted. A conducting silver paint is spread over the

back of the sample to ensure good electrical contact between all pieces for the electropolishing operation. Typical radial, tangential, and longitudinal samples are shown in Figure 15b.

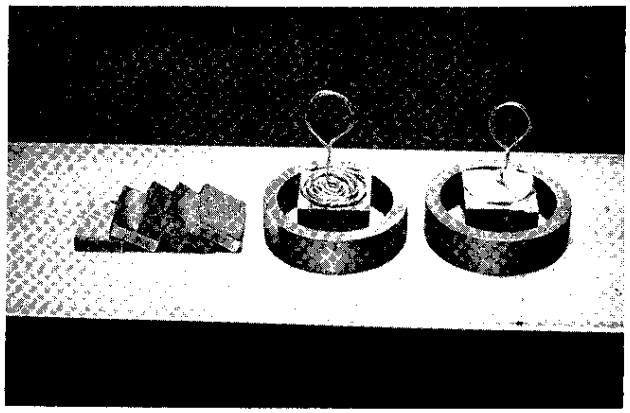

a. Method used for Mounting Radial, Tangential, and Longitudinal Pieces into Composite Samples.

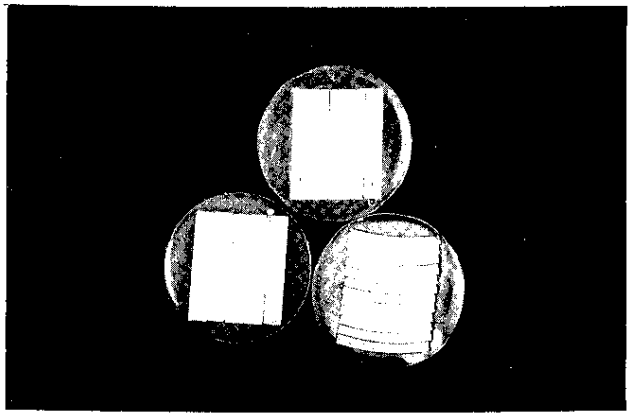

b. Typical Radial, Tangential, and Longitudinal Specimens after Mounting

FIG. 15 MOUNTING TECHNIQUE FOR X-RAY SPECIMENS

MATERIAL USED

In preparing samples from the 2.754-inch-OD x 0.420-inch-wall tube the composite samples are made large enough to completely contain a rectangular X-ray beam approximately 0.6 inch on the diagonal, as the sample is rotated. To accomplish this, the radial sample may be composed of five strips, 1/8 inch thick; the tangential samples, of twelve strips, 60 mils thick; and the longitudinal samples, of twelve ring segments, 60 mils thick.

The preparation of one radial sample, ten tangential samples (determines texture at ten points), and ten longitudinal samples requires approximately a five-inch length of an outer fuel tube.

ACKNOWLEDGMENT

In addition to the references given, the authors wish to acknowledge published articles of restricted distribution by O. K. Shupe, W. T. Kattner, and J. C. Bokros. These were the earliest known references that reported that certain kinds of heat treatments induce preferred orientation in uranium.

REFERENCES

1. Kornfeld, R. "Structures of Beta-Quenched Uranium". Process Development Quarterly Report. Part II. Pilot Plant Work. J. U. Shepardson and J. A. Nelson, Eds. Mallinckrodt Chemical Works, St. Louis, Missouri. USAEC Report MCW-1429 (Del.), pp. 145-156 (1959).

2. Chiswik, H. H. and L. T. Lloyd. Some Aspects of the Beta to Alpha Transformation in Uranium: Metallographic Structure and Orientation Relationships. Argonne National Laboratory, Lemont, Ill. USAEC Report ANL-5777 (1959).

3. Russell, R. B. and A. K. Wolff. Summary Report of the Study of Beta Treatment of Uranium. Nuclear Metals, Inc., West Concord, Mass. USAEC Report NMI-2807 (1963).

4. Sturcken, E. F. and W. R. McDonell. "An X-Ray Method for Predicting Anistropic Irradiation Growth in Uranium". J. Nucl. Mater. 7, No. 1, 85-91 (1962).

5. Morton, V. and R. N. Thudium. "Texture Gradients in Uranium Fuel Cores", Papers and Proceedings of the X-Ray Preferred Orientation Meeting Held at HAPO, June 29 and 30, 1961. W. Gary Jolley, Ed. General Electric Co., Hanford Atomic Products Operation, Richland, Wash. USAEC Report HW-74429, pp. 14-25 (1962).

6. Morton, V., R. N. Thudium, N. Crank, Jr., and C. A. Powell. "Texture Gradients in Oil Quenched, Mark VB Outer Fuel Cores", Papers Presented at the X-Ray Preferred Orientation Meeting at Savannah River Laboratory, June 7, 8, 1962. E. F. Sturcken, Ed. E. I. du Pont de Nemours & Co., Savannah River Laboratory, Aiken, S. C. USAEC Report DP-904 (1964).

7. Sturcken, E. F., B. G. LeFevre, and W. R. McDonell. "Anistropic Growth vs. Preferred Orientation in Unrestrained Uranium", Papers Presented at the X-Ray Preferred Orientation Meeting Held at Nuclear Metals, Inc., December 7-8, 1961. R. B. Russell, Comp. Nuclear Metals, Inc., West Concord, Mass. USAEC Report NMI-4992, pp. 18-42 (1963).

8. Sturcken, E. F. "Prediction of Thermal Expansion Coefficients by the Growth Index Method", Papers Presented at the X-Ray Preferred Orientation Meeting at Savannah River Laboratory, June 7, 8, 1962. E. F. Sturcken, Ed. E. I. du Pont de Nemours & Co., Savannah River Laboratory, Aiken, S. C. USAEC Report DP-904 (1964).

9. Sturcken, E. F. "The Use of Powder Reflection Intensities to Predict Physical Properties in Oriented Materials". Norelco Reporter XI, No. 1, 24-28, 43 (1964).

10. Buckley, S. N. Irradiation Growth. United Kingdom Atomic Energy Authority Research Group, Atomic Energy Research Establishment, Harwell, Berkshire, England, Report AERE-R-3674 (1961).

11. Sturcken, E. F. and J. W. Croach. "Predicting Physical Properties in Oriented Metals". Trans. AIME 227, 934 (1963).

12. Lloyd, L. T. Thermal Expansion of Alpha-Uranium Single Crystals. Argonne National Laboratory, Lemont, Ill. USAEC Report ANL-5972 (1959).

DETERMINATION OF GRAIN SIZE IN URANIUM FROM STATISTICAL FLUCTUATIONS IN X-RAY DIFFRACTION INTENSITY

E. F. Sturcken and W. E. Gettys

E. I. du Pont de Nemours & Co.
Savannah River Laboratory

INTRODUCTION

An X-ray technique was developed by Warren[1] for determining grain size from measurements of statistical fluctuations in X-ray diffraction intensity. Warren's equation for grain size was modified by Sturcken and Gettys[2] to make it valid for materials with high absorption coefficients and/or large grain size.* The modified equation is:

$$\langle D^2 \rangle = \frac{jA_o \Omega r \gamma}{\pi^2 \sin \theta} \quad \frac{\langle (Y-\overline{Y})^2 \rangle}{\overline{Y}^2} \qquad (1)$$

where $\langle D^2 \rangle$ is the average squared grain diameter, j is the multiplicity of the diffraction peak, A_o is the X-ray beam area, Ω is the solid angle containing the plane normals that contribute to the diffraction peak, Y is the number of counts from any one sample position, $\overline{Y}$ is the average number of counts, θ is the Bragg Angle, $r = \rho'/\rho$ = relative density of the sample, ρ' = density of the sample, ρ = density of a crystal ($\rho = \rho'$ for a metal and $r = 1$). If there is preferred orientation in the sample, the integrated intensity of the peak is γ times what it would have been for random orientation.

The modified equation was tested in the present report by applying it to grain size measurements of beta quenched and annealed uranium.

* In these cases the penetration of the X-ray beam is smaller than the grain dimensions.

SUMMARY

The modified grain size equation was tested for quench-annealed uranium. Values calculated from equation 1 using the X-ray statistical fluctuation method agreed well with metallographic measurements on the same sample. Hence, it is concluded that equation 1 is correct for application to materials where the X-ray beam penetrates less than one grain depth.

The grain diameter, $\langle D^2 \rangle^{\frac{1}{2}}$, obtained from the X-ray measurements was found to depend on the solid angle, and varied from $\langle D^2 \rangle^{\frac{1}{2}} = 42$ to $\langle D^2 \rangle^{\frac{1}{2}} = 83$ microns for solid angles ranging from $\Omega = 1.25 \times 10^{-3}$ to $\Omega = 10.8 \times 10^{-3}$. The dependence of $\langle D^2 \rangle^{\frac{1}{2}}$ on Ω is primarily due to substructure within the grains and is due to a lesser extent to divergence and defocusing of the X-ray beam. (The grain size equation was derived for a perfectly parallel beam.)

A metallographic grain size distribution analysis of 463 grains yielded a grain diameter of 108 microns with 68% of them in the range 53 to 142 microns.

The agreement between the X-ray and metallographic measurements is excellent considering the limited resolution of the metallograph and the defocusing and divergence errors in the X-ray measurements.

In addition to its application to grain size measurements, equation 1 above is also valuable for computing the expected variance in texture coefficients[3] for a given number of samples and a known grain size, or for computing the number of samples required to obtain a texture coefficient with a given precision when the grain size is known.

DISCUSSION

X-RAY MEASUREMENTS OF GRAIN SIZE

Apparatus and Procedure

The object of the experiment is to measure the differences in diffraction intensity obtained, for a given reflection, (hkl), by diffracting from various positions on the surface of a uranium sample. The area of the beam is made small enough compared to the grain size so that such differences occur and are large enough to be readily measured. These counts, called Y counts, along with the beam area and the solid angle, through which the sample is rotated during a Y count, may be substituted in equation 1 to calculate the average squared grain diameter.

The uranium was prepared by heat treating a section 1/8-inch thick x 1-inch diameter at 700°C for 30 minutes, quenching in water at 23°C, and annealing at 615°C for 30 minutes. The sample was mechanically polished through #1 diamond dust and electropolished[4] to remove cold-worked metal. The sample was in the form of a disk, 31/32 inch in diameter. Conventional Norelco diffraction equipment was used in conjunction with a proportional counter and pulse height analyzer. The sample was mounted in a Norelco spinner (Figure 1). When in diffracting position the sample was rotated through the necessary solid angle by means of a motor mounted on the shaft of the Norelco spinner.

Different sample positions were obtained by rotating the spinner, which is graduated in degrees, from one position to another. The (111) plane was chosen for the measurements to obtain each count; the counter is set at the proper 2θ position for reflection from the (111) plane; and the counts are taken as the sample is rotated through the angle Φ. Counts were taken at twelve positions by rotating the spinner in steps of 30°. Steps of 30° were required to avoid overlapping positions. Additional sets of twelve counts were obtained by polishing the sample to a different grain depth

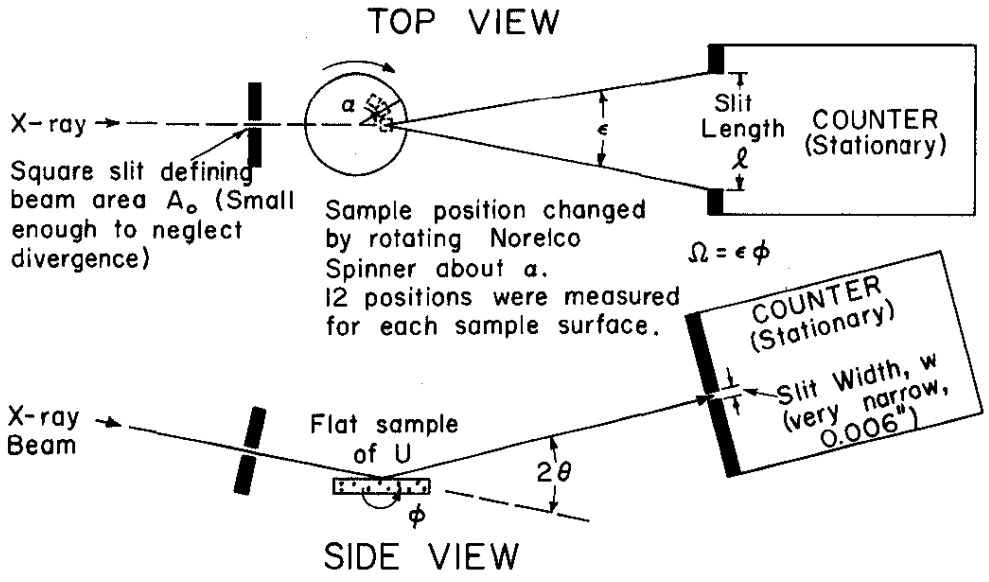

The ϕ rotation is about the same axis as the spinner. With the specimen in some position, α, (Top View) and the counter stationary at the center of a peak (we used (111)), counts are taken while the specimen is rotated through the angle ϕ. The product of ϵ, the angle subtended by the receiver slit length (Top View), and the angle ϕ gives the solid angle Ω.

FIG. 1 DIFFRACTION GEOMETRY FOR URANIUM GRAIN SIZE MEASUREMENTS WITH NORELCO DIFFRACTOMETER

and repeating the procedure. Because of the high absorption coefficient of uranium it was required that the same degree of "smoothness" exist on each surface that was measured; otherwise nonstatistical fluctuations would occur because of differences in absorption. Other details of the diffraction geometry and experimental conditions are given in Figure 1.

Number of Measurements Required

It was necessary to determine the number of diffraction intensity measurements (Y counts) required to determine the grain size. The number will vary depending on the grain size being measured and the precision desired. The number was determined by plotting $\langle D^2 \rangle^{\frac{1}{2}}$ versus the number of Y counts. $\langle D^2 \rangle^{\frac{1}{2}}$ was calculated beginning with the 24th measurement and adding one each time. A plot of $\langle D^2 \rangle^{\frac{1}{2}}$ versus the number of Y counts is shown in Figure 2. For the grain size being measured about 50 counts are required to assure a precision of about 10%, and the value of $\langle D^2 \rangle^{\frac{1}{2}}$ levels off to about ±2% after 90 counts.

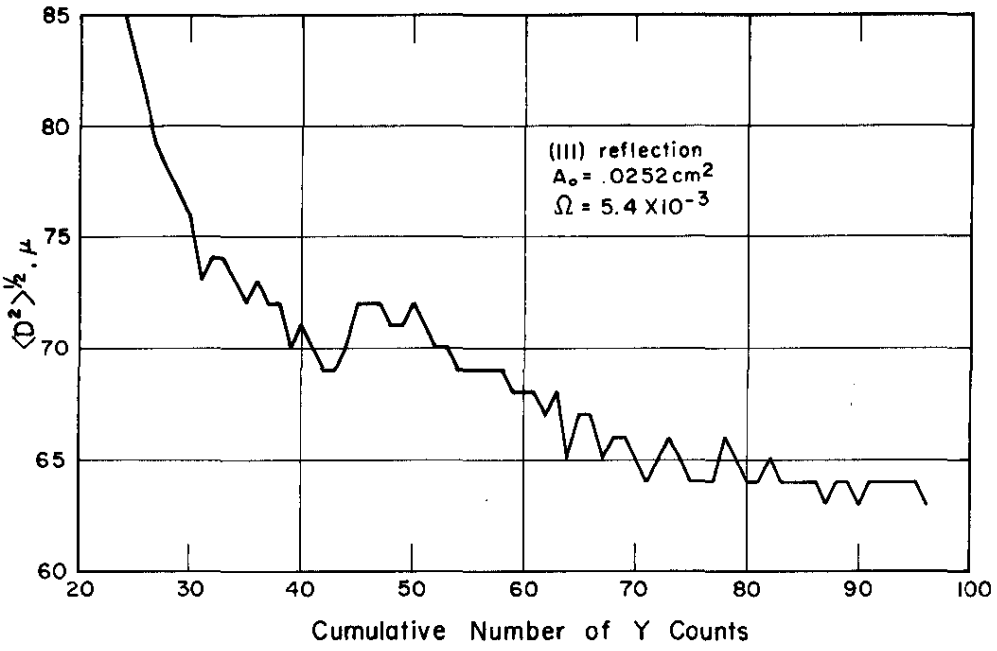

FIG. 2 GRAIN DIAMETER, $\langle D^2 \rangle^{1/2}$, VS CUMULATIVE NUMBER OF Y COUNTS

Effect of Solid Angle on Grain Size

As far as equation 1 is concerned, any solid angle that gives a sufficient number of counts above background should be acceptable. The solid angle is however affected by substructure in the grains, since a solid angle smaller than the

sub-boundary angle between two grains will cause the substructure to be resolved, and each subgrain will register as a separate grain. However, if the solid angle is larger than the sub-boundary angle between the grains, the substructure is not resolved and all the subgrains register as a single grain. From these considerations, it was decided to perform the experiment over a range of solid angles. In addition, the uranium used in the experiment was annealed to minimize substructure.

Effect of Preferred Orientation on Grain Size Measurements

The effect of preferred orientation was largely avoided by heat treating the uranium so as to produce an approximately random orientation. Orientation effects are never serious in this type of experiment for two reasons:

- The preferred orientation can be measured, and its effect is included in equation 1 as a factor, γ, which is equivalent to the texture coefficient[3] of the reflection being used.

- Equation 1 computes $\langle D^2 \rangle$, the average squared grain diameter. Hence, upon taking the square root to obtain $\langle D^2 \rangle^{\frac{1}{2}}$, the preferred orientation factor γ is reduced to $\sqrt{\gamma}$.

Results

The X-ray measurements of grain diameter are shown for a range of solid angles (Ω = 1.25 to 10.8 x 10^{-3}) in Figure 3. Note that for each solid angle the grain size is plotted as a function of the number of Y counts in groups of twelve. Groups of twelve were chosen because that was the number of Y counts obtained from a given sample surface. Hence, each unit along the abscissa of the plot was obtained by polishing the sample to a new depth. The fact that twelve Y counts are insufficient was demonstrated in Figure 2 but is shown more emphatically in Figure 4, where the grain diameter calculated from individual groups of twelve Y counts is compared with the grain diameter for cumulative groups of twelve Y counts up to a total of 120 Y counts or ten groups. It is seen that individual groups of twelve gave results ranging from 27 to 52 microns.

A plot of grain diameter $\langle D^2 \rangle^{\frac{1}{2}}$ versus solid angle is shown in Figure 5. The decrease in grain size with decreasing solid angle is due to substructure in the grains.

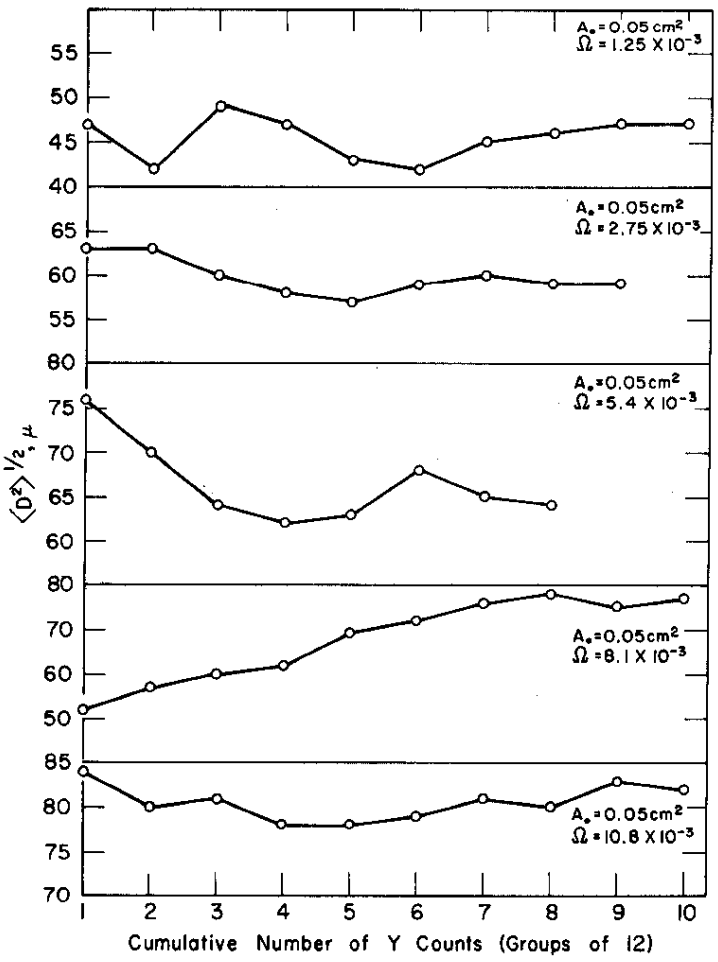

FIG. 3 GRAIN SIZE, $\langle D^2 \rangle^{1/2}$, VS CUMULATIVE NUMBER OF Y COUNTS

The continued increase in grain size at solid angles larger than the sub-boundary angles between the grains could be due to several factors:

- Defocusing caused by rotating the sample through large Φ angles. Such defocusing decreases A_o, because a certain fraction of the irradiated portion of the sample would be too far off the focal circle to be focused at the narrow receiving slit.

- There is some divergence in the X-ray beam (~ 1 degree) that is not taken into account since the grain size equation is derived for a parallel beam. The divergence angle of the beam changes slightly with changing Φ (and hence Ω).

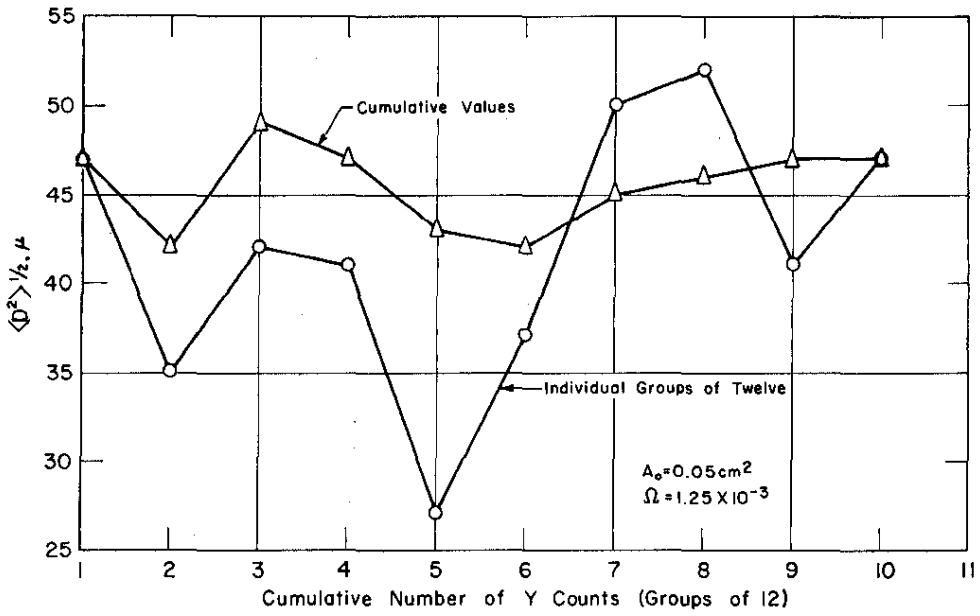

FIG. 4 CUMULATIVE VS INDIVIDUAL GROUPS OF Y COUNTS ($\Omega = 1.25 \times 10^{-3}$)

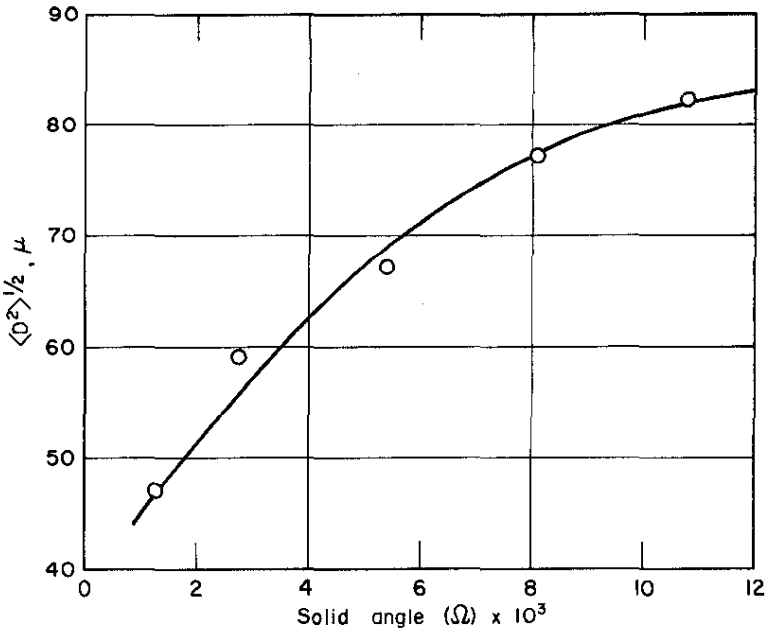

FIG. 5 GRAIN SIZE $\langle D^2 \rangle^{1/2}$ VS SOLID ANGLE (Ω)

It is therefore concluded that the continued increase in $\langle D^2 \rangle^{\frac{1}{2}}$ at large solid angles is an effect due to inperfect experimental conditions and can be decreased or eliminated by improving the focusing conditions during rotation through Φ and/or by decreasing the divergence of the X-ray beam.

METALLOGRAPHIC MEASUREMENT OF GRAIN SIZE

The metallographic measurements were made on the same sample that was used for the X-ray measurements. Photomicrographs were made on a metallograph using polarized light. To distinguish between small-angle grain boundaries, three photomicrographs were made of the same area on the sample, each for a different orientation of the specimen stage. The three photomicrographs were examined simultaneously, and all grain boundaries marked on one of them. The whole procedure was repeated for a different area on the sample. To determine the area of the grains, the grains were cut from the photographic paper and weighed. The calibration data for converting weight to area are shown in Table I and Figure 6. A total of 463 grains were measured. The grain area distribution is given in Table II and Figure 7. The mean grain area gave a mean grain diameter, $\langle D^2 \rangle^{\frac{1}{2}}$, of 108 microns. The mean grain area, $\langle A \rangle$, is computed as an area weighted[2] mean, that is:

$$\langle A \rangle = \frac{\sum_k n_k A_k^2}{\sum_k n_k A_k} \qquad (2)$$

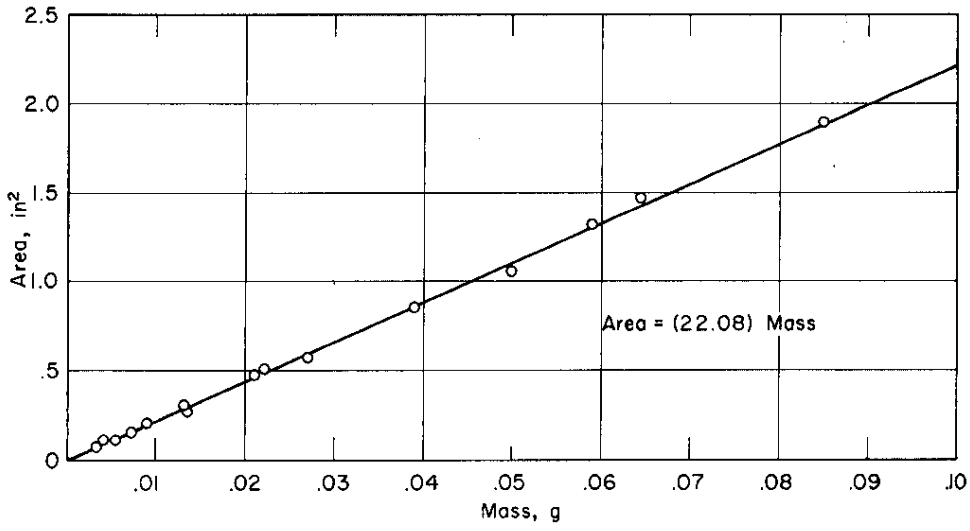

FIG. 6 CALIBRATION CURVE TO CONVERT MASS TO AREA

TABLE I

Calibration of Weight Versus Area for Photographic Paper

Area (Y), sq. in.	Weight (X), gram	Y/X	XY	$X^2 \times 10^{-4}$
0.50	.0222	22.52252	.01110	4.9284
0.30	.0132	22.72727	.00396	1.7424
1.05	.0499	21.04208	.05240	24.9001
1.32	.0590	22.37288	.07788	34.8100
0.11	.0054	20.37037	.00059	0.2916
0.28	.0134	20.89552	.00375	1.7956
0.20	.0094	21.27660	.00188	0.8836
0.47	.0212	22.16981	.00996	4.4944
0.57	.0271	21.03321	.01545	7.3441
0.85	.0389	21.85090	.03307	15.1321
1.88	.0853	22.03986	.16036	72.7609
1.47	.0645	22.79070	.09482	41.6025
0.10	.0041	24.39024	.00041	0.1681
0.15	.0072	20.83333	.00108	0.5184
0.07	.0033	21.21212	.00023	0.1089
			.46694	211.4811

$Y = mX + C$

For least squares fit:

$$C = \frac{(\Sigma x)(\Sigma xy) - (\Sigma y)(\Sigma x^2)}{(\Sigma x)^2 - N(\Sigma x^2)}$$

In this case, $C = 0$; hence $(\Sigma x)(\Sigma xy) - (\Sigma y)(\Sigma x^2) = 0$

and $\frac{\Sigma Y}{\Sigma x} = \frac{\bar{Y}}{\bar{X}} = m = \frac{\Sigma xy}{\Sigma x^2} = 22.08$

where n_k is the number of grains of area A_k, k being the kth grain. To compute the average diameter, $\langle D^2 \rangle^{\frac{1}{2}}$, it is assumed that the grains are spherical, which, of course, is not true, but is convenient for comparitive purposes.

$$\langle A \rangle = \frac{\pi}{4} \langle D^2 \rangle \qquad (3)$$

The reason for using an area weighted area to compute $\langle D^2 \rangle^{\frac{1}{2}}$ is that this is the kind of quantity that is actually measured by the X-rays.

The grain area versus the cumulative per cent of total area is plotted in Figure 8. This plot shows that 68% of the total grain area is composed of grains with diameters, $\langle D^2 \rangle^{\frac{1}{2}}$, ranging from 53 to 142 microns. The standard deviation is one half the difference between these values or ±45 microns. A micrograph of a typical area of the specimen employed for these experiments is given in Figure 9.

It should be noted that the grain size reported for both the X-ray and metallographic measurements were for

observations on plane surfaces. Such observations would yield a range of sizes even if the grains were all of the same shape and volume. A more correct analysis, called spatial grain size analysis, has been described by Scheil[5] and Johnson[6]. In the latter author's work, the variation in grain area caused purely by random sectioning is corrected for so that the grain area distrubution more nearly represents true variations in the sizes of the grains.

TABLE II

Analysis of Grain Areas For Quenched Annealed Uranium

Interval	Number of Particles	Area of Each x 10^{-4}	$(\text{Area})^2$ of Each x 10^{-8}	Total Area x 10^{-4}	$(\text{Total Area})^2$ x 10^{-8}	% Total Area	$(\%\ \text{Total Area})^2$	Cumulative % Area
1	95	.0356	.00127	3.382	.121	1.97	0.08	1.97
2	81	.1067	.01138	8.643	.922	5.04	0.59	7.01
3	50	.1778	.03161	8.890	1.581	5.18	1.00	12.19
4	43	.2492	.06210	10.716	2.670	6.25	1.70	18.44
5	38	.3204	.10266	12.175	3.901	7.10	2.48	25.54
6	32	.3917	.15343	12.534	4.910	7.31	3.12	32.85
7	23	.4629	.21428	10.647	4.928	6.21	3.13	39.06
8	11	.5342	.28537	5.876	3.139	3.43	1.99	42.49
9	10	.6054	.36651	6.054	3.665	3.53	2.33	46.02
10	11	.6766	.45779	7.443	5.036	4.34	3.20	50.36
11	15	.7478	.55920	11.217	8.388	6.54	5.33	56.90
12	9	.8190	.67076	7.371	6.037	4.30	3.84	61.20
13	2	.8903	.79263	1.781	1.585	1.04	1.01	62.24
14	5	.9615	.92448	4.808	4.622	2.80	2.94	65.04
15	3	1.033	1.0671	3.099	3.201	1.81	2.03	66.85
16	5	1.104	1.2188	5.520	6.094	3.22	3.87	70.07
17	3	1.175	1.3806	3.525	4.142	2.06	2.63	72.13
18	5	1.247	1.5550	6.235	7.775	3.64	4.94	75.77
19	2	1.318	1.7371	2.636	3.474	1.54	2.21	77.31
20	1	1.388	1.9265	1.388	1.927	0.81	1.22	78.12
21	4	1.460	2.1316	5.840	8.526	3.41	5.42	81.53
22	2	1.531	2.344	3.062	4.688	1.79	2.98	83.32
23	1	1.602	2.5664	1.602	2.566	0.93	1.63	84.25
24	0	0	0	0	0	0	0	0
25	2	1.740	3.0276	3.480	6.055	2.03	3.85	86.28
26	1	1.816	3.2979	1.816	3.298	1.06	2.10	87.34
27	1	1.887	3.5608	1.887	3.561	1.10	2.26	88.44
28	0	0	0	0	0	0	0	0
29	0	0	0	0	0	0	0	0
30	2	2.100	4.4100	4.200	8.820	2.45	5.60	90.89
31	1	2.172	4.7176	2.172	4.718	1.27	3.00	92.16
32	1	2.243	5.0310	2.243	5.031	1.31	3.20	93.47
33	1	2.315	5.3592	2.315	5.359	1.35	3.40	94.82
34-38	0	0	0	0	0	0	0	0
39	1	2.813	7.9130	2.813	7.913	1.64	5.03	96.46
40-41	0	0	0	0	0	0	0	0
42	1	3.027	9.1627	3.027	9.163	1.77	5.82	98.23
43	1	3.098	9.598	3.098	9.598	1.81	6.10	100.0
Total:	463			171.495	157.414	100.0	100.0	

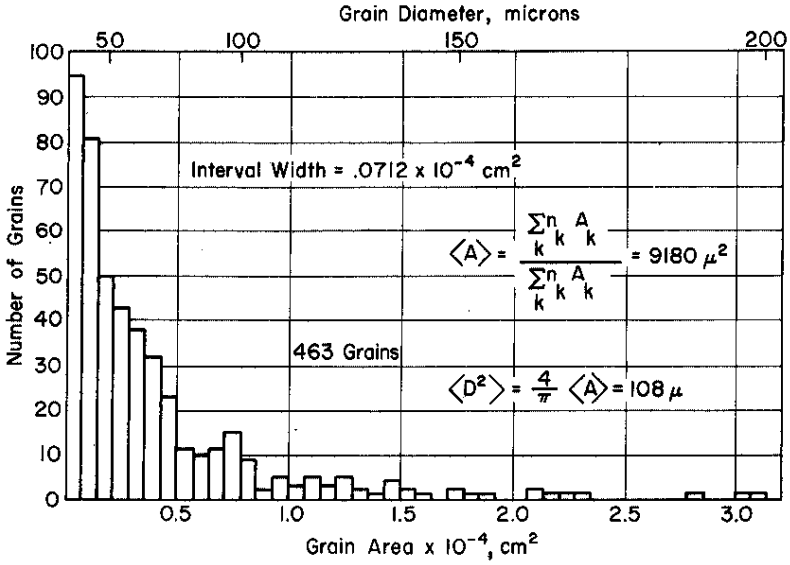

FIG. 7 DISTRIBUTION OF CROSS-SECTIONAL AREAS IN QUENCH-ANNEALED URANIUM

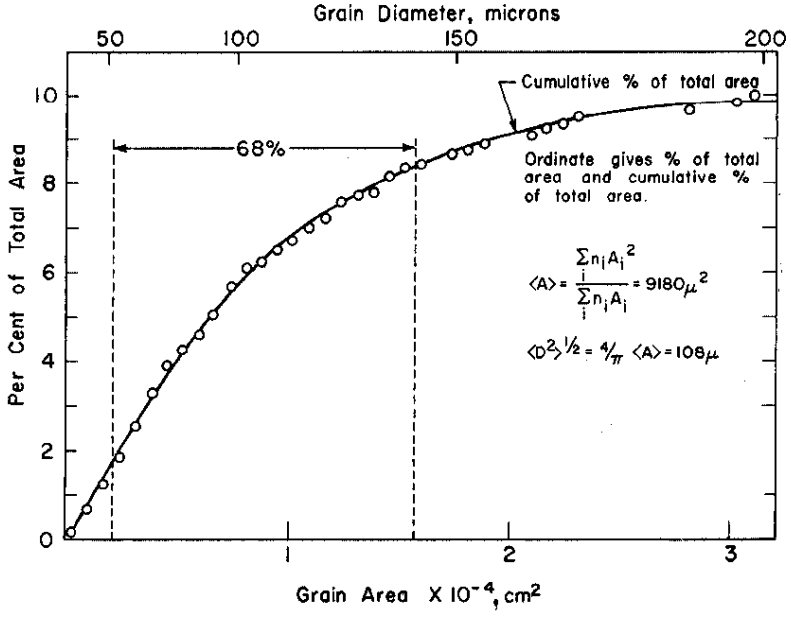

FIG. 8 GRAIN SIZE DISTRIBUTION ANALYSIS (PLANIMETER)

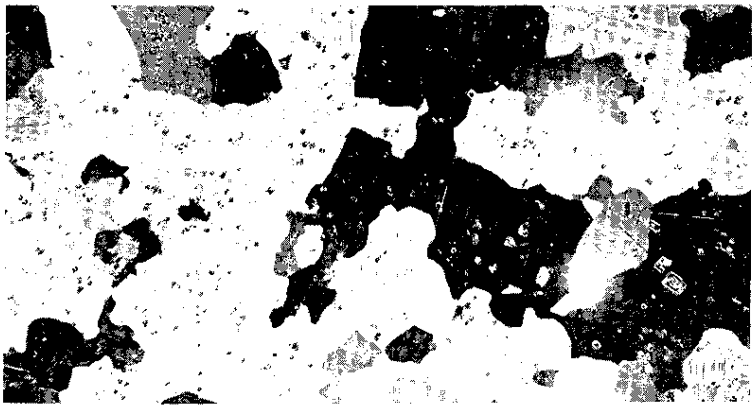

Neg. 1039

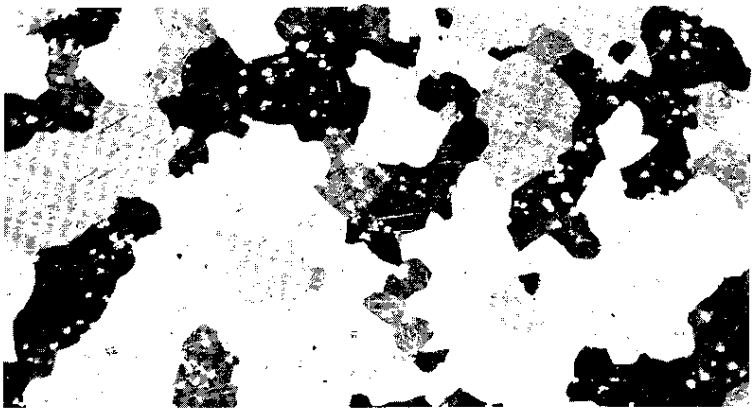

Neg. 1040

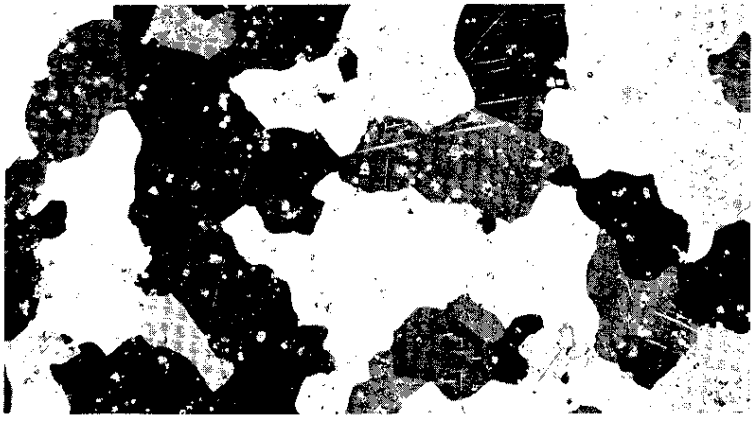

Neg. 1041

FIG. 9 PHOTOMICROGRAPH OF QUENCH-ANNEALED URANIUM (150X)

REFERENCES

1. Warren, B. E. X-ray Measurement of Grain Size. Massachusetts Inst. of Tech., Cambridge, Mass. USAEC Report NYO-4836 (1960). See also: J. Appl. Phys. 31, No. 12, 2237-9 (1960).

2. Sturcken, E. F. and W. E. Gettys. "Determination of Grain Size from Statistical Fluctuation in X-Ray Diffraction Intensity", Papers and Proceedings of the X-Ray Preferred Orientation Meeting Held at HAPO June 29 and 30, 1961. W. Gary Jolley, Ed. General Electric Co., Hanford Atomic Products Operation, Richland, Wash. USAEC Report HW-74429, pp. 45-58 (1962).

3, Morris, P. R. "Reducing the Effects of Nonuniform Pole Distribution in Inverse Pole Figure Studies". J. Appl. Phys. 30, No. 4, 595-6 (1959).

4. Sturcken, E. F. An X-Ray Method for Predicting the Stability of Natural Uranium at Low Burnup. E. I. du Pont de Nemours & Co., Savannah River Laboratory, Aiken, S. C. USAEC Report DP-251 (1958). See also: J. Nucl. Mater. 7, No. 1, 85-91 (1962).

5. Scheil, E. "Statistical Investigations of the Structure of Metals-I." Z. Metallkunde 27, 199-208 (1935).

6. Johnson, W. A. "Estimation of Spatial Grain Size." Metal Progr. 49, No. 1, 87-92 (1946).

TEXTURE GRADIENTS IN OIL QUENCHED, MARK VB OUTER FUEL CORES*

V. Morton, R. N. Thudium, N. Crank, Jr., and C. A. Powell
National Lead Co. of Ohio

Abstract

Three Mark V-B outer fuel cores were examined for texture gradients in the longitudinal, tangential, and radial directions as functions of radial position. Two of these cores were beta-treated and oil quenched with excess stock on the ID and OD. Sampling techniques are described; the G_2, G_3, and J data are tabulated; and plots of longitudinal, tangential, and radial G_3, as functions of radial position, are presented.

Introduction

Until recently, the most commonly employed technique[1] for collecting preferred orientation data on a uranium fuel core involved examination of the surface of one or more transverse samples. The X-ray beam was caused to impinge upon the specimen with the long axis of the beam centered at midwall, or, in the case of solid cores, at mid-radius, while the specimen was rotated about its axis. The data collected in this manner were used in an effort to predict dimensional changes in the longitudinal direction during thermal neutron irradiation.

The shortcomings of this technique have been demonstrated and discussed previous reports.[2,3,4,5] It has been concluded from this previous work that to predict more accurately the behavior of uranium fuel elements under neutron irradiation, it will be necessary to conduct an extensive investigation of texture gradients in three mutually perpendicular directions in uranium fuel cores having various heat treatments and geometries.

Objectives for This Quarter

1. To devise sampling plans for three mutually perpendicular directions in Mark V-B outer fuel cores.

2. To collect X-ray preferred orientation data on Mark V-B outer fuel cores which had been beta heat-treated and oil quenched with varying amounts of excess stock on the ID and OD.

Summary of Results

Sampling plans were devised and specimens machined to permit examination of surfaces normal to the longitudinal, tangential, and radial directions in three Mark V-B outer fuel cores.

While data obtained to date are insufficient to establish "typical" textures for a given heat treatment, or to permit an estimate of the variation to be expected among cores subjected to the same heat treatment, these preliminary findings indicate that little improvement is to be expected in dimensional stability as a result of heat treating with excess stock. All cores examined to date have displayed positive growth tendencies in the tangential direction. In general, there is a tendency toward large negative growth (shrinkage) in the radial direction at the inner and outer surfaces, rising to positive growth near midwall. The longitudinal direction generally shows a behavior somewhat inverse to that displayed in the radial direction, assuming a positive growth tendency near inner and outer surfaces, and decreasing to near zero or negative growth at midwall. All cores examined to date are expected to increase slightly in OD, show a somewhat more pronounced increase in ID, and increase in length due to the effects of anisotropic growth. Effects contributing to volume increases are not included in this analysis.

Experimental Equipment

Preferred orientation data were obtained with a General Electric XRD-V diffractometer. A 1 degree divergence slit with a 0.063-inch wide confining slit was used to limit the beam to the increment of interest. Since the error encountered when the rectangular X-ray beam strikes the sample at low angles is small, due to the relatively large sam-

* The Mark VB Outer Fuel Core is a uranium tube 2.682-inch OD x 1.972-inch ID. Paper reproduced from USAEC Report NLCO-850.

ple diameter, curved slits were not required. The effect of using rectangular slits is illustrated in Figure 1.

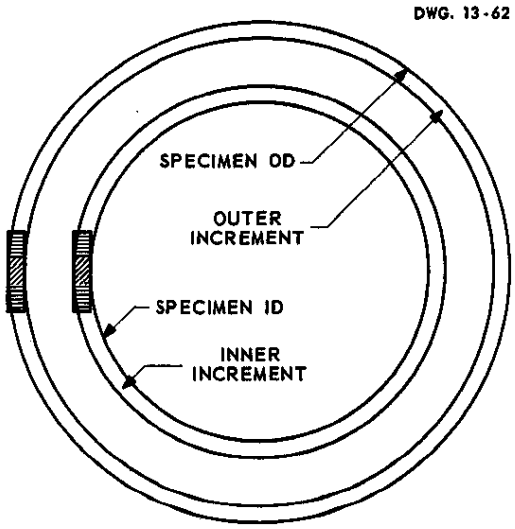

FIGURE 1 Longitudinal Specimen Showing the Divergence of a Rectangular Beam at High and Low θ Angles

Experimental Procedures

Three Mark V-B outer fuel cores were heat-treated in molten NuSal (50 w/o NaCl, 50 w/o KCl) for 10 minutes at 1350 ± 10°F, delayed in air for 11 seconds, and quenched in Houghto K oil at 130°F. One core was heat-treated with 0.125-inch excess stock on the wall (distributed equally between the ID and OD), one with 0.075-inch, and one at finished dimensions.

The first samples taken were $\frac{7}{16}$-inch-thick transverse rings which were used to collect data for the longitudinal direction. A steel ring was placed around each sample, and the space between the specimen and the ring was filled with epoxy resin. The steel rings were used to prevent beveling of the sample during grinding and to prevent the outer edge of the specimen being covered by the rotator flange. The beam-confining slit was attached to the divergence slit, and stacking plates were used to elevate the specimen and rotator to the proper height so that the confined X-ray beam fell upon the increment of interest. The specimen assembly is shown in place in the specimen rotator in Figure 2. Preferred orientation data were obtained on successive radial increments.

Samples were obtained for the tangential direction by machining 0.473-inch-long transverse ring sections with a 10 degree concave bevel on each face (see Figure 3). An expanding mandrel was inserted in the ID of the ring, and the assembly was placed in the angular dividing head of a milling machine. A $\frac{1}{16}$-inch-thick slitting cutter was used to make cuts at 20 degree intervals around the circumference to within $\frac{1}{16}$-inch of the ID. The final $\frac{1}{16}$-inch was removed with a hack saw and ground by hand using silicon carbide paper. One side of each cut was coplanar with a radius. The finished slices were placed with their radius planes downward on a flat surface and with their 10 degree beveled sides together. A steel ring was placed around the composite and filled with epoxy resin. The back edges of the individual samples were left exposed, and conductive epoxy resin (Eccobond Solder 56 C, Low Resistance Conducting Cement) was used to provide electrical contact, so that the composite sample could be electroetched.

Data were obtained from the tangential samples by the same method used on the transverse rings to obtain longitudinal orientation data. Figure 4 shows this composite in place in the specimen rotator.

FIGURE 2 Diffractometer with Longitudinal Specimen in Specimen Rotator

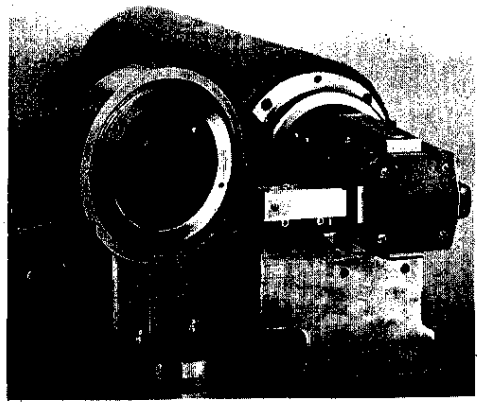

FIGURE 4 Diffractometer with Tangential Specimen in Specimen Rotator

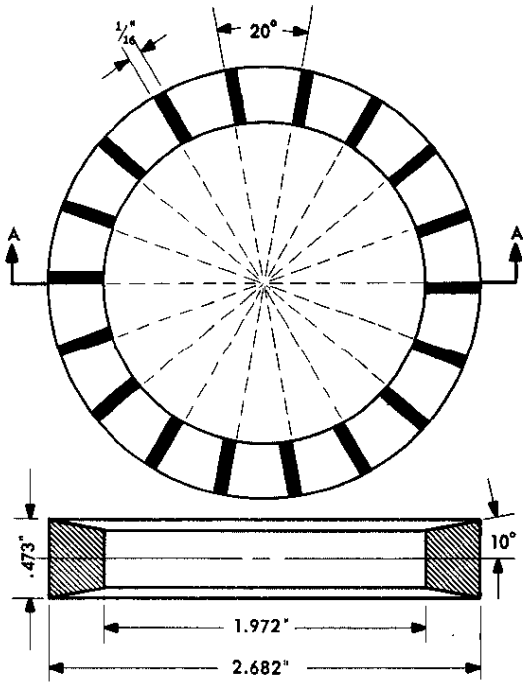

SECTION A-A
SHADED AREAS INDICATE METAL REMOVED BY CUTTING TOOL

FIGURE 3 Sampling Plan for Tangential Direction

To obtain specimens for the radial direction, ¾-inch-long cylinders were taken from the tube. An expanding mandrel was inserted in the cylinder, and the assembly was placed in the dividing head of a milling machine. Two $\frac{1}{16}$-inch slitting cutters were placed on the mandrel with a 0.173-inch spacer between them. Each cut was made so that the slice left between the cutters was equally distributed about a radius (Figure 5). The cuts were made to within $\frac{1}{16}$-inch of the ID. Again, it was necessary to remove the final $\frac{1}{16}$-inch with a hack saw. Each specimen was finish-machined on a surface grinder.

It was necessary to hand grind 0.004-inch from both lateral faces of each specimen to remove the cold work induced by the milling cutters and surface grinder. Each radial slice was 0.165-inch thick, representing a maximum deviation of the milled surfaces from a radius of less than 5 degrees on the ID and less than 4 degrees on the OD. The finished samples were stacked together with their original ID surfaces downward and mounted in a steel ring with epoxy resin. It was necessary to grind the composite specimen after each examination to reach the next radial location of interest.

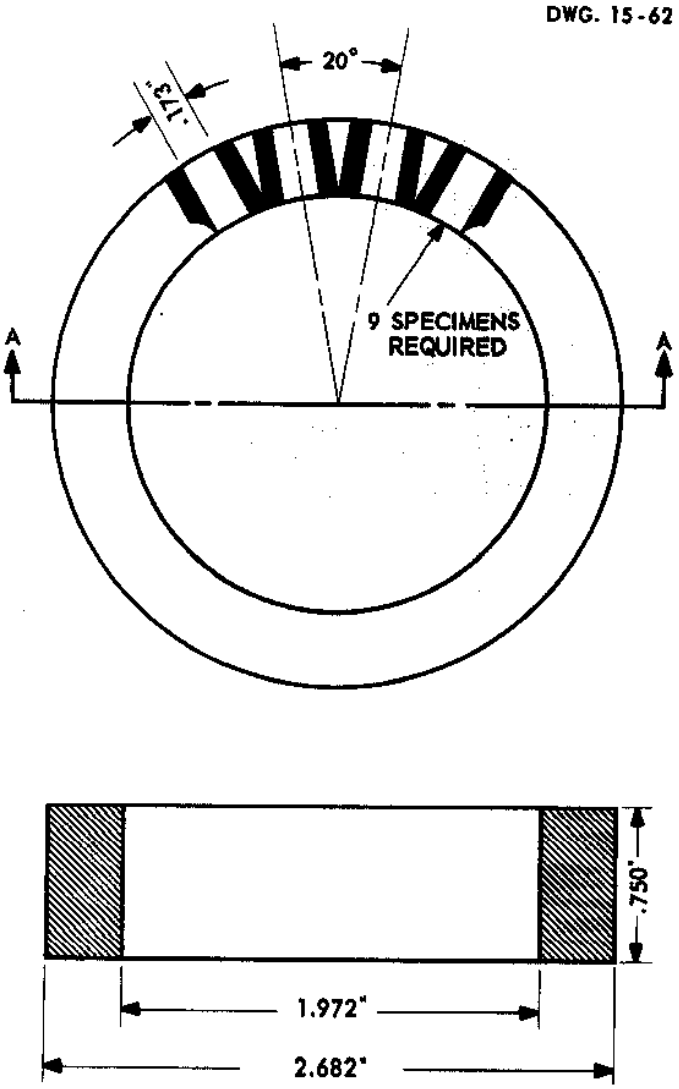

SECTION A-A
SHADED AREAS INDICATE METAL REMOVED BY CUTTING TOOL

FIGURE 5 Sampling Plan for Radial Direction

Twenty-two diffraction planes were scanned in each of the three principal directions to obtain integrated intensities. Each increment was scanned a sufficient number of times to bring the 95% confidence interval limits on the mean of the G_2 and G_3 values within approximately ± .03. The growth indices were calculated by computer.

Tables 1, 2, and 3 list the G_2, G_3, and J values and 95% confidence interval limits on their mean values. Plots of G_3 in the radial, tangential, and longitudinal directions as functions of radial position are shown in Figures 6, 7, and 8.

TABLE 1 Core I
Excess

Radius	G_3
	L
1.028	+.018 ± .01
1.090	−.012 ± .01
1.170	+.006 ± .01
1.233	+.065 ± .01
1.310	+.062 ± .01
	T
1.020	+.044 ± .01
1.097	+.027 ± .02
1.125	+.030 ± .02
1.170	.00 ± .02
1.210	+.006 ± .01
1.250	+.035 ± .02
1.312	+.029 ± .02
.994	+.036 ± .02
1.024	−.023 ± .01
1.054	−.015 ± .01
1.113	+.030 ± .01
1.144	+.039 ± .007
1.176	−.009 ± .004
1.208	−.023 ± .017
1.238	−.062 ± .004
1.269	−.080 ± .011
1.299	−.055 ± .024
1.331	−.068 ± .017

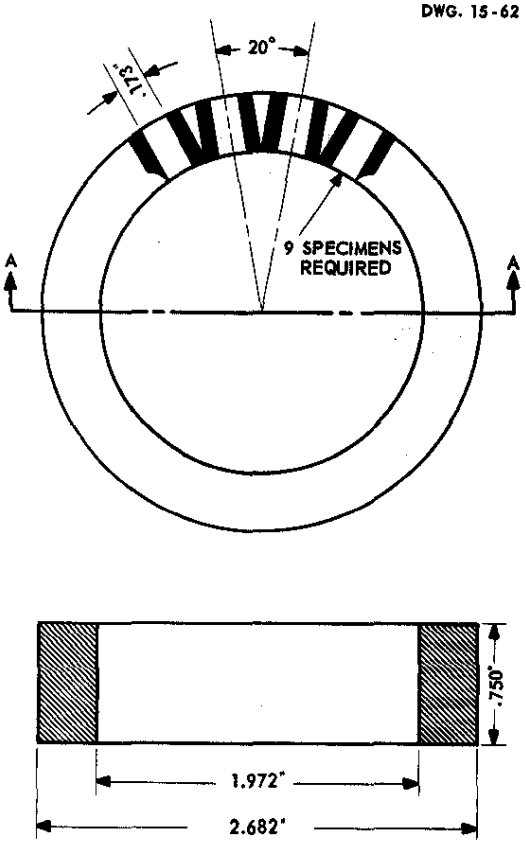

FIGURE 5 Sampling Plan for Radial Direction

Twenty-two diffraction planes were scanned in each of the three principal directions to obtain integrated intensities. Each increment was scanned a sufficient number of times to bring the 95% confidence interval limits on the mean of the G_2 and G_3 values within approximately ± .03. The growth indices were calculated by computer.

Tables 1, 2, and 3 list the G_2, G_3, and J values and 95% confidence interval limits on their mean values. Plots of G_3 in the radial, tangential, and longitudinal directions as functions of radial position are shown in Figures 6, 7, and 8.

TABLE 1 Core Heat-Treated with 0.125-Inch Excess Stock on Wall

Radius	G_3	G_2	J
	Longitudinal		
1.028	+.018 ± .015	+.022 ± .017	1.03 ± .01
1.090	−.012 ± .013	−.003 ± .014	1.05 ± .02
1.170	+.006 ± .014	+.019 ± .015	1.03 ± .01
1.233	+.065 ± .019	+.066 ± .016	1.04 ± .04
1.310	+.062 ± .018	+.073 ± .012	1.05 ± .02
	Tangential		
1.020	+.044 ± .015	+.058 ± .039	1.04 ± .03
1.097	+.027 ± .028	+.025 ± .024	1.01 ± .01
1.125	+.030 ± .028	+.025 ± .030	1.02 ± .01
1.170	.00 ± .025	+.018 ± .015	1.02 ± .02
1.210	+.006 ± .013	+.014 ± .038	1.01 ± .01
1.250	+.035 ± .023	+.052 ± .028	1.02 ± .01
1.312	+.029 ± .022	+.035 ± .022	1.03 ± .01
	Radial		
.994	+.036 ± .022	+.030 ± .010	1.02 ± .02
1.024	−.023 ± .015	−.030 ± .040	1.01 ± .01
1.054	−.015 ± .013	−.007 ± .011	1.01 ± .00
1.113	+.030 ± .014	+.026 ± .013	1.03 ± .01
1.144	+.039 ± .007	+.040 ± .010	1.01 ± .01
1.176	−.009 ± .004	−.010 ± .010	1.01 ± .01
1.208	−.023 ± .017	−.020 ± .010	1.02 ± .01
1.238	−.062 ± .004	−.060 ± .010	1.02 ± .01
1.269	−.080 ± .011	−.080 ± .010	1.04 ± .01
1.299	−.055 ± .024	−.060 ± .020	1.02 ± .01
1.331	−.068 ± .017	−.080 ± .010	1.03 ± .01

TABLE 2 Core Heat-Treated with 0.075-Inch Excess Stock on Wall

Radius	G_3	G_2	J
	Longitudinal		
.977	+.065 ± .022	+.086 ± .021	1.06 ± .00
1.063	+.045 ± .008	+.057 ± .017	1.03 ± .02
1.128	−.035 ± .035	−.013 ± .030	1.03 ± .01
1.205	−.030 ± .018	−.007 ± .008	1.03 ± .01
1.270	+.026 ± .031	+.043 ± .021	1.04 ± .02
1.347	+.060 ± .032	+.084 ± .025	1.05 ± .01
	Tangential		
.979	+.026 ± .032	+.033 ± .029	1.03 ± .03
1.052	+.014 ± .023	+.040 ± .022	1.02 ± .01
1.125	+.029 ± .031	−.043 ± .035	1.02 ± .01
1.198	+.030 ± .016	−.040 ± .020	1.02 ± .01
1.271	+.034 ± .001	+.050 ± .011	1.02 ± .01
1.348	+.048 ± .029	+.077 ± .033	1.05 ± .03
	Radial		
.948	−.172 ± .016	−.174 ± .008	1.16 ± .01
.957	−.038 ± .015	−.048 ± .014	1.05 ± .01
.967	−.078 ± .025	−.090 ± .026	1.09 ± .02
.975	−.075 ± .018	−.070 ± .020	1.05 ± .01
.985	−.097 ± .014	−.086 ± .011	1.07 ± .02
.995	−.062 ± .024	−.059 ± .011	1.03 ± .03
1.005	−.086 ± .020	−.082 ± .018	1.04 ± .01
1.016	−.059 ± .012	−.048 ± .012	1.02 ± .02
1.026	−.088 ± .018	−.074 ± .018	1.03 ± .01
1.046	+.012 ± .020	+.020 ± .013	1.07 ± .01
1.051	−.051 ± .016	−.038 ± .013	1.02 ± .00
1.071	−.028 ± .019	−.014 ± .016	1.01 ± .01
1.091	−.001 ± .005	−.010 ± .010	1.02 ± .01
1.113	+.011 ± .035	−.017 ± .020	1.01 ± .00
1.132	+.041 ± .002	+.048 ± .008	1.03 ± .01
1.152	+.046 ± .016	+.066 ± .020	1.04 ± .01
1.175	+.074 ± .013	+.088 ± .013	1.04 ± .01
1.195	+.097 ± .009	+.099 ± .007	1.02 ± .01
1.217	+.069 ± .013	+.072 ± .007	1.03 ± .01
1.238	+.065 ± .018	+.083 ± .001	1.04 ± .01
1.260	+.037 ± .018	+.048 ± .015	1.02 ± .01
1.279	+.027 ± .024	+.036 ± .019	1.02 ± .01
1.289	+.019 ± .014	+.031 ± 0.18	1.01 ± .01
1.328	−.018 ± .021	−.012 ± .014	1.01 ± .01
1.348	−.069 ± .021	−.055 ± .020	1.02 ± .01
1.353	−.078 ± .019	−.061 ± .008	1.02 ± .01
1.358	−.091 ± .026	−.069 ± .026	1.03 ± .01
1.363	−.082 ± .028	−.069 ± .022	1.04 ± .01
1.367	−.089 ± .006	−.077 ± .010	1.03 ± .01
1.372	−.119 ± .029	−.107 ± .032	1.06 ± .03
1.378	−.138 ± .009	−.130 ± .010	1.11 ± .01

TABLE 3 Core Heat-Treated at Finished Dimensions

Radius	G_3	G_2	J
	Longitudinal		
1.027	+.040 ± .018	+.055 ± .033	1.04 ± .03
1.089	+.003 ± .017	+.020 ± .013	1.03 ± .01
1.169	−.008 ± .016	+.001 ± .014	1.02 ± .01
1.232	+.026 ± .011	+.039 ± .013	1.03 ± .01
1.311	+.033 ± .016	+.053 ± .013	1.04 ± .01
	Tangential		
1.029	+.046 ± .020	+.059 ± .018	1.03 ± .01
1.066	+.022 ± .022	+.039 ± .030	1.03 ± .01
1.154	−.003 ± .031	+.018 ± .032	1.02 ± .01
1.259	+.041 ± .019	+.050 ± .005	1.03 ± .01
1.296	+.035 ± .005	+.063 ± .011	1.04 ± .01
	Radial		
.988	−.017 ± .012	−.010 ± .009	1.09 ± .01
.996	−.042 ± .017	−.034 ± .007	1.03 ± .01
1.006	−.033 ± .016	−.023 ± .012	1.03 ± .06
1.016	−.035 ± .019	−.030 ± .024	1.01 ± .01
1.026	−.040 ± .023	−.025 ± .018	1.01 ± .00
1.036	−.046 ± .021	−.038 ± .014	1.01 ± .00
1.056	−.003 ± .017	+.006 ± .017	1.01 ± .00
1.076	+.006 ± .007	+.014 ± .007	1.01 ± .00
1.101	+.032 ± .021	+.042 ± .016	1.01 ± .01
1.120	+.046 ± .014	+.052 ± .016	1.02 ± .01
1.140	+.057 ± .013	+.062 ± .021	1.03 ± .01
1.162	+.048 ± .020	+.059 ± .024	1.03 ± .02
1.182	+.024 ± .008	+.038 ± .007	1.01 ± .01
1.206	+.028 ± .023	+.040 ± .007	1.01 ± .00
1.228	+.014 ± .006	+.022 ± .006	1.01 ± .00
1.249	+.006 ± .010	+.010 ± .008	1.01 ± .00
1.269	−.029 ± .006	−.024 ± .008	1.01 ± .00
1.292	−.059 ± .024	−.056 ± .011	1.02 ± .00
1.311	−.056 ± .016	−.049 ± .017	1.02 ± .01
1.316	−.078 ± .023	−.067 ± .024	1.03 ± .01
1.321	−.089 ± .015	−.084 ± .015	1.03 ± .01
1.326	−.085 ± .007	−.074 ± .004	1.03 ± .00
1.331	−.045 ± .018	−.045 ± .024	1.03 ± .01
1.336	−.029 ± .018	−.024 ± .018	1.02 ± .01

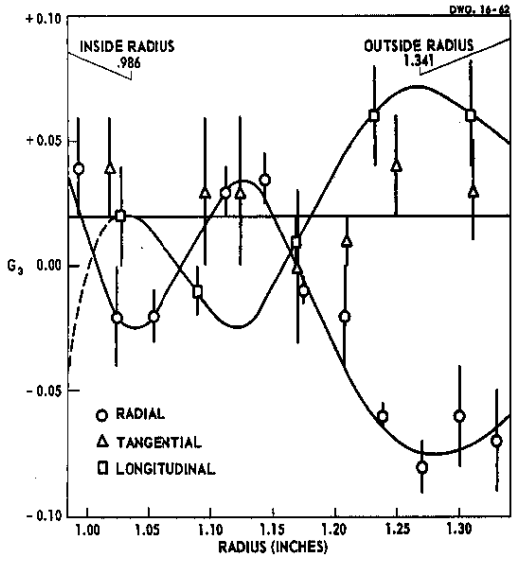

FIGURE 6 Mean Values of G_3 (with 95% Confidence Limits) as a Function of Radial Position in the Three Directions Investigated; Mark V-B Outer Core Beta Heat-Treated with 0.125-Inch Excess Stock on Wall, but Machined to Finished Dimensions Before Examination.

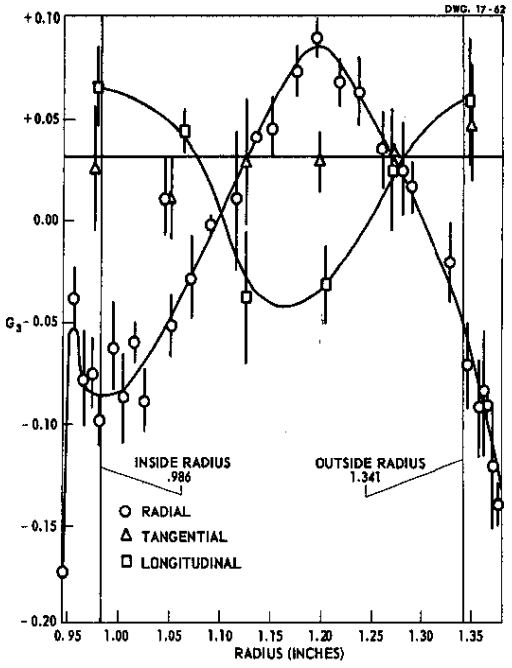

FIGURE 7 Mean Values of G_3 (with 95% Confidence Limits) as a Function of Radial Position in the Three Directions Investigated; Mark V-B Outer Core, Beta Heat-Treated with 0.075-inch Excess Stock on Wall.

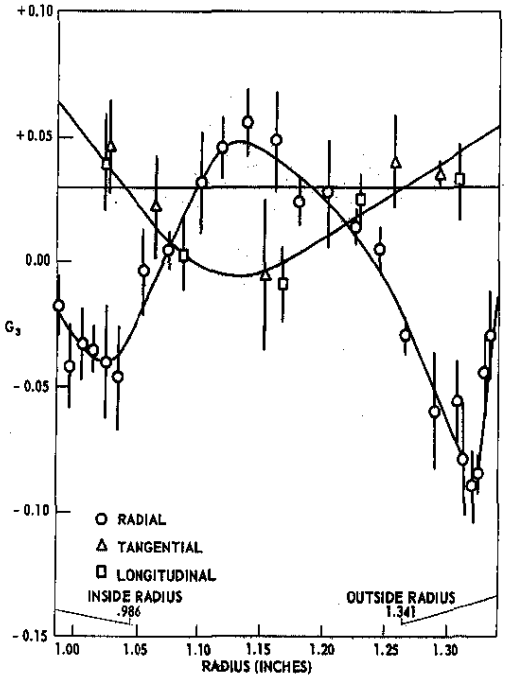

FIGURE 8 Mean Values of G_3 (with 95% Confidence Limits) as a Function of Radial Position in the Three Directions Investigated; Mark V-B Outer Core, Beta Heat-Treated at Finished Dimensions.

Future Work

Investigations of the texture gradients in the radial direction, near the outer periphery of roller-die quenched fuel cores is in process. Texture gradients in fuel cores with varying heat treatments are being investigated.

Acknowledgment

The writers are indebted to R. W. Fisher for machining the samples used in this study.

Addendum

Errors in reported[5] radii of curved slits used in examining longitudinal and tangential specimens from HAPO I&E core blanks have been brought to our attention by Bruce LeFevre of E. I. du Pont de Nemours and Company's Savannah River Laboratories. The correct radii required to approximate the beam curvature shown in Figure 10.2 on page 68 of the reference cited should be: R_1 = 0.067 inch, R_2 = 0.092 inch, and R_3 = 0.119 inch. Slits having the correct radii are currently being machined, and will be employed in future studies of this material.

References

[1] J. W. Starbuck and H. C. Kloepper, Jr. "X-Ray Evaluation of Cores Processed in the Seventh Alpha-Extrusion Campaign," Process Development Quarterly Progress Report, July-September, 1960, USAEC Report MCW-1459, pp. 81-85. November 1, 1960.

[2] R. B. Russell and L. R. Aronin. "Balanced Texture in Uranium," Fundamental and Applied Research and Development in Metallurgy, Progress Report for February, 1959, USAEC Report NMI-2075, pp. 17-25. March 30, 1959.

[3] R. B. Russell and L. R. Aronin. "Balanced Texture in Uranium," Fundamental and Applied Research and Development in Metallurgy, Progress Report for March, 1959, USAEC Report NMI-2076, pp. 15-25. May 13, 1959.

[4] J. W. Starbuck and H. C. Kloepper, Jr. "Preferred Orientation Studies of End-Quenched Jominy Bars," Process Development Quarterly Report, April-June, 1959, Part I — Laboratory Work, USAEC Report MCW-1430, pp. 89-104. July 1, 1959.

[5] V. Morton and R. N. Thudium. "Texture Gradients in Uranium Fuel Cores," Summary Technical Report for the Period July 1, 1961, to September 30, 1961, USAEC Report NLCO-840, pp. 67-71. October 20, 1961 (Classified).

THE GRAIN STRUCTURE AND ORIENTATION OF AS-EXTRUDED URANIUM TUBES MARK VB PRODUCTION

M. F. Garufi, R. J. Wallionis, and L. Robins

Bridgeport Brass Company
A Division of National Distillers and Chemical Corporation

SUMMARY

The uniformity of texture values and microstructural observations for alpha-extruded uranium for Mark VB production were evaluated for this interim report. The results, consisting of preferred orientation and irradiation growth indices, grain size, and inclusion distribution data, indicate that the characteristics of the extruded metal are relatively uniform between extruded tubes and stable during the production of hundreds of tubes over periods of months. The variation in properties along the length of the tubes, from front to rear, are discussed. The distinctive inclusion distribution observed in the rear section of some extruded tubes was related to the structure from the bottom of the cast ingots employed for extrusion billets.

INTRODUCTION

A continuing program to inspect the grain structure and orientation of as-extruded uranium tubes is in progress. The data is analyzed to see if it is consistent, indicating the uniformity of the metal produced, or whether significant differences occur, indicating that the fabrication conditions are varying. This information aids us in maintaining control over the process and in the production of high quality extruded metal. In addition, knowledge of the basic characteristics of alpha-extruded uranium and means to improve the properties, if so desired, are accumulated.

A previous report on this program showed that, under the extrusion conditions employed for Mark VB production, the as-extruded metal is all fine grained and the axial preferred orientation varies from front to rear.[1] The (110) poles

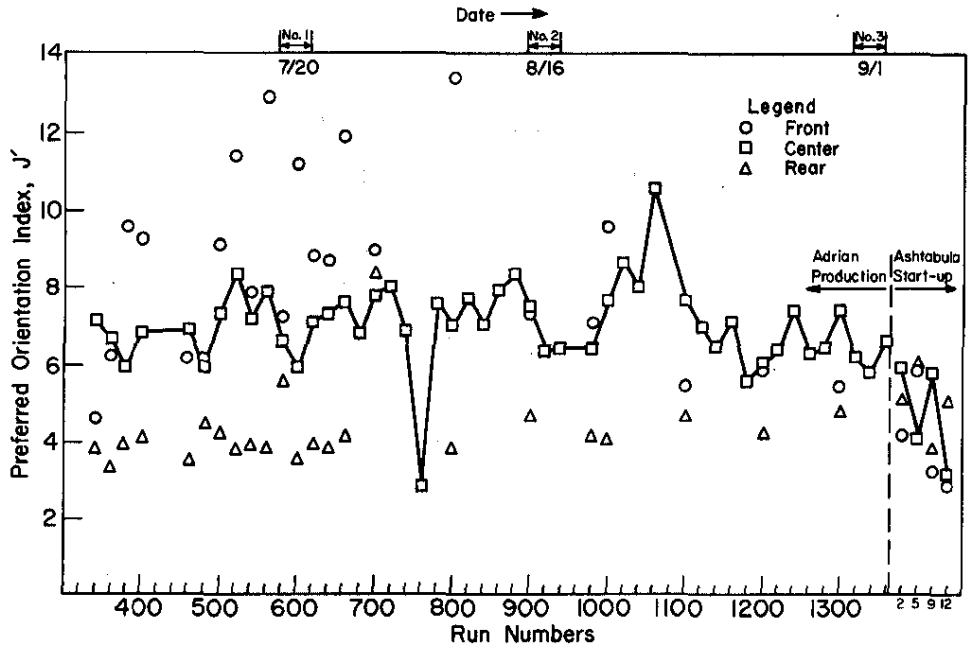

FIG. 1 AXIAL PREFERRED ORIENTATION INDEX DATA FOR AS-EXTRUDED URANIUM MARK VB TUBE SAMPLES

The noted dates were employed to illustrate the within-tube, tube-to-tube, and time-to-time variations (Table I).

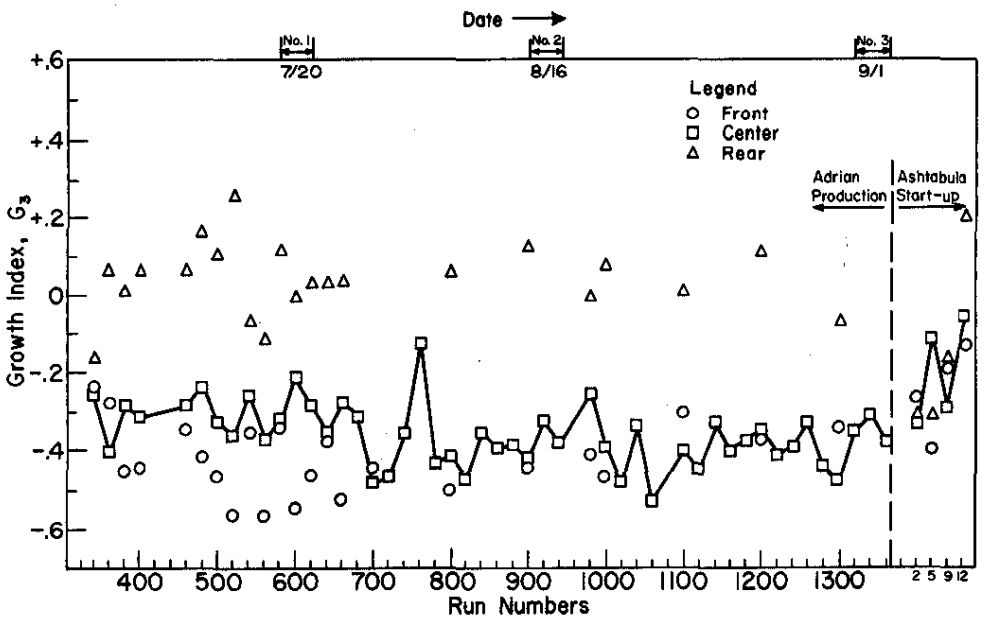

FIG. 2 AXIAL GROWTH INDEX DATA FOR AS-EXTRUDED URANIUM MARK VB TUBE SAMPLES

The noted dates were employed to illustrate the within-tube, tube-to-tube, and time-to-time variations (Table II)

are preferentially oriented in the front, and this changes to preferred (130) poles at the rear of the extruded tube. The differences in texture result in a front-to-rear increase in growth index and decrease in PO index (J') (Figures 1 and 2). The type of texture change suggests that the effective working temperature is decreasing towards the rear of the extruded tube.

Additional data has been obtained for evaluating the preferred orientation and microstructure. It is some of this data which is presented in the following interim report.

PROCEDURES

The procedures employed were essentially the same as those presented in detail in the previous report.[1] Briefly, they are are as follows:

Cast hollow ingots of unalloyed, reactor-grade uranium are cut in half to provide two extrusion billets, a "B" billet from the bottom half of the ingot and a "T" billet from the top half. The billets are triple beta treated and then heated to 1170°F (632°C) in molten chlorides (Liquid Heat H-980). The 7-3/8-inch-OD x 2-inch-ID x 20-inch-long billets are extruded out of a 7.50-inch liner to 2.81-inch-OD x 1.85-inch-ID x 20-foot-long tubes employing an 11.4:1 area reduction ratio, a ram speed of 15-20 inches/min, and a tool temperature of 650°F (343°C).

Transverse ring samples are taken 6 inches from the front, from the midlength, and from the last good metal at the rear of every 20th extruded tube for our metallographic and X-ray diffraction laboratory evaluations. This report includes data for 48 as-extruded tubes, representing 1020 pushes, from the production at our Adrian plant, and for four tubes selected from the start-up trial at our new Ashtabula plant extrusion facilities. The Adrian plant data represents 2-1/2 months of Mark VB production at that facility. Three dates were chosen to represent the variation in properties during production over a period of time at the Adrian site. The dates cover a period of about six weeks and each date is separated from the next one by at least two weeks. In addition, this data is compared to the limited data for tubes produced during the first extrusion day at the new Ashtabula plant.

Transverse surfaces were prepared for metallographic and X-ray diffraction evaluations employing conventional techniques and ending in fine mechanical polishing and electropolishing to remove any cold work from the surface of the mounted composite

specimens. To evaluate the axial texture coefficients (P_1), the irradiation growth index (G_3), and the preferred orientation index (J'), Morris's area weight method for an 18-plane set of diffraction lines was employed. The equipment and methods consisted of a Geiger-counter X-ray diffractometer, nickel-filtered copper radiation (40 kv - 20 ma), a rotating flat-specimen holder, a scanning speed of 1° (2θ)/min, and divergence-, receiving-, and scatter-slits of 1°, 0.003 inch, and 1°. Integrated X-ray line intensities were measured with a planimeter. A computer program was employed to calculate P_1, G_3, and J'.

The microstructure was evaluated employing (a) the conventional 100X, polarized-light grain size chart for alpha uranium and (b) a set of 100X, bright-field photomicrographs showing the three distinguishable types of inclusion distributions which have been observed in the as-extruded Mark VB tubes (Figure 3). A test showed that only about 5% of the cases of assigning inclusion distribution involved any doubt as to which of two possible inclusion rating groups to designate for the photomicrograph of a sample. These few cases were resolved by close inspection by two observers.

DISCUSSION OF RESULTS

The grain structure and orientation data for the Mark VB production at Adrian are relatively uniform for the period of months observed. There were only a few erratic points, and no significant trends were noted during this period, on the basis of the PO index (J'), growth index (G_3), and grain size values for samples from the center of the extruded tubes (Figures 1 and 2 and Table III). These figures also illustrate the variation in structure from front to rear. In addition, the values for the Ashtabula start-up trial fall within the range obtained from the Adrian production. Additional data will be required to determine whether the Ashtabula values may have shifted due to the change in facilities. The consistency of the texture and grain structure are discussed in further detail in the following sections.

TEXTURE

The results obtained from the axial PO index (Table I and Figure 1) and growth index (Table II and Figure 2) data are in general agreement. They will be discussed together in terms of the difference found

- within a tube, i.e., between locations along the length

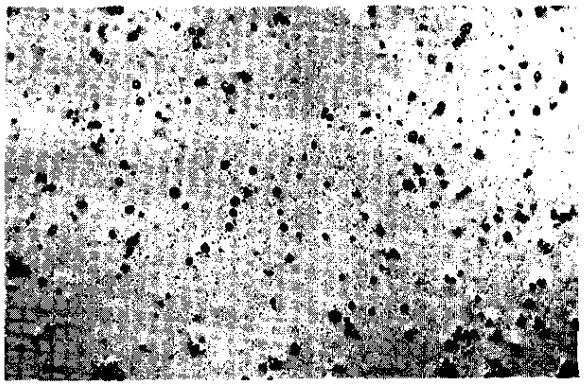

a. Type A Inclusion Distribution

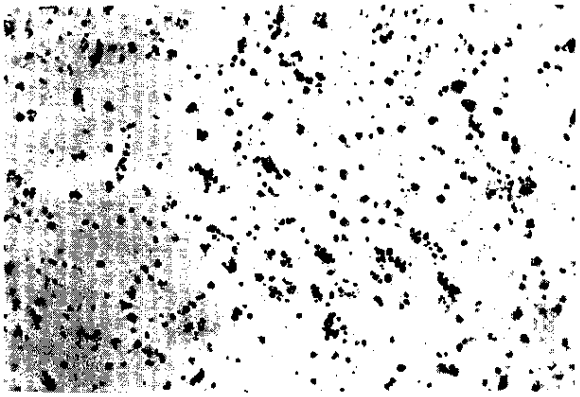

b. Type B Inclusion Distribution

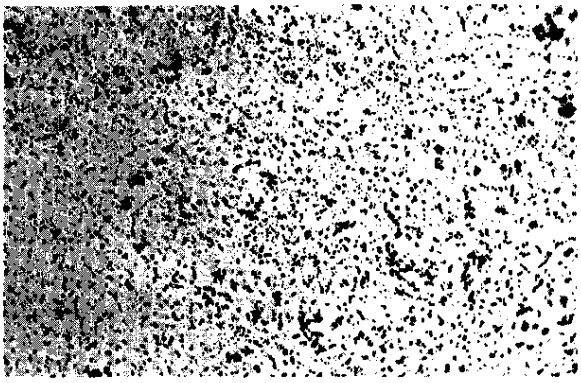

c. Type C Inclusion Distribution

FIG. 3 REPRESENTATIVE TYPES OF INCLUSION DISTRIBUTIONS OBSERVED IN AS-EXTRUDED MARK VB TUBES (Bright Field, 100X)

Type C inclusions have been observed always and only in samples from the rear of tubes from "B" (bottom) billets (Table III).

TABLE I

Representative Longitudinal Preferred Orientation Index Values for As-Extruded Uranium Tubes Mark VB Production

(Numbers in brackets are the Extrusion Run No.)

A. PO Indices Along the Length of Tubes Extruded During the Same Day (7/20)

Tube Designation	PO Index, J' (axial)				
				Within Tubes	
	Front	Center	Rear	Avg	Range
[580]	7.20	6.56	5.64	6.47	1.56
[600]	11.15	5.92	3.48	6.85	7.67
[620]	8.80	7.08	3.90	6.59	4.90
Tube-to-Tube: Avg	9.05	6.52	4.34		
Range	3.95	1.16	2.16		

B. PO Indices for Tubes Extruded on the Same Day and Over a Period of Months (Data for samples from the center of tubes)

Tube Designation	PO Index, J' (axial)			
	Adrian Production			Ashtabula Start-up Trial
	Day #1 (7/20)	Day #2 (8/16)	Day #3 (9/1)	
A	6.56 [580]	7.40 [900]	6.05 [1320]	5.80 [2]
B	5.92 [600]	6.28 [920]	5.68 [1340]	4.00 [5]
C	7.08 [620]	6.32 [940]	6.48 [1360]	5.68 [9]
D	-	-	-	3.04 [12]
Tube-to-Tube: Avg	6.52	6.67	6.07	4.63
Range	1.16	1.12	0.80	2.76

Time to Time: Grand Avg $\bar{J}'$ = 6.42 Range of Averages = .060

TABLE II

Representative Longitudinal Growth Index Values for As-Extruded Uranium Tubes Mark VB Production

(Numbers in brackets are the Extrusion Run No.)

A. Growth Indices Along the Length of Tubes Extruded During the Same Day (7/20)

Tube Designation	Growth Index, G_3 (axial) Front	Center	Rear	Within Tubes Avg	Range
[580]	-0.33	-0.32	+0.12	-0.18	0.45
[600]	-0.54	-0.21	0.00	-0.25	0.54
[620]	-0.46	-0.28	+0.04	-0.23	0.50
Tube-to-Tube: Avg	-0.44	-0.27	+0.05		
Range	0.21	0.11	0.12		

B. Growth Indices for Tubes Extruded on the Same Day and Over a Period of Months (Data for samples from the center of tubes only)

Tube Designation	Growth Index, G_3 (axial) Adrian Production Day #1 (7/20)	Day #2 (8/16)	Day #3 (9/1)	Ashtabula Start-up Trial
A	-0.32 [580]	-0.42 [900]	-0.35 [1320]	-0.33 [2]
B	-0.21 [600]	-0.32 [920]	-0.31 [1340]	-0.11 [5]
C	-0.28 [620]	-0.38 [940]	-0.38 [1360]	-0.29 [9]
D				-0.05 [12]
Tube-to-Tube: Avg	-0.27	-0.37	-0.35	-0.20
Range	0.11	0.10	0.07	0.28

Time to Time: Grand Avg $\bar{G}_3$ = -0.33 Range of Averages = 0.10

- from tube-to-tube, i.e., between tubes produced on the same day for the midlength position

- from time-to-time, i.e., between tubes produced over a period of months.

The J' and G_3 values varied along the length of the extruded Mark VB tubes. The J' values decreased along the length, and the G_3 values increased from negative values at the front to near zero and slightly positive at the rear. This is attributed to the change in extrusion conditions along the length, e.g. effective extrusion temperature and flow of metal through the die. It is also conceivable that this longitudinal variation could be due to variations in the starting material, e.g. a variation in structure and composition from the top to the bottom of the ingot due to the ingot cooling. The range of values for the samples decreased in the following order: front, rear, and center. Thus, the most consistent values were found for samples from the center of the extruded tubes.

The J' and G_3 values for center samples were relatively uniform between tubes and over a long period of time. The tube-to-tube and time-to-time range values were much smaller than the within-tube variation. In addition, there appears to be a possible trend towards decreasing range values with time over the period studied during the Adrian production. This could occur, for example, if experience and practice led to a gradual decrease in average billet transfer time from the furnace to the extrusion press.

The above results indicate that the area to concentrate on to obtain a more uniform product is to decrease the texture variation along the length of the extruded tubes. Uniformity may potentially be improved by adjusting the extrusion conditions to keep the flow of metal and actual extrusion temperature constant along the length of the tubes by, for example, adjusting the ram speed and tool temperature.

It should be noted that if the extrusion conditions prevailing at the time when G_3 passes through zero, as it increases from front to rear, were determined and could be maintained, it would be possible to produce a fine-grained tube with potential axial dimensional stability during irradiation due to the presence of a "balanced" texture. Longitudinal texture and thermal expansion coefficient gradients can result in dimensional variations and distortion when the slugs are beta-treated.

GRAIN STRUCTURE

Grain Size

The grain size of the metal extruded in the alpha phase was fine grained and relatively uniform (Table III). The size values ranged between 15 and 35 microns. Two types of minor grain size variation along the length of the as-extruded tubes were observed. One type (A) consisted of a general decrease in size from front to rear. The other type (B) consisted of peaking to a maximum grain size in the samples from the center of the tubes. Case A indicates an overall continuous billet cooling during extrusion and a decrease in the working temperature as the metal is extruded through the dies. Case B indicates that an increase in billet temperature predominates toward the end of the extrusion. The predominance is due to (a) overheating from the work of deformation and (b) friction between the work and the tools (the tools loose heat and contract down on the work piece). The finest grain size in a tube was observed in the sample from the rear for the majority of the tubes examined.

Inclusion Distribution

It was observed in all cases that the type C inclusion distribution was always found and only found in samples from the rear of tubes extruded from "B" billets, i.e., billets from the bottom half of cast ingots (Table III). This location corresponds to metal from the bottom position of the ingot, since the extrusion billets employed are obtained by cutting the cast ingots into a bottom and a top half. These billets are placed in the extrusion container liner with the top-facing end surface towards the extrusion die exit, i.e., in the extrusion direction. This unique type C inclusion distribution is distinguished from the other types in that it consists of a relatively heavy and uniform distribution of finer inclusions in comparison to types A and B (Figure 3). Inclusion gradients in the cast ingots could result from gravity segregation of particles with varying densities due to insufficient mixing of the molten metal.

It is likely that the inclusion amount, size, and distribution will influence the mechanical properties and irradiation behavior of the uranium cores. Thus the inclusion variation in the tubes noted above, which is probably retained in the fuel element, could result in some variation in the reactor performance of the metal. If this is the case, then a more uniform structure and properties could be

TABLE III

The Grain Structure of As-Extruded Uranium Tubes
Mark VB Production

Extrusion Billet No.(a)	Tube Designation (Run No.)	Sample Location	Grain Size, mm	Inclusion Distribution Type (See Figure 3) A	B	C
92399-T	340	Front	.033	X		
		Center	.033		X	
		Rear	.027		X	
92350-B	360	Front	.027		X	
		Center	.027	X		
		Rear	.020			X
92475-T	380	Front	.015	X		
		Center	.020		X	
		Rear	.015		X	
92374-T	400	Front	.015	X		
		Center	.027		X	
		Rear	.020		X	
92594-T	460	Front	.020	X		
		Center	.027	X		
		Rear	.020		X	
92586-T	480	Front	.033	X		
		Center	.027		X	
		Rear	.020		X	
92592-T	500	Front	.020	X		
		Center	.027	X		
		Rear	.020		X	
92512-T	520	Front	.027	X		
		Center	.020		X	
		Rear	.015		X	
92582-B	540	Front	.020	X		
		Center	.027	X		
		Rear	.020			X
92664-B	560	Front	.027	X		
		Center	.027	X		
		Rear	.020			X
92623-T	580	Front	.033	X		
		Center	.027		X	
		Rear	.020		X	
92611-B	600	Front	.020	X		
		Center	.025		X	
		Rear	.018			X
92370-T	620	Front	.033		X	
		Center	.033	X		
		Rear	.025		X	
92602-B	640	Front	.025	X		
		Center	.033		X	
		Rear	.020			X
92763-B	660	Front	.020		X	
		Center	.020		X	
		Rear	.020			X
92783-T	800	Front	.020	X		
		Center	.020		X	
		Rear	.015		X	
92833-B	1100	Front	.027	X		
		Center	.027		X	
		Rear	.020			X

(a) T = billet from top half of cast ingot; B = billet from bottom half of ingot.

obtained be, e.g., some adjustment of the casting procedures or modification of the beta heat treatment conditions, or by removing or excluding the metal from the bottom of the cast ingot. The latter may be accomplish by cutting and scrapping a slice from the bottom of the ingot or cropping a longer length from the rear of tubes extruded from bottom ("B") billets.

CONCLUSIONS

1. The texture of the as-extruded tubes from the Mark VB production at Adrian varies along the length of the tubes.

2. The texture and grain size at the same location in the tubes are relatively uniform from extruded tube to tube, during the extrusion of hundreds of Mark VB tubes produced over a period of months.

3. A significant trend or change in texture and microstructure characteristics was not observed during Mark VB production over a period of months. In general the texture is strong and the grain size is fine.

4. The unique inclusion distribution observed at the rear of tubes extruded from "B" billets is apparently related to the "different" structure at the bottom of cast ingots.

FUTURE WORK

Additional data will be obtained so that Mark VB production at the Ashtabula facility can be analyzed. This will include a change in the uranium composition of the billet stock from unalloyed to low-additive material. The evaluations will be expanded to include additional data such as dimensions and perhaps extrusion pressures, to obtain further details on the characteristics of the extruded metal. Special tests will be made to substantiate the reported quality variations on a within tube, tube-to-tube, and time-to-time basis.

REFERENCES

1. Robins, L. "Axial Textures In As-Extruded Uranium Tubes - Mark VB Production." Papers Presented at the X-Ray Preferred Orientation Meeting Held at Nuclear Metals, Inc., on December 7-8, 1961. R. B. Russell, Comp. Nuclear Metals, Inc., West Concord, Mass. USAEC Report NMI-4992, pp. 52-61

(1963). See also: Garufi, M. F., R. J. Wallionis, and L. Robins. "Axial Textures in As-Extruded Uranium Tubes - Mark VB Production." Quarterly Progress Summary, July to September, 1962. Bridgeport Brass Co., Seymour, Conn. USAEC Report BRB-72, pp. 27-33 (1963).

TEXTURES IN ALPHA URANIUM WHICH HAD BEEN GAMMA EXTRUDED

J. W. Starbuck

Mallinckrodt Chemical Works

SUMMARY

X-ray diffraction measurement of orientation in alloyed dingot uranium that had been gamma-extruded revealed near random structures in the axial direction. A tendency toward slight excess of [002], [023], [022], and [021] poles parallel to the extrusion axis was observed.

INTRODUCTION

With an ultimate goal of achieving a process for gamma extruding 1.5-inch-diameter rods directly from a dingot, an interim two-step process has been used for development purposes. Boland et al.[1] reported results of heat treating core blanks from a two-step gamma extrusion. Since a high degree of randomization was found in the beta-treated rods, information concerning the axial textures of as-gamma-extruded rods was desired. An additional incentive for this investigation is the absence from the literature of studies of the crystallographic orientation in as-gamma-extruded uranium. This report contains the results of preliminary studies.

EXPERIMENTAL

The material studied was alloyed dingot uranium containing 160 ppm iron and 110 ppm silicon as additives. The fabrication history consisted of gamma extrusion of the dingot to a 6.4-inch-diameter billet. An 18-inch section was heated in a salt bath to 1600-1625°F for 2 hours. The billet was then extruded via a double-hole die arrangement that yields two 1.5-inch-diameter rods. Four transverse samples were taken near each of three locations - 12, 44, and 88 inches,

respectively, as measured from the lead end of the rod. (This corresponds to the 2nd, 6th, and 11th core positions.) A typical macrostructure of this material is shown in Figure 1.

FIG. 1 PHOTOMACROGRAPH OF AS-GAMMA-EXTRUDED, ALLOYED DINGOT URANIUM STRUCTURE
(3X; HNO_3, HCl macroetch)

The texture measurements were determined in accordance with procedures and parameters described in the reports NLCO-804[2] and ANL-6359.[3] A statement concerning texture in metal with such large grains as gamma-extruded uranium necessitates sampling a large cross-sectional area. To do this, a special flat specimen spinner was used which allows X-ray scanning of an annular area having a 0.46-inch ID and a 1.22-inch OD.

RESULTS AND DISCUSSION

X-ray intensity data were gathered from a single scan of each of the twelve transverse sections, and computations

by the integral and area weight methods were carried out for each. The statistical summaries of these data are shown in Tables I and II.

These data indicate the tendency for a small but statistically significant amount of [002], [023], [022], and [021] axial texturing. This texturing is possibly the result of cooling through the beta-to-alpha transformation, wherein the resultant [200] radial texture would lead to the build-up in the axial direction of the above mentioned poles which are perpendicular to the [200] pole. A study of the radial texture may verify this.

The indicated orientation parameters J and J' are, no doubt, biased high by virtue of their sensitivity to the individual scans wherein a single measured plane could be deficient due to the large-grained material. This is borne out by the results of summing the measured X-ray intensities from the 12 scans and computing on a single sample basis. Under these conditions the J and J' factors were 1.05 and 1.06, respectively.

CONCLUSIONS

Alpha uranium which had been gamma extruded and air cooled shows very little preferred orientation in the axial direction. This conclusion must be restricted to the central 1.2 inches of a 1.5-inch-diameter rod.

FUTURE WORK

Study of gamma-extruded textures will continue on material which was held at higher temperatures prior to extrusion. Efforts will be made to characterize the axial and radial textures which might develop.

ACKNOWLEDGMENT

The contributions of Mr. G. R. Gower to the experimental work and of Mr. S. H. Huston to the statistical evaluation of data are gratefully acknowledged.

TABLE I

Axial Texture Data - Integral Method

hkl	Avg P (u,Φ)	Uncertainty of Mean (95% C. L.)	Range
020	1.09	0.27	0.56 - 1.85
110	1.04	.16	0.65 - 1.09
020	1.22	.22	0.82 - 1.99
002	1.44	.20	1.17 - 2.22
111	0.77	.11	0.43 - 1.06
022	1.47	.30	0.99 - 2.55
112	0.73	.12	0.45 - 0.95
130	0.89	.17	0.51 - 1.15
131	0.85	.08	0.72 - 1.09
023	1.55	.33	0.96 - 2.80
200	1.02	.13	0.70 - 1.40
041	1.11	.15	0.68 - 1.41
113	0.90	.10	0.69 - 1.26
132	0.89	.16	0.53 - 1.26
133	1.04	.13	0.57 - 1.30
114	1.05	.10	0.88 - 1.44
150	0.94	.17	0.55 - 1.33
223	0.70	.13	0.34 - 1.00
152	0.97	.13	0.63 - 1.19
312	0.86	.13	0.65 - 1.37
Avg G_2 =	+0.046	.024	-0.031 - +0.081
Avg J =	1.11	.05	1.02 - 1.31

TABLE II

Axial Texture Data - Area Weight Method

hkl	Avg P_1	Uncertainty of Mean (95% C. L.)	Range
020	1.04	0.31	0.50 - 2.07
110	1.02	.17	0.60 - 1.75
021	1.22	.27	0.76 - 2.26
002	1.41	.24	0.88 - 2.36
111	0.85	.11	0.59 - 1.10
112	0.77	.12	0.50 - 1.05
130	0.85	.18	0.35 - 1.34
131	0.99	.15	0.69 - 1.63
023	1.76	.46	1.01 - 3.18
200	1.08	.14	0.74 - 1.43
113	0.95	.16	0.70 - 1.52
132	0.90	.17	0.55 - 1.30
133	0.90	.12	0.58 - 1.32
114	1.04	.18	0.70 - 1.62
150	0.90	.20	0.38 - 1.49
223	0.68	.12	0.42 - 1.07
152	0.98	.15	0.68 - 1.45
312	0.79	.25	0.49 - 1.93
Avg G_3 =	+0.045	.037	-0.048 - +0.100
Avg J' =	1.17	.07	1.03 - 1.40

REFERENCES

1. Boland, J. F., H. C. Kloepper, Jr., and N. F. Neumann. "Heat Treatment of Gamma-Extruded Uranium Rods". Process Development Quarterly Progress Report July-September 1961, J. A. Nelson, Ed. Mallinckrodt Chemical Works, Uranium Division, Weldon Spring, Mo. USAEC Report MCW-1469, pp. 37-42 (1961).

2. Morris, P. R., Ed. Papers Presented at the X-ray Preferred Orientation Meeting Held at National Lead Company of Ohio, November 9-10, 1959. National Lead Company of Ohio, Cincinnati, Ohio. USAEC Report NLCO-804 (1960).

3. Mueller, M. H., Ed. Papers and Discussion from the X-ray Preferred Orientation Meeting Held at Argonne National Laboratory, December 15-16, 1960. Argonne National Laboratory, Argonne, Ill. USAEC Report ANL-6359 (1961).

SUMMARY REPORT ON THE STUDY OF BETA TREATMENT OF URANIUM*

R. B. Russell and A. K. Wolff

Nuclear Metals, Inc.

Unalloyed dingot and ingot rods and tubes have been studied for a variety of beta treatments. Tube outer diameters ranged from 4 to 1 inch, inner diameters from 3.5 to 0.5 inch, and wall thicknesses from 0.9 to 0.1 inch. Rod diameters were 1.8, 1.1, and 0.5 inch. Certain auxiliary studies involved 1-inch-diameter discs 0.03 inch thick. Cooling rates from the beta phase ranged from about 800 to 1°C/sec. The degree of preferred orientation (texture) has been described chiefly by the growth index, G_3, which predicts the direction and extent of anisotropic growth in alpha uranium under neutron irradiation.

GRAIN SIZE AND SHAPE

Delta Condition

Unalloyed dingot and ingot uranium have been shown to be very sensitive to prior delta heat treatment. A change in delta treatment before a final water quench from the beta phase may cause a shift of about four FEDC grain size numbers.

Beta Treatment Time and Temperature

Grain sizes found after oil quenching 1-inch-diameter by 1/4-inch-thick ingot discs that were beta treated over ranges of 2 to 64 minutes at 690 to 755°C were slightly coarser (1/2 to 1 FEDC grain size) in the region of 10 to 64 minutes at 690 to 735°.

Cooling Rate

For a given delta condition, the cooling rate from the beta phase is of major importance in determining the final

* A more complete report of this work was published as USAEC Report NMI-2807 (1963).

alpha grain size, which is usually finest for a water quench, intermediate for oil, and coarsest for an air cool. The macro (3X) grain size or shape does not provide a good indication of the extent or severity of texture present.

Air Delay Before Oil Quenching

An air delay before oil quenching coarsens the grain size towards the size realized by an ordinary air cool.

Recrystallization

Post-beta-treatment recrystallization at 600°C slightly refines the grain size, except in the case of air-cooled specimens, which do not recrystallize.

Applied Stress

Limited experiments on the application of stress in the beta phase, beta-alpha phases, and high alpha phase do not show any detectable effect on the final alpha grain size or shape.

DISTORTION

Most of the dimensional changes seem to be caused by the difference in texture before and after beta treatment. The relation between percent length and diameter changes (ΔL and ΔD) in rods, and the axial G_3 before beta treatment, is given approximately by the relations

$$\% \Delta L = -2.2\ G_{3Ax} - 0.23$$

$$\% \Delta D = +0.64\ G_{3Ax}$$

Distortion after beta treatment is more uniformly distributed with slower cooling rates from the beta phase; the effect, in rods, of increasing the cooling rate is generally to increase the tendency to lengthen or to decrease the tendency to shorten.

In tubes the relation between dimensional changes and G_{3Ax} before beta treatment is not apparent from plots that show large scatters in this relationship.

No differences in distortion have so far been observed among beta-treated pieces with different delta histories.

In general, no differences in distortion can be attributed to compositional differences between dingot and ingot.

TEXTURE AND GROWTH INDEX

Radial Texture Distribution

A preferred orientation (texture) of crystallites is induced by any cooling rate (within the range studied) from the beta phase. This texture is such that the G_3 is negative parallel to the thermal gradient experienced by the uranium during cooling from the beta phase. The induced texture tends to vanish (G_3 approaches zero) when the thermal gradient vanishes, as in the radial direction near the midwall of tubes or near the center of rods. These characteristics of induced texture cause the radial distribution of radial G_3 to have a large negative value at the cooling surfaces and an approximately zero value at a tube midwall; accordingly, the G_3 distribution curve usually assumes an inverted "U" shape in both dingot and ingot. In one case (beta quench of dingot into 500°C molten salt) a "U" radial G_3 distribution was observed.

Parameters have been introduced to describe the degree of radial texture penetration or the extent of total texture induced by beta treatment:

radial merit = $w_o/2r$

where r is the radial depth where G_3 has increased to -0.10

integrated net radial texture, $\pi_r = \int_0^{w_o} G_3(2r/w_o)\, dr$

integrated absolute radial texture, $|\pi_r| = \int_0^{w_o} |G_3(2r/w_o)\, dr|$

where w_o is the wall thickness, and

$G_3(2r/w_o)$ is the experimental curve showing the dependence of radial G_3 on radial depth expressed as $2r/w_o$.

Larger values of radial merit indicate shallower texture penetration.

Beta Treatment Time and Temperature

Beta treatment times longer than 8 minutes at beta temperature do not affect final G_s after an oil quench, but shorter times seem to make G_s slightly more negative.

No effect of beta temperatures between 695 and 755°C is observed on the G_s after an oil quench.

Dingot was not studied under these conditions.

Prior Delta Condition

In drastically quenched ingot and dingot bars that have enough differences in delta histories to cause a grain size change, a G_s increase of about 0.01 is associated with a unit decrease in FEDC grain size number.

Cooling Rate from Beta Phase

In ingot, the severity of induced radial texture penetration as judged by radial merit is influenced substantially by the cooling rate R_β, but in dingot is somewhat less influenced by cooling rate. Cooling rates of about 50 to 100°C/sec produce the shallowest texture penetration in ingot, but dingot seems less sensitive to this rate. However, a study of the effect of cooling rate in integrated radial texture in both ingot and dingot shows that slow cooling rates (less than about 2°C/sec) and fast cooling rates (greater than about 200°C/sec) produce substantially more integrated texture than intermediate cooling rates (about 50 to 100°C/sec).

Comparison of OD and ID Tube Integrated Textures

In general, the asymmetry in radial G_s radial distribution is greater in tubes with lower ID:wall ratios, where the circulation of the cooling medium is somewhat more restricted. A study of 45 tubes of different sizes and cooling rates showed that an average of about one half of the total integrated texture developed was formed on the outer cooling surfaces, and that there was about twice as much texture on the outer surfaces as on the inner surfaces of tubes.

Air Delay Before Oil Quench

An air delay before an oil quench increased the radial texture penetration in ingot, and an increase in air delay increased the texture penetration toward the maximum found after an ordinary air cool.

Hot-Salt Quenching of Thin Discs

A study of surface G_3 on thin (0.030-inch) ingot and dingot discs quenched from the beta phase into molten salt at 660 to 200°C for 10 minutes at temperature and then water quenched indicated that there is a region of hot-salt quenching temperatures that produces the least textured transformation products by quenching in Houghton LH-235 salt at 550 to 425°C; except, that the least textured products in ingot correspond to a surface G_3 of about -0.10, and in dingot to a surface G_3 of about -0.16 at these temperatures. However, if a different molten salt (Houghton DT-275) is used on dingot discs at these temperatures, the texture appears to vanish at a quench temperature of about 535°C. (Ingot discs have not been studied under the same conditions.)

The study of thin discs indicated strongly that a certain range of hot-salt quenches of dingot tubes would lead to a decreased penetration of radial texture as compared with that induced by continuous cooling.

Hot-Salt Quench of Tubes

A limited study of hot-salt (Houghton Draw-Temp 275) quench (10 minutes in bath) of 1.5 inch-OD by 0.5-inch-ID ingot tubes at 400 or 200°C and dingot tubes at 500, 400, and 300°C showed that intermediate quenching rates (R_β) can be obtained and that these intermediate rates, like those allowed by oil quenches, successfully produce shallow texture penetration and small values of integrated radial texture. Results on both ingot and dingot indicated that, for this size, hot-salt quench temperatures of 400 to 500°C induce less texture than do lower temperatures.

Internal Free Surfaces

The insertion of internal free surfaces within ingot bar is found to cause a sharp positive increase in G_3 in a direction perpendicular to the free surface at the interface, after a drastic quench, when the interface is in a region of

high thermal gradient and in a region believed to have a very low thermal gradient, but not at an intermediate gradient. A further study of drastically quenched ingot and dingot bars electroplated with 0.002-inch nickel seems to confirm the sharp increase in G_α in a high thermal gradient near the plating. The same results were not found in ingot tube under 0.020 to 0.005 inch of Zircaloy cladding, possibly because of a superior metallurgical Zircaloy-uranium interface, or a greater similarity of thermal conductivity between Zircaloy and uranium, which would not cause such a large interruption of the thermal gradient as may have occurred under the nickel electroplate.

Applied Stress

Stress applied during the beta-to-alpha transformation seems to be more effective in modifying induced textures than stress applied only in the beta phase, but the reason is not understood.

INFLUENCE OF FABRICATION CONDITIONS ON THE GRAIN STRUCTURE AND ORIENTATION OF EXTRUDED URANIUM TUBES

M. F. Garufi, R. J. Wallionis, and L. Robins

Bridgeport Brass Company
A Division of National Distillers and Chemical Corporation

SUMMARY

A "random balance" designed extrusion experiment, employing 28 unalloyed, reactor-grade uranium billets, was performed. The objective of the experiment was to screen the effects of many extrusion conditions on the quality of the as-extruded tubes, to determine the few most significant conditions to work with for optimization purposes. The eight independent variables, each of which was randomly varied between a low and a high level value during the 28 extrusion runs, were as follows:

(a) Billet location: bottom vs. top half of ingot (7-3/8-inch-diameter x 42-inch-long cast hollow ingots)
(b) Billet furnace temperature: 550°C vs. 625°C
(c) Extrusion tooling temperature: 232°C (450°F) vs. 468°C (875°F)
(d) Billet area reduction ratio: 12:1 vs. 19:1
(e) Cone angle (for flow-type extrusion): 60° vs. 130°
(f) Billet transfer time (furnace-to-press): 1.1 min vs. 1.5 min
(g) Ram speed: 15 in/min vs. 45 in/min
(h) Cooling medium for the hot-extruded tube: air vs. water-spray quench

The range of measured values for the dependent variables, employing data for samples from the midlength of the alpha-phase extruded tubes only, were as follows:

(a) Preferred orientation index (axial J'): 4.9 to 10.6
(b) Growth index (axial G_3): -0.51 to -0.08
(c) Grain size: 0.012 to >0.1 mm (coarse)

(d) Coarse-grained area (in duplex or fine- and coarse-grained structure): 0 to 55% of the cross section (the majority of the tubes were all fine grained)
(e) Hardness: 75 to 80 R_G

The data from each set of test results were plotted on a scatter diagram for each of the eight variables. The evaluations showed that the most important factors influencing the dependent variables were as follows:

(a) Preferred orientation: area reduction ratio and cone angle
(b) Grain size: billet furnace temperature and ram speed
(c) Hardness: ram speed and billet temperature

The complete and detailed report will be published in the future as a BRB issue. The report will include evaluations of texture coefficients (P_{hkl}), dimensional variations in the extruded tubes (eccentricity, ovality, and I. D. range), and extrusion data (pressures, tool temperature changes during each run). The characteristics will be evaluated along the length of the tubes. The significance of each independent variable and the analyses of interactions will be presented.

SLIP AND TWINNING IN ALPHA-URANIUM SINGLE CRYSTALS SUBJECTED TO COMPRESSIVE LOADING*

P. R. Morris

National Lead Co. of Ohio

Abstract

Stereographic projections have been prepared of the fraction of an arbitrarily directed compressive stress resolved as shear stress on the (010) – [100] slip system, and on the various modes of the {130} – <310>, {~172} – <312>, and {~176} – <512> twinning systems. In the {130} and {176} systems, the $(\bar{1}30)$ – $[\bar{3}\bar{1}0]$ and $(\bar{1}76)$ – $[\bar{5}\bar{1}\bar{2}]$ modes are favored. In the {172} system, a composite projection indicating regions favoring the $(\bar{1}72)$ – $[\bar{3}\bar{1}2]$, $(\bar{1}7\bar{2})$ – $[312]$, and $(17\bar{2})$ – $[3\bar{1}\bar{2}]$ modes has been prepared. Estimates of critical shear stresses for {130} and {172} twinning of ~0.74 kg/mm^2 and ~0.89 kg/mm^2, respectively, have been drawn from the work of Lloyd and Chiswik. If a critical shear stress for {176} twinning exists, it must be of the order 10 kg/mm^2.

Introduction

Uranium fuel elements undergo dimensional changes during neutron irradiation. These dimensional changes, if excessive, can seriously impair reactor operation. For this reason, considerable effort[1,2,3,4,5,6,7,8] has been devoted to the development of theories for the prediction of such dimensional changes. These theories seek to combine the directional dependence of certain physical processes in an alpha-uranium single crystal according to the frequency of crystals in each orientation.

Previous Work on Project

Experimental preferred orientation data were used[9] to test the adequacy of a previously proposed[5] elastic solution. For the irradiation conditions assumed, the stresses calculated from the elastic solution were well in excess of those required for the initiation of creep and plastic flow. The elastic solution is thus considered inadequate. The form of a solution incorporating the effects of creep and plastic flow has been proposed.[10]

Objective

The objective of this work is the development of a satisfactory theory for the prediction of dimensional changes which uranium fuel elements undergo during irradiation.

Discussion

In a previously proposed[10] form of a solution for the prediction of dimensional changes of uranium fuel cores during irradiation, the following were assumed:

1. Anisotropic irradiation growth experienced by individual crystallites is unaffected by stresses of the magnitude which can be occasioned by mechanical constraints.

2. In general, the strains produced in neighboring crystallites by anisotropic irradiation growth will be incompatible due to differences in spatial orientation. The preservation of a continuous medium requires compatibility of strain between neighboring crystallites. This compatibility is achieved initially by an elastic adjustment resulting in the creation of stresses which vary from point to point within an individual crystallite. As irradiation proceeds, these stresses increase.

3. Stress relief is provided by the mechanisms of creep and plastic flow. As in all crystalline materials, the applied stress necessary to cause plastic deformation in an alpha-uranium single crystal displays a pronounced dependence on the crystallographic direction in which the stress is applied. The dependence of strain rate on stress and temperature (creep) is also expected to be a function of crystallographic direction.

* Paper reproduced from USAEC Report NLCO-855.

A mathematical description of the proposed solution incorporating plastic flow requires the definition of yield criteria for the various deformation mechanisms which are expected to be active in the temperature range of interest. Deformation mechanisms operative in alpha-uranium single crystals at room temperature, reported by Lloyd and Chiswik,[11] and arranged in order of frequency of occurrence and ease of operation are: (1) (010) – [100] slip, (2) {130} twinning, (3) {~172} twinning, and (4) kinking, cross-slip, {176} twinning, and {011} slip. The resolved critical shear stress for slip on the (010) – [100] slip system is reported as 0.34 kg/mm^2. In subsequent work,[12] the authors report a value of 0.29 kg/mm^2 for the initiation of (010) – [100] slip at 600°C. Butcher[13] has observed (010) – [100] slip, {130}, and {172} twinning at 450°C and observes that operative deformation mechanisms at this temperature are very similar to those at room temperature.

We may conclude from this evidence that if satisfactory yield criteria can be obtained for room temperature deformations, these same criteria should suffice between room temperature and 450°C. Strain hardening (which accompanies finite deformation), and stress, strain-rate relationships show definite temperature dependence, and must be considered separately.

In an effort to define yield criteria for alpha-uranium single crystals subjected to compressive loading in the temperature range ~26°C to 450°C, stereographic projections were prepared of the fraction of a compressive stress resolved on the (010) – [100] slip system (Figure 1), and on the {130} (Figures 2a and b), {172} (Figures 3a, b, c, d, and e), and {176} (Figures 4a, b, c, and d) twinning systems. The last projection (Figures 1, 2b, 3e, and 4d) for each system illustrates the favored mode (or modes). In the {130} system, the $(\bar{1}30) - [\bar{3}\bar{1}0]$ mode (Figure 2b) is favored, except along the [010] – [001] boundary, where the $(130) - [3\bar{1}0]$ mode is equally probable. In the

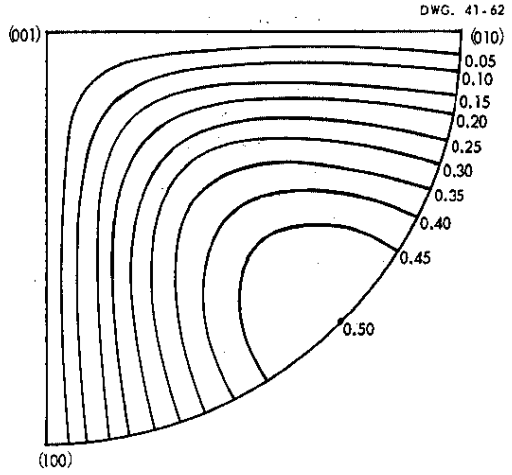

FIGURE 1 Stereographic Projection of Resolved Shear Stress on (010) – [100] Slip System.

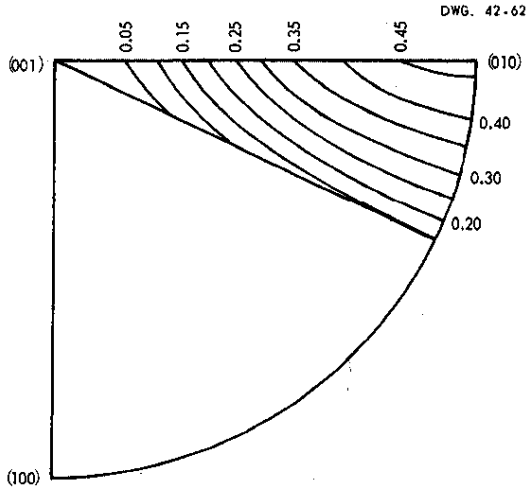

FIGURE 2a Stereographic Projection of Resolved Shear Stress on $(130) - [3\bar{1}0]$ Twin System for Compressive Loading.

{176} system, the $(\bar{1}76) - [5\bar{1}\bar{2}]$ mode (Figure 4d) is favored, except along the octant boundaries. Along the [100] – [010] boundary, the

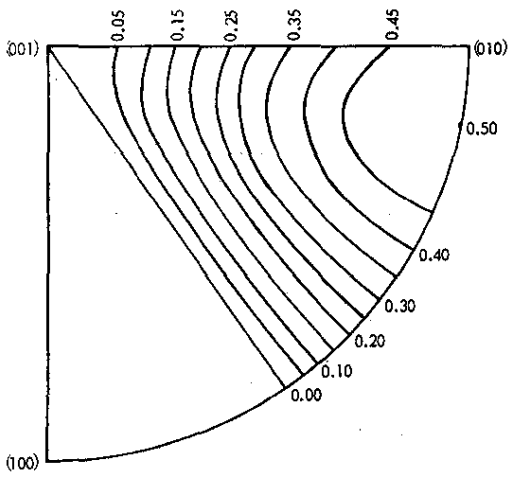

FIGURE 2b Stereographic Projection of Resolved Shear Stress on $(\bar{1}30) - [\bar{3}\bar{1}0]$ Twin System for Compressive Loading.

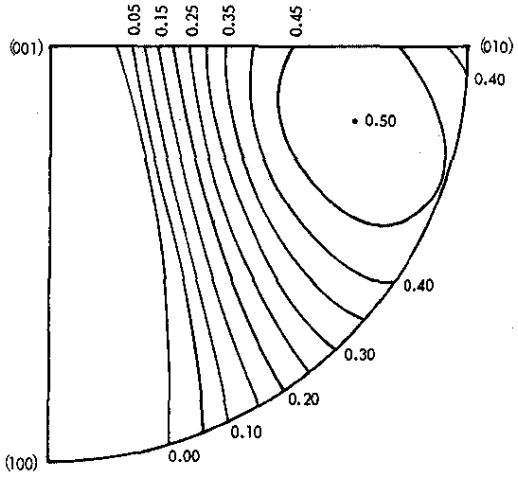

FIGURE 3a Stereographic Projection of Resolved Shear Stress on $(\bar{1}7\bar{2}) - [312]$ Twin System for Compressive Loading.

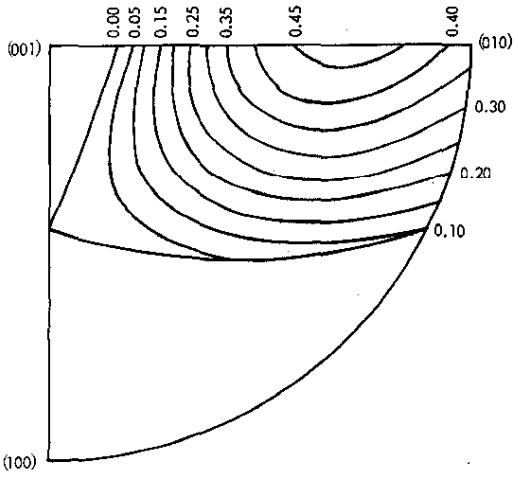

FIGURE 3b Stereographic Projection of Resolved Shear Stress on $(17\bar{2}) - [3\bar{1}\bar{2}]$ Twin System for Compressive Loading.

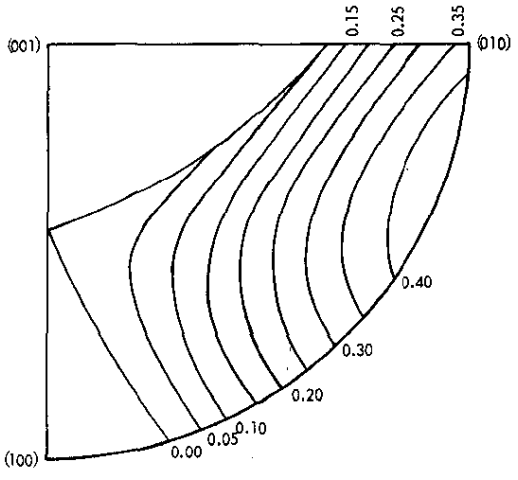

FIGURE 3c Stereographic Projection of Resolved Shear Stress on $(\bar{1}72) - [\bar{3}\bar{1}2]$ Twin System for Compressive Loading.

$(1\bar{7}6) - [5\bar{1}\bar{2}]$ mode is equally probable. Along the [010] – [001] boundary, the $(17\bar{6}) - [51\bar{2}]$ mode is equally probable. Along the [001] – [100] boundary, the $(\bar{1}\bar{7}6) - [\bar{5}\bar{1}\bar{2}]$ mode is equally probable.

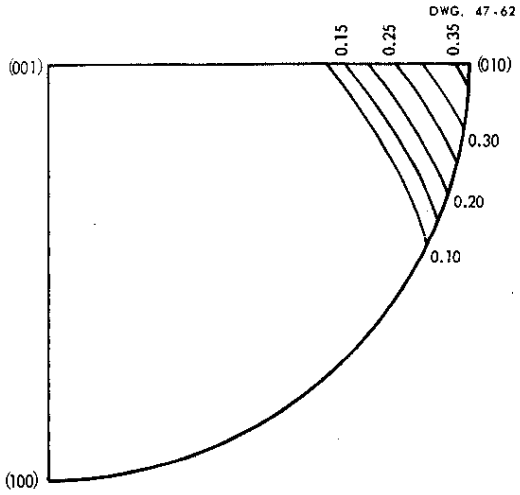

FIGURE 3d Stereographic Projection of Resolved Shear Stress on $(\bar{1}72) - [3\bar{1}2]$ Twin System for Compressive Loading.

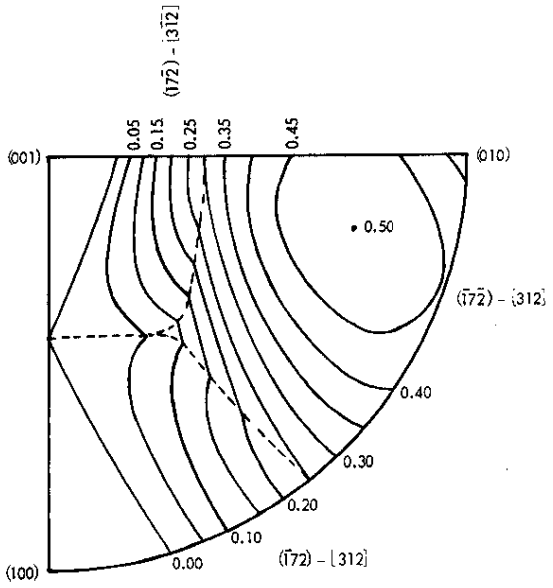

FIGURE 3e Stereographic Projection of Resolved Shear Stress on $\{172\} - \langle 312 \rangle$ Twin System for Compressive Loading.

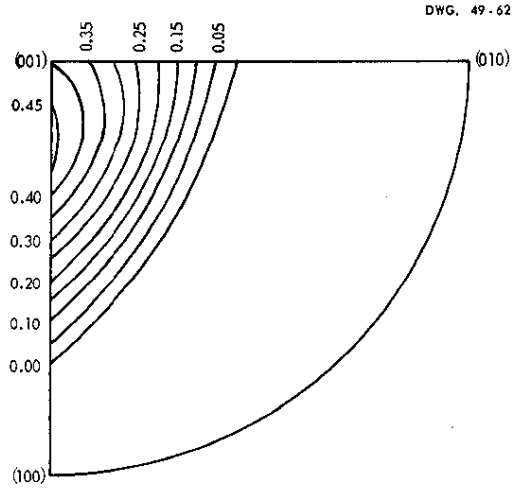

FIGURE 4a Stereographic Projection of Resolved Shear Stress on $(\bar{1}76) - [5\bar{1}2]$ Twin System for Compressive Loading.

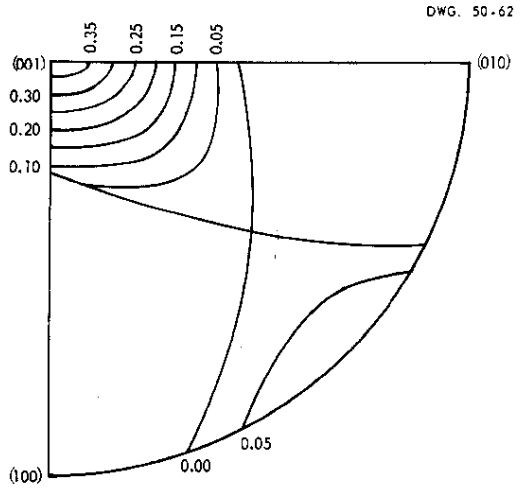

FIGURE 4b Stereographic Projection of Resolved Shear Stress on $(\bar{1}76) - [5\bar{1}2]$ Twin System for Compressive Loading.

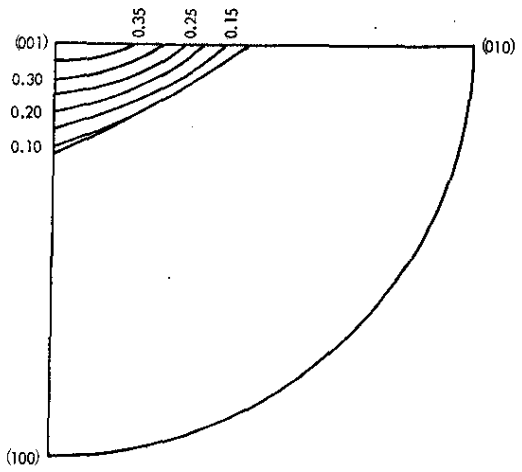

FIGURE 4c Stereographic Projection of Resolved Shear Stress on $(\bar{1}76) - [51\bar{2}]$ Twin System for Compressive Loading.

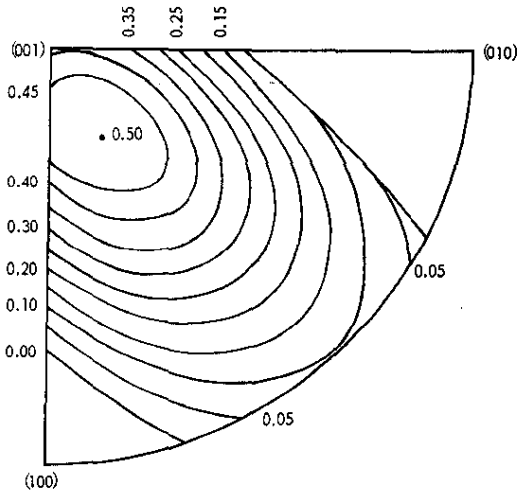

FIGURE 4d Stereographic Projection of Resolved Shear Stress on $(\bar{1}76) - [51\bar{2}]$ Twin System for Compressive Loading.

In the {172} system, a composite projection indicating regions favoring the $(\bar{1}72) - [3\bar{1}2]$, $(\bar{1}7\bar{2}) - [312]$, and $(17\bar{2}) - [3\bar{1}\bar{2}]$ modes has been prepared (Figure 3e).

The data of Lloyd and Chiswik[11], have been employed to form estimates of resolved critical shear stress for {130}, {172}, and {176} twinning. A portion of their Table I is reproduced with additions as our Table 1.

TABLE 1 Crystal Compression Directions and Fraction of Applied Stress Resolved on Various Slip, Twinning Systems

Crystal	Angular Location of Compression Direction With Respect to — (degrees)			Fraction of Applied Stress Resolved on			
	[100]	[010]	[001]	(010) – [100]	{130}	{172}	{176}
I	74	16	89.5	0.265	0.491	0.449	0.000
J	73	24.5	73	0.266	0.442	0.495	0.000
K	32	77	61.5	0.191	0.000	0.029	0.249
L	89	1.5	89.5	0.017	0.472	0.385	0.000
M	64	78	29	0.091	0.000	0.024	0.497
N	19.5	71	89	0.307	0.000	0.024	0.004
O	27	84.5	64	0.085	0.000	0.000	0.154
P	89	61	29	0.008	0.113	0.149	0.312
Q	59	88.5	31	0.013	0.000	0.000	0.441
R	47*	81.5	44	0.101	0.000	0.017	0.398
S	89.5	9.5	80.5	0.009	0.445	0.443	0.000
T	27.5	90	62.5	0.000	0.000	0.000	0.119
U	89.5	27	63	0.007	0.373	0.462	0.000
V	70	49.5	47.5	0.222	0.222	0.277	0.352
W	51.5	46	69*	0.432	0.200	0.317	0.259
X	31.5	64.5	72.5	0.367	0.000	0.114	0.206
Y	46	89	44	0.012	0.000	0.000	0.341

* Corrected value confirmed by L. T. Lloyd.

In these calculations, the following alpha-uranium lattice parameters, determined by M. H. Mueller and R. L. Hitterman of Argonne National Laboratory were employed:

$$a_o = 2.8539 \pm 0.0001\text{A},$$

$$b_o = 5.8691 \pm 0.0001\text{A},$$

$$c_o = 4.9554 \pm 0.0001\text{A}.$$

Using these lattice parameters, we obtain cos α_o = 0.28304, cos β_o = 0.91236, cos γ_o = 0.29578, for the direction cosines of the irrational composition plane for {~172} twinning, and cos α_o = 0.23218, cos β_o = 0.65294, cos γ_o = 0.72095, for the direction cosines of the irrational composition plane for {~176} twinning.

A portion of Lloyd and Chiswik's Table XV is also reproduced as our Table 2.

TABLE 2 **Operative Deformation Mechanism**

Crystal	Operative Twin System			Slip Deformation Mechanism			
	{130}	{172}	{176}	(010)	(010)–(001) Cross-Slip	Kinking	(011)
I	2	–	–	X	–	–	–
J	1	1	–	X	–	–	–
K	–	–	–	X	–	X	–
L	2	–	–	X	–	–	–
M	–	–	–	X	X	–	–
N	–	–	–	X	–	–	–
O	–	–	–	X	–	X	–
P	2	2	–	X	–	–	–
Q	–	–	–	X	X	–	–
R	–	–	–	X	X	–	–
S	2	–	–	X	–	–	–
T	–	–	–	X	X	X	–
U	2	2	–	X	–	–	–
V	1	1	–	X	–	–	–
W	–	–	–	X	–	–	–
X	–	–	–	X	–	–	–
Y	–	–	2	X	X	–	X

Table 3 is obtained from load-contraction curves shown in their Figures 34 to 50. Where evidence of twinning is observed, the loads shown correspond to the load at which twinning was evidenced. Where no evidence of twinning is observed, the loads shown correspond to the maximum applied.

Evidence of {130} twinning is observed in crystals I and L at resolved shear stresses of 0.76 kg/mm^2 and 1.21 kg/mm^2, respectively. Crystal W, with a resolved shear stress of 0.56 kg/mm^2 did not display {130} twinning. Values of 0.56 kg/mm^2 $< \sigma_{130} <$ 0.76 kg/mm^2 are consistent with the data of Tables 2 and 3, where σ_{130} is the critical resolved shear stress for {130} twinning. Both {130} and {172} twinning are observed in crystals J, P, U, and V. The ratios of resolved shear stress for {172} twinning to that for {130} twinning for these four crystals are 1.12, 1.32, 1.24, and 1.25 respectively. In crystals I, L, and S, where the ratios of resolved shear stresses are 0.91, 0.82, and 1.00, {172} twinning is not observed. Since crystal J displayed {172} twinning at a resolved shear stress of 1.57 kg/mm^2, while crystal W did not display {172} twinning at a resolved shear stress of 0.88 kg/mm^2, 0.88 kg/mm^2 $< \sigma_{172} <$ 1.57 kg/mm^2.

The failure of crystal S to display {172} twinning at a resolved shear stress of 4.52 kg/mm^2 seems to indicate a preference for {130} twinning when the ratio of shear stresses is unity. We shall assume $\sigma_{172} \approx 1.2\ \sigma_{130}$. This is in keeping with twinning on both systems at resolved shear stress ratios of 1.12, 1.32, 1.24, and 1.25 observed in crystals J, P, U, and V respectively, and also with the failure of crystals I, L, and S with resolved shear stress ratios of 0.91, 0.82, and 1.00 to display {172} twinning, if we assume twinning to occur on both systems if the critical shear stresses are exceeded, and if the ratio of resolved shear stresses is within approximately 10% of $\sigma_{172}/\sigma_{130}$. We shall choose σ_{130} = 0.74 kg/mm^2, σ_{172} = 0.89 kg/mm^2. The evidence for a critical resolved shear stress for {176} twinning is inconclusive. If a critical stress for {176} twinning exists, it must be of the order 10 kg/mm^2.

Acknowledgment

The writer is indebted to L. T. Lloyd for permission to draw from his report, and for discussions of twinning in uranium.

TABLE 3 Resolved Shear Stresses on Various Twinning Systems

Crystal	Load (lb)	Area (mm^2)	Compressive Stress kg/mm^2	Resolved Shear Stress on		
				{130} kg/mm^2	{172} kg/mm^2	{176} kg/mm^2
I	21*	6.16	1.55	0.76	0.70	0.00
J	44*	6.36	3.17	1.40	1.57	0.00
K	51	4.38	5.29	0.00	0.15	1.32
L	16.5*	2.92	2.57	1.21	0.99	0.00
M	98	3.07	14.5	0.00	0.35	7.21
N	54.5	2.74	9.04	0.00	0.22	0.04
O	52.5	1.72	13.9	0.00	0.00	2.14
P	250	2.13	53.3	6.02	7.94	16.6
Q	105	1.55	30.8	0.00	0.00	13.6
R	67.5	2.86	10.7	0.00	0.18	4.26
S	34	1.52	10.2	4.54	4.52	0.00
T	200	2.63	34.6	0.00	0.00	4.12
U	49.5*	4.49	5.01	1.87	2.31	0.00
V	65.5	3.46	8.60	1.91	2.38	3.03
W	41	6.70	2.78	0.56	0.88	0.72
X	26.5	3.92	3.07	0.00	0.35	0.63
Y	305	6.06	22.9	0.00	0.00	7.8

* Denotes evidence of twinning in load-contraction curve corresponding to load shown.

References

[1] E. F. Sturcken. An X-Ray Method for Predicting the Stability of Natural Uranium at Low Burnup, USAEC Report DP-251. November, 1957 (Classified).

[2] P. R. Morris. Comparative Measurements of the Velocity of Propagation of an Ultrasonic Pulse in Uranium Fuel Elements, USAEC Report NLCO-764, p. 13. November, 1958.

[3] E. F. Sturcken. "A Generalized Growth Index Formalism," Papers Presented at the X-Ray Preferred Orientation Meeting Held at National Lead Company of Ohio. November 9 and 10, 1959, USAEC Report NLCO-804, p. 9, July, 1960.

[4] J. P. LeGeros. "A Growth Mechanism Based Upon Lattice Distortion," Papers Presented at the X-Ray Preferred Orientation Meeting Held at National Lead Company of Ohio, November 9 and 10, 1959, USAEC Report NLCO-804, p. 25. July, 1960.

[5] P. R. Morris and R. N. Thudium. Prediction of Dimensional Changes in Uranium Fuel Elements During Irradiation — The Elastic Solution — Interim Report, USAEC Report NLCO-816. September, 1960.

[6] E. F. Sturcken. "Status of the Growth Index Formalism," Papers and Discussion from the X-Ray Preferred Orientation Meeting Held at Argonne National Laboratory, December 15 and 16, 1960, USAEC Report ANL-6359, p. 20. May, 1961.

[7] R. D. Arnell and (Mrs.) J. Clayworth. The 'p' Value Method of Determining Preferred Orientation in Uranium Fuel Rods, and its Extension to the Prediction of Irradiation Growth, UKAEA Report DEGR-292(c). July 17, 1961.

[8] P. R. Morris. "Irradiation Growth in Alpha-Uranium Single Crystals," J. Appl. Phys. 4; 1611. April, 1962.

[9] P. R. Morris and R. N. Thudium. Prediction of Dimensional Changes in Uranium Fuel Elements During Irradiation — Test of The Elastic Solution, USAEC Report NLCO-838. November, 1961 (Classified).

[10] P. R. Morris. "The Form of a Solution for the Prediction of Dimensional Changes of Uranium Fuel Cores During Irradiation," Summary Technical Report for the Period January 1, 1962 to March 31, 1962, USAEC Report NLCO-850, p. 69. April 16, 1962 (Classified).

[11] L. T. Lloyd and H. H. Chiswik. Deformation Mechanisms of Alpha-Uranium Single Crystals, USAEC Report ANL-5367. December 14, 1954.

[12] H. H. Chiswik, A. E. Dwight, L. T. Lloyd, M. V. Nevitt, and S. T. Zegler. "Advances in the Physical Metallurgy of Uranium and Its Alloys," International Conference on the Peaceful Uses of Atomic Energy Proceedings, 2nd, Vol. 6, pp 394 to 412. New York: United Nations, 1958.

[13] B. R. Butcher. The Deformation of Alpha-Uranium at 450°C and 500°C, UKAEA Report AERE-R-2898. April, 1959.

PREDICTION OF THERMAL EXPANSION COEFFICIENTS BY THE GROWTH INDEX METHOD

E. F. Sturcken

E. I. du Pont de Nemours & Co.
Savannah River Laboratory

INTRODUCTION

In general the physical properties of an oriented metal depend on the direction in which the properties are measured. Hence to predict physical properties the grain orientation must be known as a function of the direction of the specimen.

The conventional methods of expressing preferred orientation are the pole figure and the inverse pole figure. Both methods are difficult to use for predicting physical properties because they are graphical and because they are stereographic projections and hence are not "area-true."

In the present report the growth index concept[1] is used to formulate an expression analogous to the growth index for the thermal expansion coefficient of an oriented metal. In the growth index concept the volume of grains in each orientation is weighted by a strain tensor for irradiation growth, and the growth index is the average of the weighted values over all orientations.

SUMMARY

Equations were derived for the thermal expansion coefficient, α_N, of an oriented metal for cases in which the grain orientation was represented by texture coefficients (TC),[1] area weighted p values,[2] and a continuous orientation distribution function $P(u, \phi)$.[3]

The equations derived for the thermal expansion coefficient were tested on uranium rods rolled to various reductions of area at temperatures of 300°C and 600°C. Thermal expansion coefficient values measured by dilatometer were in good agreement with those calculated from the derived equations except in the case where the grain orientation was

represented by texture coefficients. The poor agreement in this case was believed to be due to the fact that TC values give disproportionate weight to strong textures.

Studies were also made of the effect of the number of planes (hkl) employed to represent the grain orientation versus the agreement between calculated and measured thermal expansion coefficient values. Only small differences were observed between measured and calculated thermal expansion coefficient values in cases where the grain orientation was represented by 10, 14, 18, 20, and 32 measured planes. The differences were more likely due to scatter in the experimental measurements of preferred orientation than to the number of diffraction planes employed to represent the grain orientation.

DISCUSSION

Development of Equations for Calculating Thermal Expansion Coefficients

Assuming homogeneous elastic deformation, the coefficient of thermal expansion, α, for a single crystal of uranium in some direction, N, is given by the equation

$$\alpha_N = \alpha_a \cos^2 \alpha + \alpha_b \cos^2 \beta + \alpha_c \cos^2 \gamma \qquad (1)$$

where $\cos^2 \alpha$, $\cos^2 \beta$, and $\cos^2 \gamma$ are the direction cosines tha the direction of interest makes with the a, b, and c crystallographic axes, respectively, and α_a, α_b, and α_c are the thermal expansion coefficients of the a, b, and c axes, respectively (note: these axes are also the principal axes). To generalize to the polycrystalline case, ignore interactions and sum over the volume of grains in each orientation.

Consider first the case for which the volume of grains in each orientation, i, is represented by the texture coefficient, TC_i, that is

$$TC_i = \frac{I_i/I^o_i}{\frac{1}{n}\sum_{i=1}^{n} I_i/I^o_i} \qquad (2)$$

where the subscript i refers to the planes hkl, I_i is the intergrated diffraction intensity measured from some plane i of the specimen, I^o_i is the calculated intensity,[4] and n is the number of planes measured. In this case generali-

zation of equation 1 yields the expression

$$\alpha_N = \frac{1}{n} \sum_{i=1}^{n} TC_i \left(\alpha_a \cos^2 \alpha_i + \alpha_b \cos^2 \beta_i + \alpha_c \cos^2 \gamma_i\right) \qquad (3)$$

where N is the direction normal to the surface upon which the preferred orientation measurements were made.

Consider next the case where the volume of grains in each orientation, i, is represented by area weighted p values, that is

$$P_i = \frac{I_i / I^o_i}{\sum_{i=1}^{n} A_{w_i} I_i / I^o_i} \qquad (4)$$

where A_{w_i} is the area weighting factor defined by P. R. Morris.[2] In this case, generalization of equation 1 yields the expression

$$\alpha_N = \sum_{i=1}^{n} p_i A_{w_i} \left(\alpha_a \cos^2 \alpha_i + \alpha_b \cos^2 \beta_i + \alpha_c \cos^2 \gamma_i\right) \qquad (5)$$

which has been reported by Morris.[2]

Consider finally the case where the volume of grains in each orientation is represented by a continuous function, $P(u,\phi)$.[3] The symbols u and ϕ specify the angles in spherical coordinates that the crystallographic axes of the grain make with the normal to the sample surface, and $P(u,\phi)$ gives the number of grains oriented in each direction (u,ϕ). $P(u,\phi)$ is obtained from a least squares fit of the I_i to an orthonormal set of spherical harmonic functions. In this case generalization of equation 1 yields the expression

$$\alpha_N = \alpha_a \int_0^1 \int_0^{\pi/2} P(u,\phi) \left(1 - u^2\right) \sin^2 \phi \, du \, d\phi$$

$$+ \alpha_b \int_0^1 \int_0^{\pi/2} P(u,\phi) \left(1 - u^2\right) \cos^2 \phi \, du \, d\phi$$

$$+ \alpha_c \int_0^1 \int_0^{\pi/2} P(u,\phi) \, u^2 \, du \, d\phi \qquad (6)$$

If $P(u,\phi)$ is represented by a ten-term set of associated Legendre functions, equation 6 reduces to[5]

$$\alpha_N = A_{00} \frac{\sqrt{\pi}}{3\sqrt{2}} (\alpha_a + \alpha_b + \alpha_c) + A_{20} \frac{\sqrt{10\pi}}{30} (2\alpha_c - \alpha_b - \alpha_a) + A_{22} \frac{\sqrt{\pi}}{\sqrt{30}} (\alpha_b - \alpha_a) \quad (7)$$

where A_{00}, A_{20}, and A_{22} are the least squares coefficients.

Application of the Equations for the Thermal Expansion Coefficient, α_N, to Hot- and Cold-Rolled Uranium Rods

The equations developed in the previous section were tested on preferred orientation data reported by Mueller, Knott, and Beck[5] for uranium rods rolled at 300°C and 600°C to reductions of area of 0, 10, 45, and 70%. The thermal expansion coefficients were also measured on these same rods.

The relative diffraction intensities, I_1, reported by Mueller, Knott, and Beck were normalized by dividing them by the calculated "random" intensities, I^o_1, and then the I_1/I^o_1 were used to calculate α_N. Table I compares the values of α_N measured with a dilatometer with those calculated for 32 diffraction planes (hkl) by equations 3, 5, and 7. The best agreement between measured and calculated α_N was obtained using the area weighted p values to represent grain orientation (equation 5). Good agreement was also obtained when $P(u,\phi)$ was used to represent the grain orientation (equation 7). However, the agreement was poor for the stronger textures when TC values were used to represent the grain orientation. The poor agreement is believed to be due to the fact that TC values are disproportionately weighted by strong textures.

The effect of the number of planes measured on the resulting α_N was studied by calculating α_N for 10, 14, 18, 20, and 32 planes using equations 3, 5, and 7. These results are summarized in Table II. The greatest variation in α_N, as a function of the number of planes employed, occurred for the case where the grain orientation was represented by TC values (equation 3) and the least variation occurred for the case where the grain orientation was represented by area weighted p values (equation 5).

Regardless of the representation used for grain orientation, the values of α_N did not level off as the number of planes was increased from 10 to 32. The failure to level off

suggests that the errors in the internal consistency of a given set of measured relative diffraction intensities was greater than the error caused by representing the grain orientation by 10 versus 32 planes. The errors in each set of measured I_i were probably due to statistical fluctuations[6] caused by grain size and to the inclusion of a number of very weak diffraction peaks which were difficult to measure. Hence the measurement of a larger number of planes does not by itself assure greater precision in α_N.

TABLE I

Comparison of Measured and Calculated α_N for Rolled Uranium Rods

	α_N in Units of $10^{-6}/°C$						
		Calculated[a] for 25-100°C Using α_a, α_b, and α_c Measured by Lloyd[7]					
% Reduction of Area	Measured at 25-100°C[5]	Eq 3	% Diff[b]	Eq 5	% Diff	Eq 7	% Diff
Rolled at 300°C							
0	15.96	14.87	7.07	17.12	7.01	17.06	6.66
10	12.80	10.75	17.41	12.77	0.23	12.71	0.71
45	10.02	6.90	36.88	8.97	11.06	8.16	20.46
70	9.17	6.08	40.52	7.94	14.38	6.90	28.25
Rolled at 600°C							
0	15.86	14.83	6.71	17.10	7.52	16.88	6.23
10	14.90	14.50	2.72	16.04	7.37	16.25	8.67
45	13.39	10.23	26.76	12.91	3.65	12.44	7.36
70	12.71	11.01	14.33	13.19	3.71	13.29	4.46
			Avg 19.05		Avg 6.87		Avg 10.35

(a) Calculated for 32 planes

(b) % Difference = $\frac{\text{Meas - Calc}}{1/2\ (\text{Meas + Calc})}$ x 100. Since neither the preferred orientation measurements nor the dilatometer measurements are known to better than 10% there is no justification for using either as the correct value.

TABLE II

Effect of the Number of Measured Planes On α_N for Rolled Uranium Rods

Rolling Temp, °C	% Reduction of Area	α_N 10 Planes	14 Planes	18 Planes	20 Planes	32 Planes	Mean Deviation(a)
Case I. α_N Calculated from Equation 3							
300	0	15.85	14.07	16.68	15.24	14.87	0.79
300	10	9.49	10.33	10.92	10.30	10.75	0.46
300	45	6.13	5.89	6.80	5.88	6.90	0.58
300	70	5.52	4.69	5.90	4.67	6.08	0.71
600	0	15.81	14.31	16.29	15.32	14.83	0.69
600	10	16.56	16.16	16.12	15.57	14.50	1.28
600	45	9.61	9.11	11.05	9.90	10.23	0.58
600	70	11.66	10.98	11.64	10.66	11.01	0.33
						Group Avg	0.68
Case II. α_N Calculated from Equation 5							
300	0	17.14	15.82	17.22	16.72	17.12	0.36
300	10	12.15	12.92	12.05	12.28	12.77	0.40
300	45	9.21	8.50	8.10	7.87	8.97	0.54
300	70	8.45	7.00	7.49	6.76	7.94	0.62
600	0	17.04	16.12	17.00	16.74	17.10	0.30
600	10	16.91	17.11	16.03	16.21	16.04	0.42
600	45	12.30	11.89	12.57	12.49	12.91	0.48
600	70	13.30	13.33	12.87	12.88	13.19	0.18
						Group Avg	0.41
Case III. α_N Calculated from Equation 7							
300	0	16.60	16.40	17.06	16.68	17.06	0.30
300	10	12.69	12.68	11.93	12.26	12.71	0.26
300	45	6.57	8.32	7.96	7.90	8.16	0.44
300	70	4.73	6.60	7.12	6.71	6.90	0.58
600	0	17.42	16.59	16.74	16.52	16.88	0.27
600	10	17.32	17.07	16.16	16.38	16.25	0.42
600	45	11.64	12.05	12.36	12.30	12.44	0.28
600	70	13.40	13.22	12.84	12.91	13.29	0.20
						Group Avg	0.34

(a) Assuming that the 32-plane case gives the correct α_N.

REFERENCES

1. Sturcken, E. F. and W. R. McDonell. "An X-ray Method for Predicting Anisotropic Irradiation Growth in Uranium". J. Nucl. Mater. 7, No. 1, 85-91 (1961).

2. Morris, P. R. "Reducing the Effects of Nonuniform Pole Distribution in Inverse Pole Figure Studies". J. Appl. Phys. 30, No. 4, 595-6 (1959).

3. Sturcken, E. F. and J. W. Croach. "Predicting Physical Properties in Oriented Metals". Trans. AIME Metallurgical Society 227, 934-40 (1963).

4. Sturcken, E. F. and B. Post. "A Precise Determination of the Atomic Position Parameters for Alpha-Uranium". Advances in X-ray Analysis 4, pp. 85-92. New York: Plenum Press, Inc. (1960).

5. Mueller, M. H., H. W. Knott, and P. A. Beck. Effect of Varying Reduction on the Preferred Orientation in Rolled Uranium Rods. Final Report. Argonne National Laboratory, Argonne, Ill. USAEC Report ANL-5194 (1954); Mueller, M. H., et al. "Preferred Orientation in Rolled Uranium Rods". Trans. AIME Metallurgical Society 212, 793-98 (1958).

6. Sturcken, E. F. and W. E. Gettys. "Determination of Grain Size from Statistical Fluctuation in X-Ray Diffraction Intensity", Papers and Proceedings of the X-Ray Preferred Orientation Meeting Held at HAPO, June 29 and 30, 1961. W. Gary Jolley, Ed. General Electric Co., Hanford Atomic Products Operation, Richland, Wash. USAEC Report HW-74429, pp. 14-25 (1962).

7. Lloyd, L. T. Thermal Expansion of Alpha-Uranium Single Crystals. Argonne National Laboratory, Lemont, Ill. USAEC Report ANL-5972 (1959).

CRYSTAL STRUCTURE VARIATIONS IN ALPHA URANIUM AT LOW TEMPERATURES*

M. H. Mueller and R. L. Hitterman
Argonne National Laboratory

and

C. S. Barrett
University of Chicago

An extensive crystal structure determination of alpha uranium at low temperatures was undertaken since a number of unusual physical property changes have been observed near 43°K, especially the elastic moduli.[1] Both X-ray and neutron diffraction intensity measurements were obtained for a series of 0k0 reflections from a single crystal. These were used to obtain the best value of the displacement, y, of the uranium atom along the b axis. The atom positional parameter, obtained from these intensities using a least squares refinement computer program, was found to decrease from 0.1025 at 298°K to 0.1019 near 43°K and then to increase rapidly to 0.1025 at 4.2°K. [The room temperature value of y measured in the present report is identical to that which was measured by Sturcken and Post[2] employing X-ray diffraction from single crystals of uranium.]

Unit cell dimensions and expansion coefficients were determined from 4.2 to 298°K by X-ray diffraction using the Bond technique with single-crystal reflections at high angles. High-order reflections of the type h00, 0k0, and 00ℓ were used for the a_o, b_o, and c_o, respectively. The results obtained in angstroms were as follows: at 298°K a_o = 2.8537, b_o = 5.8695, c_o = 4.9548; at 50°K a_o = 2.8364, b_o = 5.8666, c_o = 4.9363; and at 4.2°K a_o = 2.8444, b_o = 5.8689, c_o = 4.9316. The linear thermal expansion coefficient is abnormally high in the c direction and is negative in the a and b directions in the temperature range below 43°K. This increase in a_o below 42°K is in agreement with the observation reported previously[3] in cooling from 63 to 20°K. The calculated volume from these lattice constants shows a minimum

* A more complete description of this work was published in Physical Review 129, 625-9 (1963).

near 43°K which is in agreement with the results obtained from uranium polycrystalline samples.[4]

A few reflections, such as odd 00ℓ's, were observed with neutrons, but not with X-rays. Since these reflections are not permitted with the presently ascribed orthorhombic structure, it is possible that they may be ascribed to a magnetic scattering, and since magnetic alignment may have a bearing on the change of structure and properties in the low temperature range, these extra reflections are being further investigated. This work was performed under the auspices of the United States Atomic Energy Commission.

REFERENCES

1. Fisher, E. S. and H. J. McSkimin. "Low-Temperature Phase Transition in Alpha Uranium". Phys. Rev. 124, 67-70 (1961).

2. Sturcken, E. F. and B. Post. "The Atomic Position Parameter in Alpha Uranium". Acta Cryst. 13, 852 (1960).

3. Bridge, J. R., C. M. Schwartz, and D. A. Vaughan. "X-Ray-Diffraction Determination of the Coefficients of Expansion of Alpha-Uranium." J. Metals 8, 1282-5 (1956).

4. Schuck, A. F. and H. L. Laquer. "Low Temperature Thermal Expansion of Uranium". Phys. Rev. 86, 803 (1952).

THE FORM OF A SOLUTION FOR THE PREDICTION OF DIMENSIONAL CHANGES OF URANIUM FUEL CORES DURING IRRADIATION*

P. R. Morris

National Lead Co. of Ohio

Abstract

The form of a proposed solution for the prediction of dimensional changes in uranium fuel cores during irradiation is set forth. Present knowledge of relevant physical processes is reviewed. Areas are noted in which experimental data are required.

Introduction

Uranium fuel elements undergo dimensional change during neutron irradiation. These dimensional changes, if excessive, can seriously impair reactor operation. For this reason, considerable effort[1,2,3,4,5,6] has been devoted to the development of theories for the prediction of such dimensional changes. These theories seek to combine the directional dependence of certain physical processes in an alpha-uranium single crystal according to the frequency of crystals in each orientation.

Previous Work on Project

Experimental preferred orientation data were used[7] to test the adequacy of a previously proposed[5] elastic solution. For the irradiation conditions assumed, the stresses calculated from the elastic solution were well in excess of those required for the initiation of creep and plastic flow. The elastic solution is thus considered inadequate.

Objective

The objective of this work is the development of a satisfactory theory for the prediction of dimensional changes which uranium fuel elements undergo during irradiation.

Summary of Results

The form of a proposed solution for the prediction of dimensional changes in uranium fuel cores during irradiation is set forth. Areas are noted in which experimental data are required.

Discussion

We shall assume that the anisotropic irradiation growth experienced by the individual crystallites is unaffected by stresses of the magnitude which can be occasioned by mechanical constraints. The correctness of this assumption may be readily checked by irradiating a single crystal subject to mechanical constraint, but seems to be borne out by the presence of extensive twinning and deformation bands in irradiated polycrystalline uranium.

In general, the strains produced in neighboring crystallites by anisotropic irradiation growth will be incompatible due to differences in spatial orientation. The preservation of a continuous medium requires compatibility of strain between neighboring crystallites. This compatibility is achieved initially by an elastic adjustment resulting in the creation of stresses which vary from point to point within an individual crystallite. As irradiation proceeds, these stresses increase.

Stress relief is provided by the mechanisms of creep and plastic flow. As in all crystalline materials, the applied stress necessary to cause plastic deformation in an alpha-uranium single crystal displays a pronounced dependence on the crystallographic direction in which the stress is applied. In all probability, the dependence of strain rate on stress and temperature (creep) is also a function of crystallographic direction. In magnesium single crystals, for example, creep by slip along basal planes has been observed.[8] The

* Paper reproduced from USAEC Report NLCO-850.

relief of stresses occasioned by anisotropic irradiation growth is thus also expected to exhibit a dependence on crystallographic direction.

On the average, individual crystallites may be expected to extend in crystallographic directions in which a positive irradiation growth coefficient is coupled with "strength" which is higher than the average "strength" of the matrix. Contraction may be expected in crystallographic directions in which a negative irradiation growth coefficient is coupled with "strength" higher than the average "strength" of the matrix. No general prediction can be made for the behavior in directions for which the "strength" is appreciably lower than the average "strength" of the matrix. The individual crystallites may be expected to yield in these directions, either in extension or in contraction, in order to maintain compatibility of strain between neighboring crystallites. This yielding results in changes in orientation of the participating crystallites.

The nonlinear nature of the equations involved in this problem does not permit an analytic solution. We are thus restricted to numerical solutions of the iterative type. The framework for solutions to problems of this nature has been partially developed in relation to the effect of thermal cycling,[9] and irradiation growth,[10] on the creep of uranium, and in relation to thermal stress distribution in uranium fuel elements.[11]

At this point, it is perhaps pertinent to survey briefly the extent of our current knowledge of the relevant physical processes.

Rather complete data[12] are available on the elastic constants of alpha-uranium single crystals in the temperature range from −195°C to +35°C. Values of C_{11}, C_{22}, and C_{33} are known to 300°C; and work is in progress to extend these measurements to temperatures approaching the alpha-to-beta transformation.

Critical, resolved shear stresses have been reported for (010) - [100] slip at room temperature,[13] and[14] for (001) - [100], (010) - [100], and {110} - ⟨110⟩ slip at 600°C. The deformation mechanisms which are active at room temperature have been found[15] to persist to 450°C.

Conflicting or unconfirmed values have been reported[16,17,18,19,20] for irradiation growth coefficients of unconstrained alpha-uranium single crystals in the range −196°C to 500°C.

Information relating strain rate (creep rate) to stress and temperature is currently available only for polycrystalline uranium.[9,21,22,23,24] In all probability, the dependence of strain rate on stress and temperature for an alpha-uranium single crystal is a function of crystallographic direction.

Suggested Areas of Further Investigation

Further progress in the development of theories for the prediction of irradiation growth in uranium fuel elements is dependent on additional knowledge of the irradiation growth rates and mechanical properties of alpha-uranium single crystals over the range of temperatures of interest in the operation of a production reactor.

Experiments of creep rates for single crystals should be carried out both within and without the reactor, since experience[22] and theory[10] indicate that in-pile creep rates are higher than out-of-pile rates.

These experiments will require the growing of large numbers of alpha-uranium single crystals, and the preparation of these crystals in forms suitable for experimentation.

References

[1] E. F. Sturcken. An X-Ray Method for Predicting the Stability of Natural Uranium at Low Burnup, USAEC Report DP-251. November, 1957 (Classified).

[2] P. R. Morris. Comparative Measurements of the Velocity of Propagation of an Ultrasonic Pulse in Uranium Fuel Elements, USAEC Report NLCO-764, p. 13. November, 1958.

[3] E. F. Sturcken. "A Generalized Growth Index Formalism," Papers Presented at the X-Ray Preferred